DISSERTATION

AMPLITUDE CORRECTION FOR REDUCED AXIS SCANNING OF LAYERED MATERIALS

Submitted by

Peihong Zhang

Department of Mechanical Engineering

In partial fulfillment of the requirements

For the Degree of Doctor of Philosophy

Colorado State University

Fort Collins, Colorado

Spring, 2004

COLORADO STATE UNIVERSITY

June 10, 02

WE HEREBY RECOMMEND THAT THE DISSERTATION PREPARED UNDER OUR SUPERVISION BY PEIHONG ZHANG ENTITLED "AMPLITUDE CORRECTION FOR REDUCED AXIS SCANNING OF LAYERED MATERIALS" BE ACCEPTED AS FULFILLING IN PART REQUIREMENTS FOR THE DEGREE OF DOCTOR OF PHILOSOPHY.

Committee on Graduate Work

Robert Gotshall

Dr. R. Gotshall, Health and Exercise Science

Hiroshi Sakurai

Dr. H. Sakurai, Mechanical Engineering

Dr. D. W. Radford, Mechanical Engineering

Dr. M. L. Peterson, Advisor, Mechanical Engineering

Dr. A. T. Kirkpatrick, Department Head, Mechanical Engineering

ABSTRACT OF DISSERTATION

AMPLITUDE CORRECTION FOR REDUCED AXIS SCANNING OF LAYERED MATERIALS

This dissertation explores an amplitude correction method for reduced axis scanning of a layered structure. The technique is applicable to inspection of a component with complicated contours. Reduced axis scanning technique decreases the number of required degrees of freedom in the scanning system. The reduced axis scanning can provide a more reliable automated inspection method. Gain correction is required to accommodate the non-normal incident wave that is used when scanning with a reduced axis system. Models based on matrix solutions of the wave transmission in the component are used for gain correction. The exploration of the applicability of these methods to wave transmission in a layered elastomeric or polymeric matrix composite plate are shown.

Samples of layered elastomeric or polymeric matrix composite plates are considered both theoretically and experimentally. The transmission coefficient of multi-layered material structure at an arbitrary incident angle is considered using the transfer matrix method. The model is incrementally increased in complexity from an elastic material model to a visco-elastic material model. All of the modeling assumes an orthotropic material, although calculation is for an arbitrary incidence which reduces material symmetry. In the theoretical derivations of the transfer matrix, the use of the second rank and third rank determinant simplifies the expressions of the transfer matrix and the resulting algorithm.

The experimental method uses water immersion and a through transmission configuration. Theoretical transmission curves are reconstructed by convolving the calculated transmission coefficient with a reference signal. Experimental results for a carbon fiber/epoxy composite plate are shown which compare favorably to theoretical results for the simple lamina lay-up used for the testing.

Peihong Zhang
Mechanical Engineering Department
Colorado State University
Fort Collins, CO 80523
Spring 2004

ACKNOWLEDGMENTS

I would express my gratitude to my adviser, Dr. Michael M. Peterson. It is impossible to accomplish the dissertation without his guidance, encouragement and support. His patience and confidence are impressive, his hard work and strict scientific attitude greatly impress me. I very sincerely hope that his work and research gain a great achievement.

I wish to express my appreciation to my committee: Dr. Robert Gotshall, Dr. Donald W. Radford and Dr. Hiroshi Sakurai, for their suggestions, encouragement and patience as mentors.

As always, support of my mother is my energy source, it is impossible to study further and accomplish the dissertation without her support and understanding. I am grateful to my mother for her contributions during my studies. I hope that she is in good health and long life.

I would thank for my daughter, she lost much more time to spend with her mother in past several years. I hope she grows up joyfully and happily.

TABLE OF CONTENTS

List of Tables

List of Figures

Chapter 1

Automatic Gain Correction for Reduced Axis Scanning

Motivation and Background

1.1 Introduction

More widespread adoption of in-process and in-service inspection is dependent on reduction in cost and an increase in inspection reliability. Automation of the inspection process is key to meeting the required reliability needs and can make inspection a viable alternative for cost sensitive applications. Manual inspection is too costly except in critical applications. However, in those applications where cost is less of an issue, reliability of manual inspection is more of a concern. As a result automatic inspection is increasingly becoming the norm in both critical and non-critical applications. Fortunately many NDE processes lend themselves well to automation. In particular, ultrasonic inspection can often be performed for large parts at a reasonable cost using an automatic scanning apparatus.

One of the challenges facing automatic scanning systems is that in many cases the part geometry may not be known precisely. In other applications the geometry may be sufficiently complex that it requires a scanning system with a large number of degrees of freedom to follow the part contours during the inspection process. For ultrasonic inspection of an obliquely incident wave, refraction of the wave-front occurs across the interface between the coupling fluid and the part. However, in cases where the acoustic impedance of the coupling fluid and the part is closely matched, refraction of the wave is low. With closely matched acoustic impedance, relatively complex parts may be scanned without precisely following the part contours. It is possible in those cases to scan a complex part and to be less exact in following the profile. Alternatively, a reduced number of degrees of freedom may be used in the scanning system. Thus a close acoustic impedance match between the part and the coupling fluid can make reduced axis scanning possible for higher efficiency and lower cost. The reduction in the number of degrees of freedom in scanning system can also result in a more reliable scanning system. However, while a reasonable ultrasonic signal may be received when scanning a part using this approach, the refraction and attenuation of the wave in the material may be sufficiently high that amplitude correction of the received signal may be required.

Thus an analytical model or efficient numerical method is needed which can be used to correct the received signal to account for refraction and loss of amplitude which occurs in the part. Without such a correction it is possible to have both false positives and false negatives (detecting a flaw when none exists) depending on the part curvature. In a number of parts such as composites, the component may be modeled as a layered material. Matrix propagator methods are attractive for the creation of a model which will allow the effect of amplitude variation on the received signal to be corrected for the non-normal wave incidence. The magnitude of the received signal can be adjusted so that it is consistent regardless of the angle of incidence. Before considering the issues associated with non-normal incident wave inspection, it is useful to review the motivation for increased use of non-destructive testing methods.

1.1.1 Problem Definition

1.1.1.1 Inspection

Retirement for cause is rapidly becoming commonplace in a number of industrial and critical service application situations. As financial constraints continue to be imposed on public and private enterprise, the need to efficiently allocate resources becomes more acute. Perhaps one of the most obvious wastes of resources is the systematic replacement and destruction of components of a complex system, which have met their design life. This is routinely done in commercial and military aircraft, military systems and even in commercial surface transportation. A more efficient approach would be to periodically inspect parts, which are nearing their design life and to determine the remaining useful life of the component. This, however, will require efficient and reliable low cost inspection techniques. The use of a reduced number of axes will help to improve scanning technology in a number of relevant applications.

Aircraft

Perhaps the most notable case of the increased use of retirement for cause is in the commercial aircraft sector. While high profile incidents such as the Aloha Aircraft failure have increased the pressure to improve inspection methods and implementation, the US aircraft fleet continues to age and high reliability of the fleet is expected in an age of highly competitive environment for the airlines. This demand has been met by improved testing procedures as well as improved training of aircraft maintenance personnel. Short courses provide philosophical grounding as well as the tools required to assure the reliability of the aging aircraft fleet [Kantimathi and Sam]. However, a need remains to further improve the testing of aircraft components using high reliability techniques in large area. An example of such a system is the dripless bubbler which was developed at Iowa State University as a part of the FAA - Center For Aviation Systems Reliability [Hsiu and Patton, 1993]. This system allows areas of the skin of a jetliner to be inspected using an attachable scanning system. Such a system has the potential to detect a number of defects, which could lead to failure of the skin of a jet aircraft.

Naval systems

A need, which is similar to exists in aircraft, exists in naval operation. One important example is the inspection of large thick composite components used for either radar or sonar domes. The inspection is needed to detect manufacturing defects, as well as to detect defects due to accidents or environmental effects. These shell structures may be several feet in diameter and must be relatively defect-free to perform reliably. This is a highly challenging scanning application, which involves complex shapes of multiple layers. Similar situations are encountered in stealth related acoustic technologies, which require complex shape to be produced of layered materials. Defects can threaten the functionality of the system as well as may represent a fatal system problem for the entire platform.

Both of these applications present continuing research challenges in applied NDE which are generally referred to as the inspection of thick composite parts. Taylor and Nayfeh among others have considered the inspection of thick rectangular laminates [Taylor and Nayfeh, 1996]. Typical applications of thick composites are in submarine parts such as sonar domes and acoustic path deflection units. These composite parts are often several centimeters thick and can represent hundreds of layers of material. Inspection methods to detect disbonds between the layers and large inclusions are of interest. It is also important to perform periodic inspections due to the potential for small disbonds to grow because of diffusion of water between the layers.

The ability to inspect some of these components with a normally incident signal is limited by the complex shape and uncertainty in the shape of the component. For example, the design of a sonar dome is determined by the hydrodynamic design and manufacturing issues for the submarine rather than the need to make inspection simple.

Tires

The system, which primarily motivates this work, is shown in Figure 1.1. Truck tire casings are routinely retreaded three or more times during their service life. While a high resolution ultrasonic scanning of the entire surface of the tire would reduce the number of tire failure, the tire casing is complex in shape. In order to reduce the number of axes required to scan the tire section, four paintbrush transducers are used as transmitters. Four standard small diameter transducers are mounted in a scanning head and used as receivers. The entire sample can be scanned with two axes of motion as shown plus rotation of the tire to scan the circumference. However, the incident wave is generally not normal to the surface of the sample, for many standard casings the wave is as much as 30 degrees from normal incidence. Sensitivity of detection for disbonds and material property changes at different locations on the tire casing are of interest. The size and severity of the defect must be known regardless of the shape of the casing. The tire

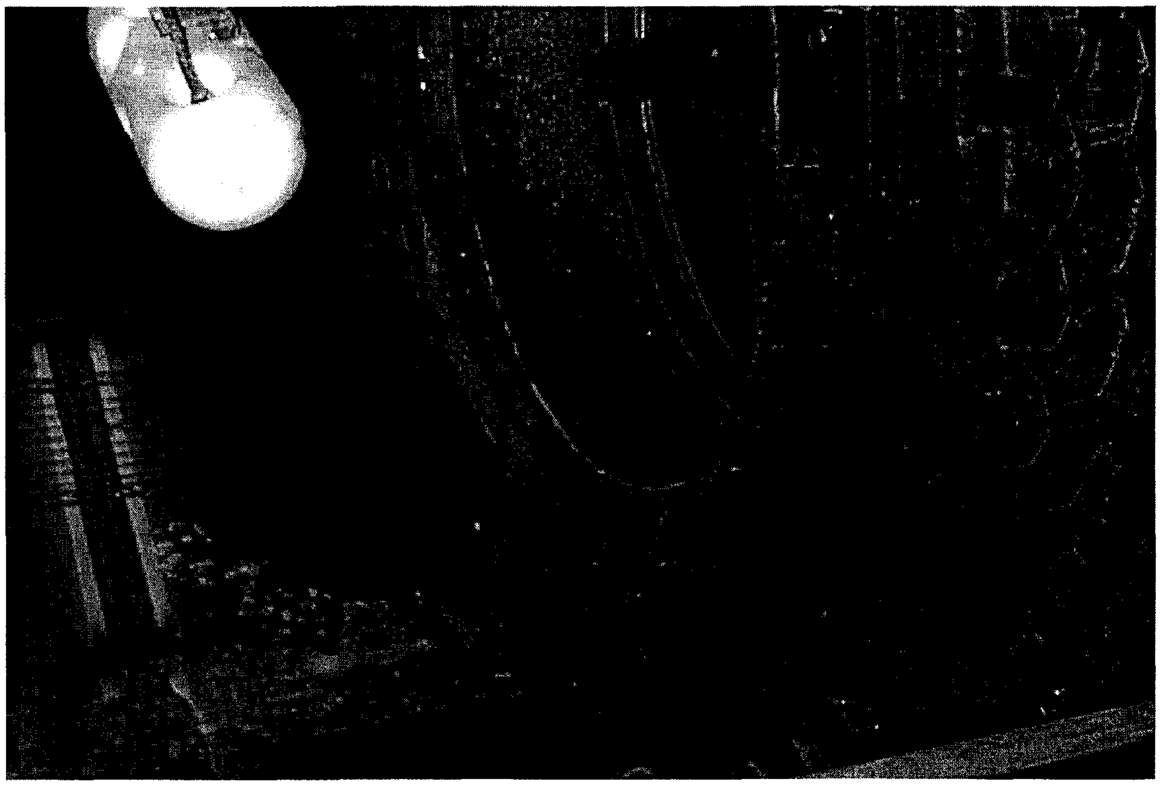

Figure 1.1a The transducers for ultrasonic inspection machine of a truck tire casing

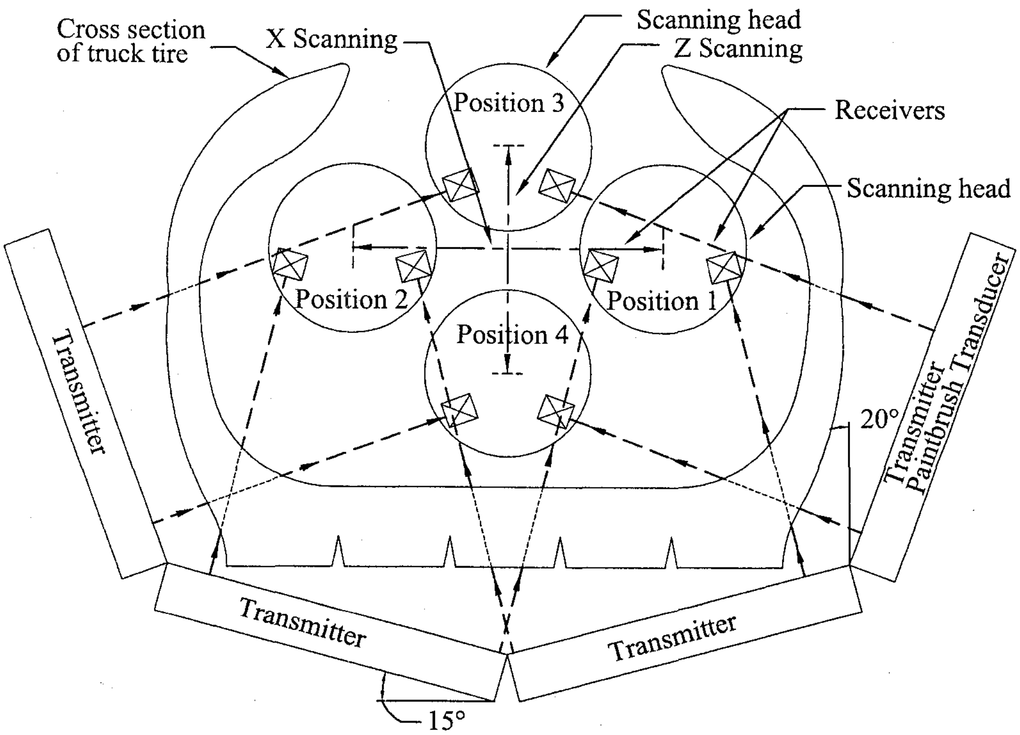

Figure 1.1b The configuration of transducers for ultrasonic inspection of a truck tire casing

casing, like the composite sonar dome, is approximately modeled as a layered system. Because of the rubber matrix material, the system is reasonably described as a linear visco-elastic solid with the steel or fabric belts also creating significant material anisotropy.

1.1.1.2 Complex part shapes

In all three applications described, the part is of a reasonably complex geometry. The potential to change the part shape to improve inspectability is limited. The shapes of the parts are defined by hydrodynamic, aerodynamic or other performance characteristics. The use of through-transmission ultrasonic inspection requires accurate alignment of the transmitting transducer and receiving transducer, in order to obtain an acceptable signal-to-noise ratio. Misalignment of the receiver and transmitter will reduce the received amplitude, which can lead to unacceptable signal-to-noise ratio in areas of slight material variation. The inspection is done quite easily but further limits the ability to follow complex contours. Proper interpretation of an ultrasonic image requires that reasonable dynamic range be available to separate defects from slight property variations. In addition, it is important to note that the highest sensitivity to defects may not be in a normal incident wave. As seen in a number of references in the literature, non-normal incidence may result in a higher change in attenuation for a number of defects [Zhang and Peterson, 1999].

Figure 1.2 shows a cross section of a typical tire casing, when the tire casing is inspected, it is clear that to exactly follow the contours of the part, at a fixed distance from the tire, at least, 3 degrees of freedom would be required in the plane of the figure. Both the transmitting and receiving transducers would have to be rotated to maintain their

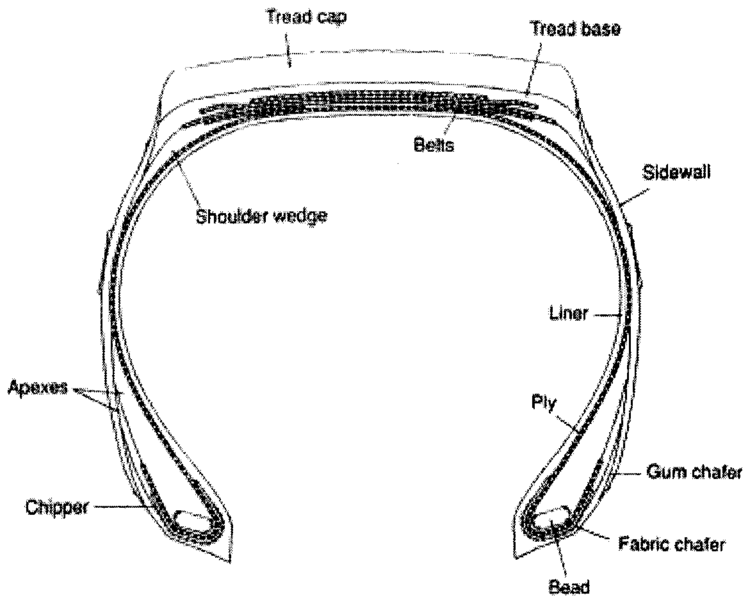

Figure 1.2 A cross section of a typical tire casing

efficiency as well. Also, one more degree of freedom is required to detect the cross-section in which the defect exists. Thus, a probable configuration for a full scanning system for a normal incident wave would require 3 degrees of freedom of the receiving transducers on the interior of the tire, as well as 2 more axes for the tire and the exterior transmitter. In all cases rotation of the tire is required to scan all of the cross section of the tire, the rotation axis would be required on the exterior transmitting transducer, to maintain parallel faces for the transmitter and receiver. Each other in addition to being in a water coupled system. The two rotational axes on the transducers would have to be performed using submersible motors or long mechanical linkages. Clearly the increase of 2 degrees of freedom, two of which must function under water would significantly increase the system complexity. The ability to remove the rotational axes is thus of great value.

1.1.1.3 Machine reliability and sensitivity to tolerance variation

While the reduction of the number of degrees of freedom reduces machine cost, it can also increase inspection reliability. Further, the two scanning axes and tire rotational axis used in the tire inspection system keeps all of the moving parts out of the water and relatively simple. The scanning motion control system is also simpler which will further enhance machine reliability. For reduced axis scanning only one axis of the system moves between scan-lines. Simultaneous control of at least three degrees of freedom would be required for normal incident inspection. Also, by reducing a-priori assumptions regarding the part shape, slight tolerance variation in the parts are less likely to result in inspection errors. Both false positives and false negatives can result if the amplitude of a transmitted signal increases or decreases due to change in part curvature. The reliability of the inspection system is thus enhanced both by improved reliability and reduced sensitivity to tolerance variation in the part shape.

1.1.2 Approach

1.1.2.1 Characterization of sensitivity to misalignment

What is evident from the discussion above is that precise alignment to maintain normal incidence of the ultrasonic wave is impractical and may not be desirable. A method to characterize the effect of the misalignment on the amplitude of the received signal is thus required. This method should account for possible visco-elasticity of the matrix material as well as anisotropy introduced by reinforcing fiber (or tire belts). Furthermore, the model must be capable of being implemented for the configurations which will be encountered during inspection.

Several additional issues are associated with the need for correction of the signal due to misalignment. Amplitude correction in all of the applications described, needs to be performed in near-real-time. As a result, the correction of the amplitude for misalignment must also be of reasonable computational complexity or, alternatively, implemented as a look up table for the results. Finally, the need for a-priori knowledge of the part shape is only reduced, not eliminated, in the correction process. A good understanding of the shape of the part is still required particularly if any sharp transition in amplitude occur at particular angles.

Non-normal incidence inspection is used in the tire scanning system shown in Figure 1.1. The bottom or crown transmitters are fixed at 15^0 from the horizontal. The vertical or sidewall, transducers are fixed at 20^0 from vertical. The basis for selection of these angles was the need to scan the entire area of the tire casing while maintaining sufficient clearance between the transducers and casing. In particular, the inspection of the area in the transition between sidewall and crown (the shoulder) requires that specific angles be used in order to completely scan the tire. The range of incident angles at which the ultrasonic wave impinges on the casing is approximately $0^0 - 30^0$. Preliminary work suggests that the transmission coefficient is almost linear between 0^0 and 12^0 [Zhang and Peterson, 1999]. However, the linear relationship exists only for a single frequency of the ultrasonic wave. Actual ultrasonic transducers are broadband units. The 3 dB drop bandwidth for the 500 kHz transducers used in the tire inspection is from approximately 300 kHz to 700 kHz. So, while the $0^0 - 12^0$ incidence angle may be suitable for some practical application, the transmission coefficient has a more complicated relation for a broadband transducer. Thus, it is likely that calculations will be required for a range of frequencies, the result of which must be convolved with the incident signal to obtain a corrected amplitude.

1.1.2.2 Optimal inspection angle

Several references also indicated that the highest sensitivity to defects may not occur when a normal incident wave is used for inspection [Zhang and Peterson, 1999, Ainlie,1995, Cervenka and Challande,1991]. In particular, in the case of disbonds in which the two faces of the discontinuity are in contact, the defects may only result in a change in amplitude if the ultrasonic signal is at non-normal incidence. For example in the tire casing application, disbonds are common in the shoulder region. The disbonds in the shoulder are likely to align with the belts in the tire crown. As a result, a wave which is normal to the surface or normal to the plane of the defect, may not be optimal for detection. If optimal detection is at an angle to the defect face of approximate 30^0 [Zhang and Peterson, 1999], then due to refraction at the rubber interface, the incident wave should impinge on the rubber at approximate a 25^0 angle. Clearly, an interesting and challenging optimization problem is faced in an attempt to provide optimal detection in a reduced axis scanning system.

1.1.2.3 Gain correction

Once the best configuration of transducers is obtained for flaw detection and scan coverage, a variation in the alignment remains due to part curvature. The angle from normal changes the amplitude of the received signal and can impact the accuracy of the inspection results. Using the model developed, it should be possible to obtain corrected received amplitude which corresponds to a particular angle of incidence. This correction cannot accurately perform for differences in sensitivity to defects at different incident angles, but it is suitable for correcting the reference gain to provide a more consistent image amplitude. Practical issues associated with implementation or the gain correction are significant in the tire inspection system. Two1024 point line scans are acquired at 10 second intervals, the line scans correspond to two positions on either the crown or the sidewall of the tire casing. Amplitude correction, in the form of an offset to the two 1024 point line scans, must be applied to the two lines as they are acquired. Thus computational efficiency of the model is a high priority. Implementation of the algorithm on existing hardware is possible because of the modular design of the tire scanning system [Downs et. al, 1999]. The model will be based on existing methods, which have the potential to be implemented in a manner which fits the requirements for real time calculation.

1.1.3 Thesis statement

A computationally efficient model can be used to correct the gain for reduced axis scanning of multi-layer structures. The dissertation demonstrates the applicability of the transfer matrix formulation to the gain correction of ultrasonic imaging for reduced axis scanning. The computer codes based on previous research – allow a user to predict the transmission through a layered visco-elastic isotropic or orthotropic plate at an arbitrary angle of incidence. Experimental methods and signal processing required to obtain material properties used in the codes are discussed, signal processing is developed, that allows the amplitude curves at discrete frequencies to be compared to experimental imaging results. The following sections in this chapter present a solution of a transmission coefficient used as a gain correction of reduced axis scanning system for isotropic multi-layered structure, and a corresponding computer code used as a gain correction is completed for the calculation of transmission coefficient. Chapter 2 explores a solution of a transmission coefficient as the gain correction of a elastic orthotropic composite plate for reduced axis scanning system, chapter 3 expands to discuss the effect of a visco-elastic property for a composite plate on the gain correction, chapter 4 develops a model to solve a delamination and disbond problem for the composite, and attempts to detect the defect of disbond in the inspection, the last chapter develops and discusses some experimental methods and signal processing for measurements of material properties.

1.2 Review of Literature

1.2.1 Transfer matrix approach

The transmission of a plane elastic wave at oblique incident through a solid medium consisting of any number of parallel plates of different materials and thickness has been the subject of considerable interest. The most important approach is based on the transfer matrix method, which systematized the analysis and made it suitable for efficient computation. Before the Thompson matrix method was presented, attempts to obtain transmission and reflection coefficients were directly attempted from the governing equations and boundary conditions of the problem. Standard boundary conditions are considered as well as continuity of the particle displacements, normal stresses and shearing stresses at the interfaces between the layers. However, using a direct approach based on the governing equations is so formidable that no attempt appears to have been made to treat cases of more than two layers [Haskell, 1953].

In 1950, Thompson introduced a matrix method which consisted of velocities, normal and shear strain components. The matrix method avoids unwieldy mathematical expressions and conveniently represents the reflection and transmission within multi-layered structures. The Thompson matrix is limited to computation of a multi-layered fluid and sandwiched solids because of an assumption in the continuity of shear strain in the interface between layers. Haskell [1953] corrected an error in the Thompson matrix formalism by changing shear strains into shear stress and expanded the special case to general multi-layered solids. Meantime, the corrected Thompson matrix formulas were used to obtain the dispersion equations of phase velocity for elastic surface waves of Rayleigh and Love type on multilayered solid media. Importantly, the Thompson matrix was used to compute phase and group velocities of Rayleigh waves for three-layer and two-layer models of the earth's crust. Brekhovskikh's [1960] treatment paralleled that of Thompson and yielded equations whose validity is limited to the same special cases as Thompson's. Both formulations are valid only for certain special cases such as multiple fluid layers or multiple solid layers with identical shear modulus sandwiched between fluid layers.

The Thompson-Haskell matrix method was first developed for elastic materials. It was later modified for linear visco-elastic materials by other investigators [Cooper, 1967. Shaw and Bugl, 1969]. A significant amount of work exists in the area of wave propagation in linear visco-elastic materials. Kolsky [1953] discussed general one-dimensional problems of the propagation of stress waves in viscoelastic solid and presented wave propagation for a Voight linear visco-elastic model and a 3-element mechanical linear visco-elastic model. Kolsky[1958] explored the characterization of pulse propagations in viscoelastic materials by Fourier transform or Laplace transform. The general background on viscoelastic waves was later applied to layered structures.

Cooper [1967] considered reflection and transmission of oblique plane waves at a plane interface between two visco-elastic media. The method of solution is the same as that used in the elastic problem. Potential functions are employed and the results are similar to elastic cases except that it leads to the definition of complex reflection and transmission angles and coefficients. The reflected and transmitted wave in this work is a general plane wave, i.e. a plane wave whose amplitude varies across the wave front. The angles of reflection and transmission depend on the incident angle in a more complicated way than in the elastic case, because the wave speeds of the reflected and transmitted wave are, in general, functions of incident angles. Shaw and Bugl [1969] combined transmission and reflection of plane waves through layered linear elastic media with transmission and reflection of plane waves in a linear viscoelastic medium. The transfer matrix method was expanded to a viscoelastic medium. The reflection and transmission coefficients, in the linear viscoelastic layered media, were formulated as the equivalent elastic plane-strain case with modified Lame' constants. The modified Lame' constants are complex and frequency dependent and replace the usual elastic Lame constants. The transfer matrix method is directly implemented in terms of stresses and displacements. The above matrix method treats any solid layers, fluid layers or sandwich structures between fluid layers. Cervenka and Challande [1991] provided a more general method that can treat any sequence of liquid and solid layers, which was based on the Thompson-Haskell matrix method.

In addition to the theoretical work, the comparison of experiments to the theory for the Thompson-Haskell matrix method has progressed as well since the method was first introduced. Barnard et al [1975] computed the acoustic reflection and transmission of thin plates at arbitrary incident angles by using Thompson's method (which he attributed to Brekhovskikh). Absorption by the material was included in theoretical equations by allowing the wave number to be complex. Experimental data was then provided which supported the results. Both reflection measurements and transmission coefficient measurements were performed. The reflection coefficient was obtained as the ratio of the received signal amplitude to the incident signal amplitude. A measure of transmission coefficient was provided by the ratio of the received signal amplitude to the incident signal amplitude, but also including losses in the material, in the transmission path. Loss in the material was obtained by comparing the amplitude with and without the sample included in the propagation path. Regardless of attribution, the Brekhovskikh or Thompson matrix method was shown to predict the transmission and reflection coefficient of a thin plate fairly accurately.

Later work by Fold and Loggin [1977] used Brekhovskikh's treatment with an appropriate correction, which paralleled the Thompson-Haskell method. Fold and Loggin determined the transmission and reflection coefficients for plane waves at oblique incidence on a system of N layers of plane parallel plates. The theoretical results showed good agreement with measured data.

However, while Thompson-Haskell transfer matrix method was directly applied, numerical algorithms were found to become unstable with increasing frequency. When using numerical techniques to evaluate the transfer matrix, the exponential term may cause large round off errors. The round-off errors are especially problematic in the presence of evanescent waves and for large values of the product of frequency and thickness. In ultrasonic applications, the problems arise when the product is on the order of 10^2 $MHz \cdot mm$, a range that is of considerable practical interest.

Dunkin [1965] prevented these numerical difficulties which are caused by computation of the squares of exponential terms. Although the terms cancel numerically, they cause a loss of significant figures in the function and in some components of certain matrix products. Dunkin introduced a matrix formulation, which avoids these difficulties and gives a natural decomposition of the model solutions into source part and receiver part. The source is caused by the distribution of incident stresses, receiver part is associated with displacements and stresses in the Nth layer.

Levesque and Piche [1992] further improved the transfer matrix approach to provide a complete description for the propagation of ultrasonic waves in a multilayered medium. Generalized expression for the reflection and transmission coefficients were derived which were then solved numerically. Problems with numerical stability are solved based on Dunkin's work with modifications which are used to maintain computational efficiency. The formulation is applicable at any arbitrary incident angles and for any sequence of solid or fluid layers. In addition, viscoelastic behavior is allowed and a method to perform calculations for arbitrary incident pulse shapes and beam profiles is described. The arbitrary pulse shape and beam profile is handled through application of two-dimensional Laplace transform, which is then inverted numerically.

The area of wave propagation in layered systems is sufficiently well developed that extensive reviews of the work exist as monographs on the subject by authors such as

Ewing and Jardetzky [1957] and Brekhoskikh [1980,1990]. Ursin further reviewed elastic wave propagation in horizontally layered media in a related paper [1983].

1.2.2 Application to anisotropic materials

The transfer matrix method has also been used for elastic wave propagation in multilayered anisotropic media. Nayfeh and Chimenti [1989] developed an approach for propagation of plane waves in a general anisotropic plate and presented numerical results of plane wave dispersion for some special cases of interest. The most general cases are the triclinic symmetry with 21 independent elastic constants and the monoclinic plate with 13 independent elastic constants. Nayfeh [1991] presented the exact analytical treatment of the interaction of harmonic elastic waves with N-layered anisotropic plates. The solution was obtained by combining the transfer matrix method with the linear transformation approach. By satisfying appropriate continuity conditions at interlayer interfaces a global transfer matrix can be constructed which relates the displacements and stresses on one side of the plate to those on the other. Taylor and Nayfeh [1996] expanded the analysis for the exact three-dimensional viscoelastic solution for simply supported, thick multilayered composite plates, in which each layer is assumed to posses orthotropic or higher material symmetry. The damping characteristics of a composite plate, as well as its natural modes of vibration, were obtained with aid of the matrix transfer method. Nayeh [1995] further reviewed wave propagation in layered anisotropic media. Spies [1994] also considered elastic waves in homogeneous and layered transversely isotropic media.

All of the models require knowledge of the elastic constants for the anisotropic material. While the elastic constants of the anisotropic materials play an important role for elastic wave propagation, ultrasonic wave speed measurements appear to be the most widely used method for the determination of the elastic properties of anisotropic solids. Aristegui and Baste [1997] have considered the optimal identification of the 21 independent elastic constants for the most general linear homogeneous anisotropc elastic solid. The constants are obtained from wave speed measurements of obliquely incident ultrasonic bulk waves. A number of more general reviews of anisotropic elasticity include works by Ting [1996] among other.

Clearly, the development of an appropriate model of wave propagation in a layered elastic solid requires that a method of calculation be available. However, reasonable values of the elastic and visco-elastic constants must also be available. Both of these problems have been previously considered. However, the implementation into a single practical system represents a significant effort and the contribution of this dissertation.

1.2.3 Visco-elastic material Research

Rubber is generally modeled as being a linear viscoelastic material. Rubber exhibits significant internal damping and the stiffness tends to increase as the frequency of loading is increased. In order to model a visco-elastic material, it is necessary not only to obtain elastic constants for the material but also to obtain the visco-elastic properties.

Nolle and Mowry [1949] and Nolle and Sieck [1950] measured velocities and attenuation of both transverse and longitudinal ultrasonic waves for a synthetic rubber. Measurements were performed using a fluid coupled ultrasonic method and a solid coupled ultrasonic transmission method. The visco-elastic properties of the material were obtained for a Voight visco-elastic model. Snowdon [1963] also considered the dynamical properties of rubber and rubber-like materials using a linear visco-elastic model. Nichols [1973] also measured the acoustic properties of rubber, and measured the material properties including: transmission loss at normal incident angles, reflectivity at normal incident angle and transmission loss at arbitrary incident angles. From these basic measurements the complete visco-elastic properties of bulk rubber samples may be obtained. However, this becomes significantly more difficult for anisotropic materials. Further, the visco-elastic properties are the same in all directions with only elastic properties being dependent on direction.

1.2.4 Application of theory

A large number of investigators have described the interaction of an elastic wave with a multi-layered elastic or viscoelastic material. However, few investigators have attempted to integrate this theory into practical systems except for some simple ultrasonic and some geophysical application. However, between the application and the current work in few cases where the theory has been applied, significant differences exist.

The geophysical applications differ somewhat in the use of the theory since the physical configuration of the source and receiver is typically one sided. The transmitting and receiving transducers are both located on the surface of the earth or in a relatively shallow well. The problem of interest is propagation of a surface or plate wave in a multi-layered structure. While mathematically similar to the current approach, a number of practical differences in transducer sensitivity, design and signal to noise characteristics exist. In addition, only a single signal or a small number of signals need to be processed at one time.

In contrast to the geophysical applications, the transducer characteristics and configurations of the present application are quite typical of ultrasonic non-destructive evaluation systems. However the practical ultrasonic applications typically assume that the geometry is well defined, that the beam is normal to the surface of the part and that, even in the case of the inverse problem, the material is well characterized. None of these restrictions are appropriate in the current work. The applicability of the general approach to this application was demonstrated by the simplified model by Cheng and Achenbach [1996], and the extended model by Zhang and Peterson [1999]. Both of these papers consider the use of models to perform signal calibration for inspection of multi-layer systems.

1.3 Theory

Several steps will constitute the development of a model which can be used for amplitude correction of the reduced axis scanning system. The general model will, first, be developed for isotropic materials. Anisotropic materials will then be considered as an extension. Extension for a finite beam field would allow a synthetic image to be created of the tire casing or other multi-layer structure. The theory will first be developed for a plane wave incident on a homogeneous isotropic layered material

1.3.1 Obliquely incident waves in layered media

For the typical system, several layers of homogeneous isotropic layers will be used as a model. Figure **1.3** shows the configuration of a simple model of five layers of plane homogeneous visco-elastic or elastic material which is immersed in a fluid (typically water). In the absence of body forces, the displacement-stress equation of motion is:

$$\rho \frac{\partial^2 u_j}{\partial t^2} = \frac{\partial \sigma_{ij}}{\partial x_i} \tag{1.1}$$

where u_j is the displacement in j direction, t is time, ρ is the mass density, σ_{ij} is the stress tensor and x_i $(i = 1,2,3)$ denotes the x, y and z axes. The summation convention used. From Hooke's law for an isotropic material (2 independent Lame's constants), stresses are related to displacements as:

$$\sigma_{ij} = \lambda^* \frac{\partial u_k}{\partial x_k} + \mu^* \left(\frac{\partial u_i}{\partial x_j} + \frac{\partial u_j}{\partial x_i} \right) \tag{1.2}$$

where λ^* and μ^* are the complex Lame' constants, the Lame' constants can then be defined as:

$$\lambda^* = \frac{1}{3}(Y_v - Y_s) \text{ and } \mu^* = \frac{1}{2} Y_s \tag{1.3}$$

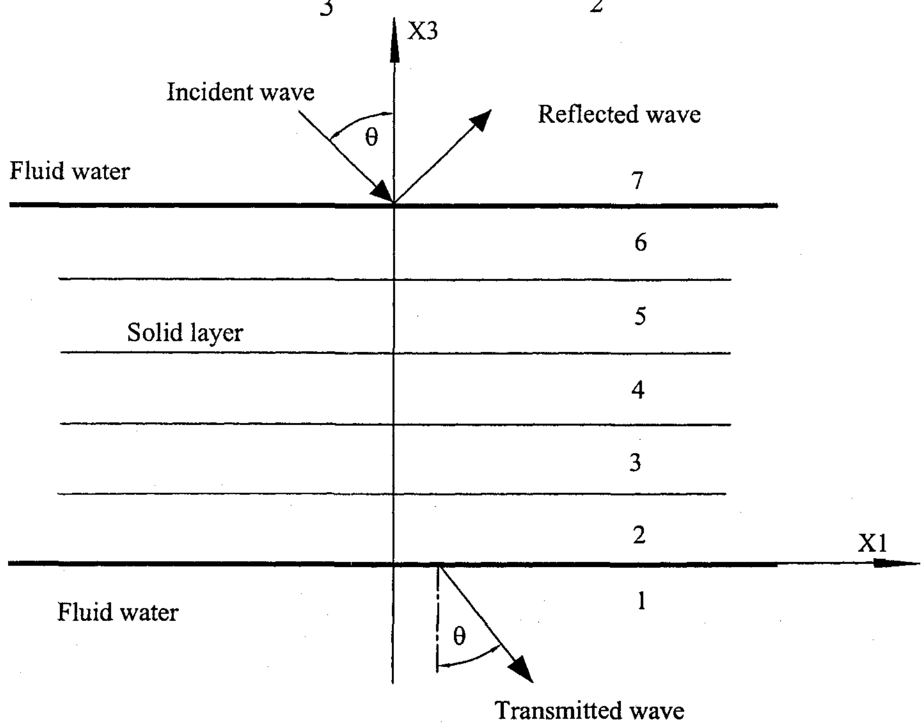

Figure 1.3 A 5-layer solid structure immersed in fluid water

where Y_s and Y_v are the derivatoric and dilatational complex moduli. For a linear viscoelastic material, this is a reasonably general description of the system.

The displacement equation of motion can then be obtained from equation (1.1) and equation (1.2) as:

$$\rho\frac{\partial^2 u_j}{\partial t^2}=\frac{\partial}{\partial x_j}\left(\lambda^*\frac{\partial u_k}{\partial x_k}\delta_{ij}\right)+\frac{\partial}{\partial x_i}\left[\mu^*\left(\frac{\partial u_i}{\partial x_j}+\frac{\partial u_j}{\partial x_i}\right)\right] \tag{1.4}$$

which may be rewritten in vector operator form as:

$$\rho\frac{\partial^2\vec{u}}{\partial t^2}=\left(\lambda^*+\mu^*\right)\nabla\left(\nabla\cdot\vec{u}\right)+\mu^*\nabla^2\vec{u}+\nabla\lambda^*\nabla\cdot\vec{u}+\nabla\mu^*\times\nabla\times\vec{u}+2\left(\nabla\mu^*\cdot\nabla\right)\vec{u} \tag{1.5}$$

From the definition above, a homogeneous solid can then be described as:

$$\frac{\partial^2\vec{u}}{\partial t^2}=\frac{\lambda^*+2\mu^*}{\rho}\nabla\left(\nabla\cdot\vec{u}\right)-\frac{\mu^*}{\rho}\nabla\times\left(\nabla\times\vec{u}\right) \tag{1.6}$$

Equation (1.6) is consistent with Helmholtz's theorem such that the displacements may be decomposed into scalar and vector field. The displacement may be written into the vector superstition of longitude wave displacement u_l and shear wave displacement u_t:

$$\vec{u}=\vec{u}_l+\vec{u}_t \tag{1.7}$$

Substitution of displacement representation (1.7) into equation (1.6) yields:

$$\frac{\partial^2\vec{u}_l}{\partial t^2}-\frac{\lambda^*+2\mu^*}{\rho}\nabla^2\vec{u}_l+\frac{\partial^2\vec{u}_t}{\partial t^2}-\frac{\mu^*}{\rho}\nabla^2\vec{u}_t=0 \tag{1.8}$$

The most familiar approach to the solution of the wave equation employs potential functions. Using φ and $\vec{\phi}$ as the scalar and vector potential respectively, a solution can be described. The two functions φ and $\vec{\phi}$ describe the longitudinal and shear waves that propagate in the solid. If $\vec{u}_l$ is the displacement associated with the longitudinal wave and $\vec{u}_t$ is the displacement associated with the shear wave, then

$$\vec{u}_l = \nabla\varphi, \qquad \vec{u}_t = \nabla\times\vec{\phi} \tag{1.9}$$

and equation (1.7) may be rewritten as

$$\vec{u} = \nabla\varphi + \nabla\times\vec{\phi} \tag{1.10}$$

the displacement representation (equation 1.9) satisfies the equation (1.8) of motion if

$$\frac{\partial^2\varphi}{\partial t^2} - c_l\nabla^2\varphi = 0 \tag{1.11}$$

and

$$\frac{\partial^2\vec{\phi}}{\partial t^2} - c_t\nabla^2\vec{\phi} = 0 \tag{1.12}$$

where $c_l = \sqrt{\dfrac{2\mu^* + \lambda^*}{\rho}}$ is the longitudinal wave velocity, and $c_t = \sqrt{\dfrac{\mu^*}{\rho}}$ is the shear wave velocity in an unbounded media. For time harmonic plane waves, the vector potential of 2-dimensional problem is expressed as:

$$\vec{\phi} = (0, \phi, 0) \tag{1.13}$$

For the isotropic materials, from equation (1.13), (1.10) and (1.2), the displacement and stress are related to potentials, respectively as:

$$\vec{u} = \left(i\xi\varphi - \frac{\partial\phi}{\partial z},\ 0,\ \frac{\partial\varphi}{\partial z} + i\xi\phi\right) \tag{1.14}$$

$$\vec{\sigma}_3 = \left[-2\mu^*\xi\left(\gamma\phi - i\frac{\partial\varphi}{\partial z}\right),\ 0,\ 2\xi\mu^*\left(\gamma\varphi + i\frac{\partial\phi}{\partial z}\right)\right] \tag{1.15}$$

where $\xi = k_l \sin\theta_l$, $\gamma = \xi - k_t^2 / 2\xi$, $k_l = \omega / c_l$, $k_t = \omega / c_t$ is wave number, and θ is an incident angle. The subscript l indicates a longitudinal wave, subscript t indicates a shear wave. The solution for a solid layer, omitting $\exp i(\xi x - \omega t)$ term, is then of the form:

$$\varphi = \varphi_1 \exp(-i\alpha z) + \varphi_2 \exp(i\alpha z) \tag{1.16a}$$

$$\phi = \phi_1 \exp(-i\beta z) + \phi_2 \exp(i\beta z) \tag{1.16b}$$

$$\alpha = k_l \cos\theta_l \tag{1.17a}$$

$$\beta = k_t \cos\theta_t \tag{1.17b}$$

φ_1 and ϕ_1 are the amplitude coefficient of the incident longitudinal and shear wave, and φ_2 and ϕ_2 are the reflection coefficients for the longitudinal and shear waves. The potential vector is defined as:

$$\vec{\varphi} = [\varphi_1 \quad \varphi_2 \quad \phi_1 \quad \phi_2]^T$$

for fluids such as water, the scalar potential and vector potential are expressed as:

$$\varphi^{(7)} = \exp(-i\alpha(z - z_6)) + V\exp(i\alpha(z - z_6)) \tag{1.18a}$$

$$\phi^{(7)} = 0, \qquad z > z_6 \tag{1.18b}$$

$$\varphi^{(1)} = W\exp(-i\alpha z) \tag{1.18c}$$

$$\phi^{(1)} = 0, \qquad z \le 0 \tag{1.18d}$$

where W is the transmission coefficient, and V is the reflection coefficient.

1.3.2 Waves in layered media

The applications of interest all share a series of common defects. The defects represent either discontinuities in the boundary conditions between layers (disbonds) or spatial variation of material properties. Either type of defect can represent a stress concentration which can lead to separation of layers under stress. Both types of defects should be detectable using ultrasonic waves. Prior to considering the impact of defects on the propagation of an elastic wave through a layered structure, a model will be described which will be used to represent the system. The general description of the model will be for a defect free system. A disbond and inclusion will be added to the model.

1.3.2.1 Multi-layer structure model

For the five-layer system shown in Figure 1.3, a model of the system is required which can be used for efficient computation. The boundary condition of a multi-layered structure consists of interfaces between several solid layers. The normal and shear stresses are continuous across the interface, as are the displacements. Notationally, continuous stresses and displacements at the interface are shown as:

$$[\sigma_{xz}]^{+} = [\sigma_{xz}]^{-} \text{ and } [\sigma_{zz}]^{+} = [\sigma_{zz}]^{-} \tag{1.19}$$

$$[u_x]^{+} = [u_x]^{-} \text{ and } [u_z]^{+} = [u_z]^{-} \tag{1.20}$$

where the axes are shown in Figure 1.3. The superscript "+" represents the positive side of the interface and the superscript "-" represents the negative side of the interface. A displacement-stress vector can be defined as:

$$\vec{f} = [u_x, u_z, \sigma_{zz}, \sigma_{xz}]^T \tag{1.21}$$

which is continuous across the interface. Then: $\vec{f}(z_j^{-}) = \vec{f}(z_j^{+})$

The displacement-stress vector for each layer of isotropic material can then be rewritten in terms of potential functions as:

$$\vec{f}=[B(z,z_{j-1})]\vec{\varphi}\,,\quad z_{j-1}\le z\le z_j \tag{1.22}$$

$$B(z,z_{j-1})=\begin{bmatrix} i\xi & i\xi & -i\beta & i\beta \\ i\alpha & -i\alpha & i\xi & i\xi \\ 2\mu^*\xi\gamma & 2\mu^*\xi\gamma & -2\mu^*\xi\beta & 2\mu^*\xi\beta \\ -2\mu^*\xi\alpha & 2\mu^*\xi\alpha & -2\mu^*\xi\gamma & -2\mu^*\xi\gamma \end{bmatrix}\begin{bmatrix} e^{i\alpha(z-z_{j-1})} & 0 & 0 & 0 \\ 0 & e^{-i\alpha(z-z_{j-1})} & 0 & 0 \\ 0 & 0 & e^{i\beta(z-z_{j-1})} & 0 \\ 0 & 0 & 0 & e^{-i\beta(z-z_{j-1})} \end{bmatrix}$$

$$\tag{1.23}$$

where, for every homogeneous layer, we consider that potential vector $\vec{\varphi}$ to be the same.

Then, the displacement-stress vector from one layer to the next layer is found to be:

$$\vec{f}(z_j)=[B(z_j,z_{j-1})]\vec{\varphi}\,,\ \vec{f}(z_{j-1})=[B(z_{j-1},z_{j-1})]\vec{\varphi} \tag{1.24}$$

$$\vec{f}(z_j)=[B(z_j,z_{j-1})][B(z_{j-1},z_{j-1})]^{-1}\vec{f}(z_{j-1}) \tag{1.25}$$

Let $[A^{(j)}]=[B(z_j,z_{j-1})][B(z_{j-1},z_{j-1})]^{-1}$, from layer 1 to layer 5, the displacement stress vector is then:

$$\vec{f}(z_6)=[A]\vec{f}(z_1) \tag{1.26}$$

and the displacement-stress matrix has the form

$$\begin{bmatrix} u_x^{(6)} \\ u_z^{(6)} \\ \sigma_{zz}^{(6)} \\ \sigma_{xz}^{(6)} \end{bmatrix}=[A]\begin{bmatrix} u_x^{(1)} \\ u_z^{(1)} \\ \sigma_{zz}^{(1)} \\ \sigma_{xz}^{(1)} \end{bmatrix} \tag{1.27}$$

where $[A]=[A^{(6)}][A^{(5)}][A^{(4)}][A^{(3)}][A^{(2)}]$. For each layer, the matrix $A^{(j)}$ coefficients are shown in Appendix A.

For the boundary conditions between a solid and a fluid, the shear stresses that vanish in the fluid are expressed as:

$$\sigma_{xz}^{(6)}=0\,,\ \sigma_{xz}^{(1)}=0 \tag{1.28}$$

for a fluid the normal stresses are

$$\sigma_{zz}^{(1)} = -\omega^2 \rho W \, , \; \sigma_{zz}^{(6)} = -\omega^2 \rho (1+V) \tag{1.29}$$

from which the displacements are found to be:

$$u_z^{(1)} = -i\alpha W \, , \; u_z^{(6)} = i\alpha (V-1) \tag{1.30}$$

The equations of the displacement and the stress matrix are:

$$\begin{bmatrix} u_x^{(6)} \\ u_z^{(6)} \\ \sigma_{zz}^{(6)} \\ 0 \end{bmatrix} = [A] \begin{bmatrix} u_x^{(1)} \\ u_z^{(1)} \\ \sigma_{zz}^{(1)} \\ 0 \end{bmatrix} \tag{1.31}$$

Consider the normal stress, the normal displacement and the boundary condition from the zero shear stress.

$$\begin{aligned} u_z^{(6)} &= A_{21} u_x^{(1)} + A_{22} u_z^{(1)} + A_{23} \sigma_{zz}^{(1)} \\ \sigma_{zz}^{(6)} &= A_{31} u_x^{(1)} + A_{32} u_z^{(1)} + A_{33} \sigma_{zz}^{(1)} \\ 0 &= A_{41} u_x^{(1)} + A_{42} u_z^{(1)} + A_{43} \sigma_{zz}^{(1)} \end{aligned} \tag{1.32}$$

The equations of the normal displacement and the normal stress are found to be:

$$\begin{aligned} u_z^{(6)} &= M_{22} u_z^{(1)} + M_{23} \sigma_{zz}^{(1)} \\ \sigma_{zz}^{(6)} &= M_{32} u_z^{(1)} + M_{33} \sigma_{zz}^{(1)} \end{aligned} \tag{1.33}$$

where

$$M_{ik} = A_{ik} - A_{i1} A_{4k} / A_{41}$$

Substituting equations (1.29) and (1.30) for the displacement and stress representations into the equation (1.33), the transmission coefficient and reflection coefficient are given by

$$W = \frac{-2i\omega\, Z_1 \rho_1 \rho_7^{-1}}{M_{32} - i\omega\, Z_1 M_{33} - (M_{22} - i\omega\, Z_1 M_{23}) i\omega\, Z_7} \tag{1.34}$$

$$V = \frac{M_{32} - i\omega\, Z_1 M_{33} + (M_{22} - i\omega\, Z_1 M_{23}) i\omega\, Z_7}{M_{32} - i\omega\, Z_1 M_{33} - (M_{22} - i\omega\, Z_1 M_{23}) i\omega\, Z_7} \tag{1.35}$$

this formulation gives the transmission and the reflection coefficients in the absence of a defect. However, it is necessary to extend this result to the case of a defect in the layered material.

1.3.2.2 Defective layer

In order to model defects in the tire or a thick composite, it is necessary to consider the types of defects which occur in both the present application and more generally in layered systems.

Reversion of tire layer

Reversion occurs in aircraft tire rubber under certain circumstances when landing on a wet runway. The problem occurred frequently in aircraft tires when jets were first landing on aircraft carriers [Hsiu, 1993]. The reversion of rubber requires high contact pressures and results from superheated steam being created between the tire and runway. The superheated steam creates an area of reduced material integrity that can produce localized porosity in the tread rubber. The reversion condition is represented in the calculations by replacement of the tread materials in one layer by the material properties of a soft unvucanized rubber. This layer is the surface layer of the casing. A similar defect would be expected for a thick composite with uncured resin in one belt. The tread rubber devulcanizes and becomes essentially like raw rubber. When the required material properties for proper operation are lost it represents a significant safety hazard.

Heat damage to layer

Heat damage within the matrix of the casing occurs under a number of conditions, most notably, over inflation and under inflation of the casing can result in a range of tire casing defects. Some of these defects may be characterized as heat damage. Heat is generated both in the hysterysis in the deflection of the tire as well as due to action between the rubber and wire reinforcements. Once localized heating occurs, the different materials (wire and rubber) have non-uniform heat strains. Thus the heating action can produce cracks or disbonds between materials as well as cross-linking and hardening of the rubber matrix. If the damage is localized, then the interaction of the defect with the ultrasonic wave may be understood as a distribution of scatterers. However, damage will tend to propagate along the belt interface and produce delaminations in the casing. This condition can be modeled as altered material properties in one or more layers in the tire.

1.3.2.3 Defective boundary conditions

In addition to defects which correspond to altered material properties within layers, the tire casing can also have disbonds between layers. The disbonds can initiate from separations of the wires in the belts from the matrix or from existing porosity in the casing. Potential types of disbonds include both complete disbonds and disbonds in which the separate faces are in contact (kissing disbonds).

Slip in axial plane, discontinuous boundary conditions

Figure 1.3 shows the layered system with the continuity conditions discussed above. For the disbond defect, assume a slip boundary condition exists between two layers. It will be assumed that interlayer slip occurs between layer 4 and layer 5, but the development is suitable for any boundary between layers. Although the boundary conditions are discontinuous, the matrix method may be used to solve this problem. Slip conditions are expressed as shear stress free surfaces on the crack:

$$\sigma_{xz}^{(4+)} = 0, \quad \sigma_{xz}^{(4-)} = 0 \tag{1.36a}$$

$$\begin{bmatrix} u_z^{(4+)} \\ \sigma_{zz}^{(4+)} \end{bmatrix} = \begin{bmatrix} u_z^{(4-)} \\ \sigma_{zz}^{(4-)} \end{bmatrix} \tag{1.36b}$$

The displacement stress vector from layer 1 to the top of layer 4 is then expressed as:

$$\vec{f}(z_4^-) = [A^{(4)}]\vec{f}(z_3) \tag{1.37}$$

$$\vec{f}(z_4^-) = [A_1]\vec{f}(z_1) \tag{1.38}$$

where the matrix $[A_1] = [A^{(4)}][A^{(3)}][A^{(2)}]$, and the matrix coefficients $[A^{(j)}]$ are the same as the continuous boundary conditions problem. The displacement-stress vectors between layer 1 and the top of layer 4 are expressed

$$\vec{f}(z_4^-) = \begin{bmatrix} u_x^{(4-)} \\ u_z^{(4-)} \\ \sigma_{zz}^{(4-)} \\ 0 \end{bmatrix}, \quad \vec{f}(z_1) = \begin{bmatrix} u_x^{(1)} \\ u_z^{(1)} \\ \sigma_{zz}^{(1)} \\ 0 \end{bmatrix} \tag{1.39}$$

From the normal displacement, normal stress and the zero shear stress boundary equation, the normal displacement and normal stress matrix can be expressed as:

$$\begin{bmatrix} u_z^{(4-)} \\ \sigma_{zz}^{(4-)} \end{bmatrix} = [M_1]\begin{bmatrix} u_z^{(1)} \\ \sigma_{zz}^{(1)} \end{bmatrix} \tag{1.40}$$

$$M_{1ik} = A_{1ik} - A_{1i1}A_{14k} / A_{141} \tag{1.41}$$

where A_{1ik} is the coefficient of the matrix $[A_1]$.

Also, the displacement-stress vector from the bottom of layer 5 to layer 6, gives:

$$\vec{f}(z_6) = [A^{(6)}]\vec{f}(z_5) \tag{1.42}$$

$$\vec{f}(z_6) = [A_2]\vec{f}(z_4^{\ +}) \tag{1.43}$$

where $[A_2] = [A^{(6)}][A^{(5)}]$, the representations of the displacement-stress vector for the slip boundary conditions are:

$$\vec{f}(z_6) = \begin{bmatrix} u_x^{\ (6)} \\ u_z^{\ (6)} \\ \sigma_{zz}^{\ (6)} \\ 0 \end{bmatrix}, \ \vec{f}(z_4^{\ +}) = \begin{bmatrix} u_x^{\ (4+)} \\ u_z^{\ (4+)} \\ \sigma_{zz}^{\ (4+)} \\ 0 \end{bmatrix} \tag{1.44}$$

Similarly, the normal displacement and normal stress matrix is given by

$$\begin{bmatrix} u_z^{\ (6)} \\ \sigma_{zz}^{\ (6)} \end{bmatrix} = [M_2]\begin{bmatrix} u_z^{\ (4+)} \\ \sigma_{zz}^{\ (4+)} \end{bmatrix} \tag{1.45}$$

$$M_{2ik} = A_{2ik} - A_{2i1}A_{24k} \,/\, A_{241} \tag{1.46}$$

Substituting equation (1.36) and (1.40) into matrix equation (1.45), the matrix representation of the displacement and stress relationships is derived as:

$$\begin{bmatrix} u_z^{\ (6)} \\ \sigma_{zz}^{\ (6)} \end{bmatrix} = [M_s]\begin{bmatrix} u_z^{\ (1)} \\ \sigma_{zz}^{\ (1)} \end{bmatrix} \tag{1.47}$$

where $[M_s] = [M^{(2)}][M^{(1)}]$. The steps in the development are similar to the solution of multi-layered rubber immersed in water with continuous solid boundary condition. By substituting equation (1.29) and (1.30) into equation (1.47), we can derive expressions of transmission coefficients and reflection coefficients with interlayer slip between solids. The solutions are the same as equation (1.34) and (1.35), but the matrix $[M]$ coefficients are different for the two cases.

Discontinuous shear and normal tensile stress

The case for a discontinuous tensile and shear stress is relatively straight forward to make and is of more practical interest. For compressive stress, the same situation exists as in the previous section. For tensile stresses, the stresses and strains at the boundary are discontinuous. The 5-layered structure is the same as above as well, shear and tensile forces are not transmitted between layer 4 and layer 5. The transmission coefficients are expressed by the same relationship as equation (1.34), when the stress at layer 4, $\sigma_{zz}^{(4+)}$ is a compressive stress. Equation (1.36) and (1.47) are applied for this case. In contrast, the transmission coefficient is zero, when the stress $\sigma_{zz}^{(4+)}$ calculated from equation (1.45) is a tensile stress.

1.3.3 Material models

Linear elastic isotropic materials are described using two independent Lame's constants. However, rubber is typically described as being a linear visco-elastic material. Rubber exhibits internal damping and the stiffness increases as the frequency of loading is increased. Two simple models are commonly used to describe the response of rubber: a 2-element Voight model and a 3-element model. The Voight model is more straight forward but does not account for the stiffness increase as the frequency of loading increases.

1.3.3.1 Voight model

The simplest model used for linear viscoelasticity is the Voight model which is shown schematically in Figure 1.4a. The relation between stress and strain in the Voight model is:

$$\sigma = \left(\mu + \eta \frac{\partial}{\partial t} \right) \varepsilon \tag{1.48}$$

where σ is stress, ε is strain, μ is elastic modulus and η the viscosity coefficient. In general, for a linear visco-elastic material, the stress and strains can be written in term of the operators P and Q as: $P\sigma = Q\varepsilon$. For 3-dimensional visco-elastic rubber material, under moderate or small hydrostatic pressure the responses can be considered to be elastic. Then the relationship is:

$$\sigma_{kk} = 3k\varepsilon_{kk} \tag{1.49}$$

where k is the bulk modulus and

$$P\sigma_{ij} = 2Q\varepsilon_{ij} \tag{1.50}$$

In general then by definition [Tschoegl, 1989]:

$$\sigma_{ij}' = Y_s \varepsilon_{ij}' \tag{1.51a}$$

$$\sigma_{kk}' = Y_v \varepsilon_{kk}' \tag{1.51b}$$

where Y_s and Y_v are the derivatoric and dilatational complex modulus, respectively, and

$$\sigma_{ij}' = \sigma_{ij} - \frac{1}{3} \sigma_{kk} \delta_{ij} \tag{1.52a}$$

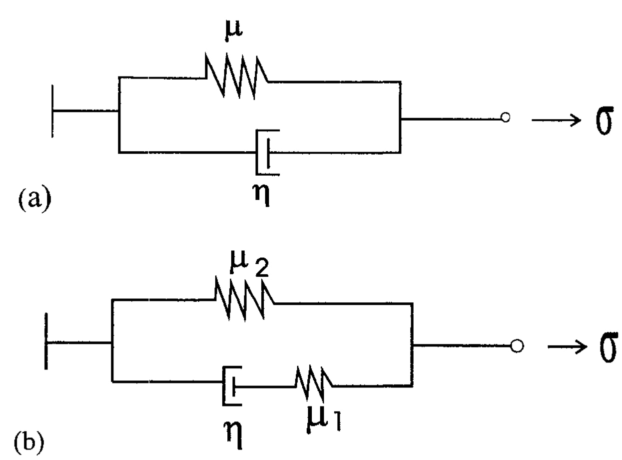

Figure 1.4. Visco-elastic models of rubber materials (2-element Voight model and 3-element mechanical model)

$$\varepsilon_{ij}' = \varepsilon_{ij} - \frac{1}{3}\varepsilon_{kk}\delta_{ij} \tag{1.52b}$$

gives the deviatoric stress σ_{ij}' and deviatoric strain ε_{ij}', respectively. The relationships for the complex Lame' constants may be obtained for use directly in the mechanics modeling. The deviatoric complex modulus is then:

$$Y_S = 2\frac{Q}{P} \tag{1.53a}$$

and the dilatational complex modulus is:

$$Y_v = 3k \tag{1.53b}$$

$$\lambda^* = \frac{1}{3}(Y_v - Y_s),\ \mu^* = \frac{1}{2}Y_S \tag{1.54}$$

For the Voight model, $Y_S = 2(\mu + \eta D)$ and $Y_v = 3k$. The complex Lame' constants are the expressed as:

$$\lambda^* = \lambda - \frac{2}{3}\eta\frac{\partial}{\partial t} \tag{1.55}$$

$$\mu^* = \mu + \eta\frac{\partial}{\partial t} \tag{1.56}$$

1.3.3.2 Three element model

A slightly more complex model of rubber is the 3-element mechanical model, shown in Figure 1.4b. The 3-element model allows the stiffness of the rubber to be modeled as having frequency dependence. This behavior more closely represents the behavior of actual rubber materials. The relationship between the stress and the strain for the 3-element model is:

$$(\mu_1 + \eta D)\sigma = (\mu_1\mu_2 + (\mu_1 + \mu_2)\eta D)\varepsilon \tag{1.57}$$

Similarly

$$Y_s = \frac{2[\mu_1\mu_2 + (\mu_1 + \mu_2)\eta D]}{\mu_1 + \eta D} \tag{1.58a}$$

$$Y_v = 3k \tag{1.58b}$$

and the complex Lame' constants are then:

$$\lambda^* = k - \frac{2}{3}\mu_2 - \frac{2}{3}\frac{\mu_1 \eta D}{\mu_1 + \eta D} \tag{1.59a}$$

$$\mu^* = \mu_2 + \frac{\mu_1 \eta D}{\mu_1 + \eta D} \tag{1.59b}$$

Experimentally the three elements model requires that 4 unknown material parameters be obtained. The parameters required are, μ_1, μ_2, η and k. The properties must be obtained for all materials used in the modeling. As mentioned above, however, the visco-elastic properties, unlike the elastic properties, are isotropic since they are primarily related to matrix properties.

1.3.4 Implementation as complex modulus

If, for an incident plane wave, the complex modulus are based on the Voight model:

$$\lambda^* = \lambda + \frac{1}{3}i\omega\eta \tag{1.60a}$$

$$\mu^* = \mu - i\omega\eta \tag{1.60b}$$

The real part of the complex modulus is the elastic modulus, and the imaginary part changes with frequency and with the viscosity coefficient.

For a 3-element mechanical model, the complex Lame' constants are expressed

$$\lambda^* = k - \frac{2}{3}\mu_2 + \frac{2}{3}\frac{\mu_1 i\omega\eta}{\mu_1 - i\omega\eta} \tag{1.61a}$$

$$\mu^{*} = \mu_2 - \frac{i\omega \mu_1 \eta}{\mu_1 - i\omega \eta} \tag{1.61b}$$

or

$$\lambda^{*} = \lambda(\omega) + \lambda'(\omega) i \tag{1.62a}$$

$$\mu^{*} = \mu(\omega) + \mu'(\omega) i \tag{1.62b}$$

The real part and imaginary part of the constitutive model simultaneously depend on the frequency and viscosity coefficient. The model like the Voight model can be directly implemented in existing models as a complex elastic modulus.

1.3.4.1 Anisotropic materials

The previous development assumes that it is reasonable to model the materials as linear visco-elastic homogeneous and isotropic materials. In most of the applications which are of interest, such as thick composites and tire casings, the material must be modeled as being anisotropic. However, at the length scales of interest the material may be modeled as being homogeneous with the isolated scatterers being the defects. Further simplification of the model is possible for most applications such as tire belts and thick composites. The layers may be assumed to be orthotropic. The matrix method has already been used to solve orthotropic problems [Nayef, 1991, 1995]. Chapter 2 presents some details of the use of matrix methods for anisotropic materials.

1.4 Preliminary Theoretical Results

The theoretical calculation for homogeneous, isotropic, plane incident waves is the fundamental problem which underlies the proposed work. Results have been obtained for transmission coefficients that are suitable for use in gain correction based on transfer matrix method calculations. The preliminary input data and calculation results are described in the following sections.

1.4.1 Material data

Calculations are shown for the Voight material model for the case of the 5-layer system with both continuous and interlayer slip. The input data is shown in Table 1.1. Material properties are based on measurements unless noted. The attenuation is extrapolated from published data [Nolle, 1952] assuming a linear dependence of attenuation on frequency. For the case of reversion of the tread rubber (layer 2) materialproperties of soft (unvulcanized) rubber is used [Krautkramer and Krautkramer, 1977].

1.4.2 Calculation results

Results for the transmission coefficient with continuous boundary conditions and interlayer slip are shown in Figure 1.5. These figures show the dependence of the transmission coefficient on both frequency and angle of the incident wave. The plots of attenuation for different angles at a range of frequencies show the importance of

Table 1.1 Input data for 5-layer structures of rubber

	Thickness (mm)	Velocity (m/s) (L and SV wave[Shaw,1968])		Attenuation (Nep) (L, S) [Shaw, 1968]		Density (g/cm3)
Layer 2	15	1648 (L)	787 (S)	0.02	0.07	1.16
Layer 20 Unvulcanized	15	1480	706	0.02	0.07	0. 9
Layer 3	2	1639	782	0.02	0.07	1. 5
Layer 4	2	2413	1150	0.03	0.10	1. 6
Layer 5	2	2783	1326	0.03	0.12	1. 6
Layer 6	7	2164	1030	0.03	0.09	1. 5

correction for misalignment as well as the altered sensitivity to these two types of defects at some incident angles. The slip boundary condition shown is, however, only an approximation to the simple slid boundary condition which was described above. However, the type of variation of sensitivity to angle and frequency which would be encountered may be representative.

A comparison of the sensitivity of the continuous boundary conditions, interlayer slip in solids and reversion layer with angle is shown in Figure 1.6. These figures show the three cases at 500 kHz, the nominal center frequency of the transducer used in the system. Additional figures show similar sensitivity to angle at 300 kHz and 700kHzfrom the central frequency. The 300KHz and 700KHz frequency correspond to the 3 dB bandwidth of the transducer.

It is evident from these figures that the impact of the misalignment of the transducers in the orientation show in Figure 1.1 cannot be neglected. What remains to be demonstrated is if the calculations shown are of sufficient accuracy given the uncertainty in the material properties, as well as the incident angle, to be used to correct the received signal.

1.4.3 Result explanations

The transmission coefficient is defined as the ratio of the amplitude of the acoustic pressure in the transmitted wave to the amplitude in the incident wave. As an illustration, the theoretical curves of the power transmission coefficient as a function of the angle of incidence are shown in Figure 1.6a for a 5-layer rubber structure immersed in water, at the frequency 500 KHz, the frequency corresponds to different acoustic wavelengths for the individual layers in the multi-layered structure. The strong increase

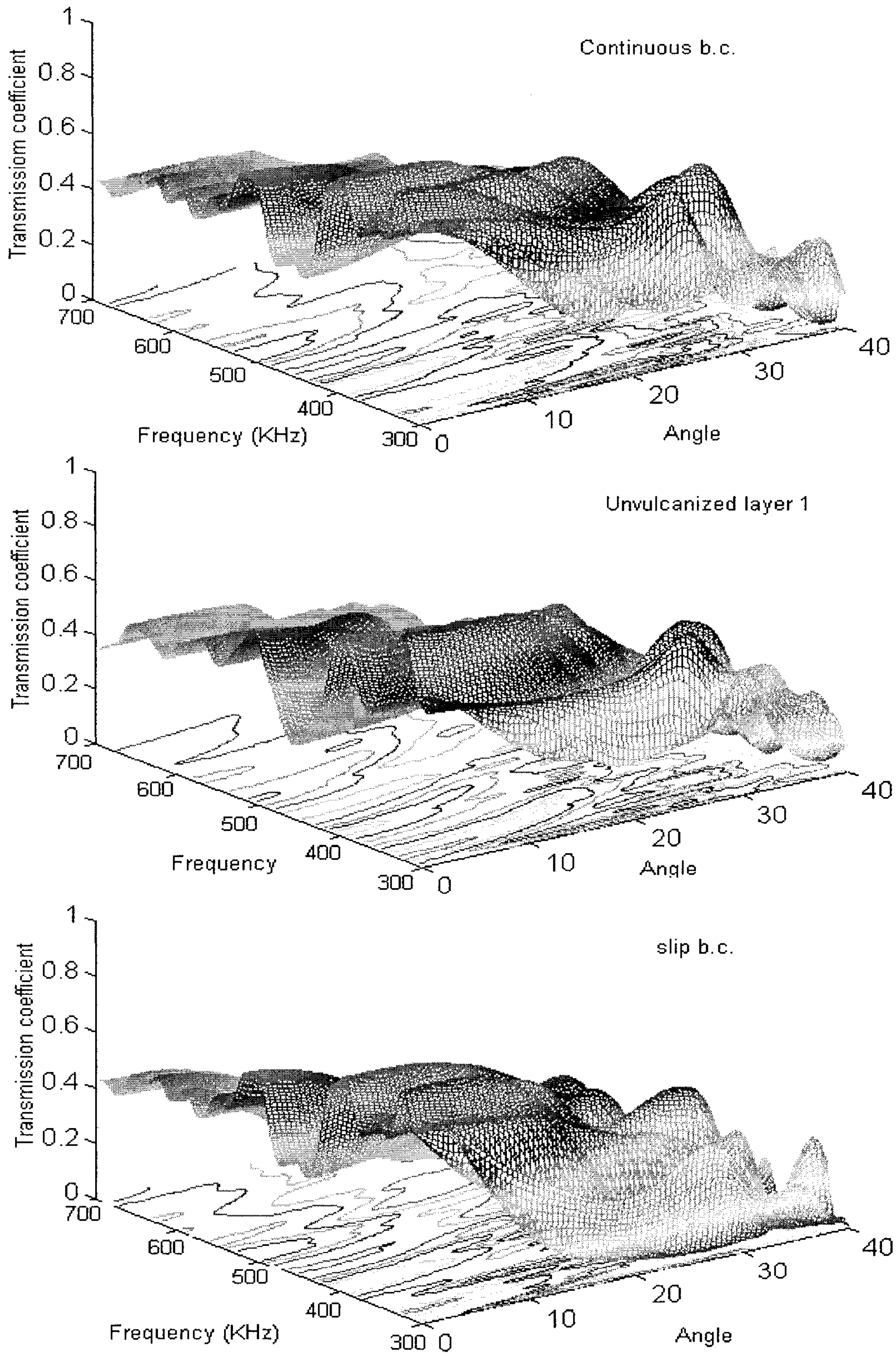

Figure 1.5 Transmission coefficients at different boundary conditions for isotropic materials

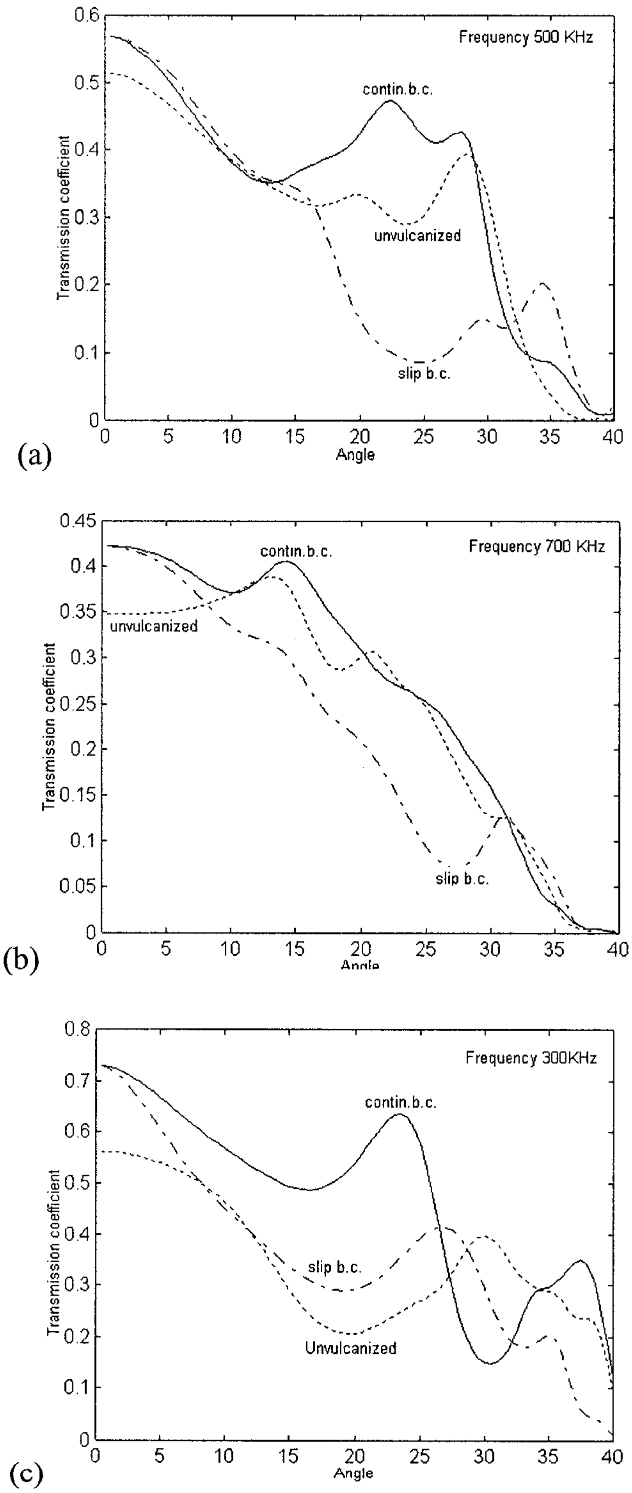

Figure 1.6 Transmission coefficients versus angles at different frequencies for isotropic materials

of the transmission in the region of 22^0 is explained by the effects, which are similar to a quarter wave transmission in a single layer. However, it is difficult to estimate the influence on the transmission coefficient of the individual layers. Therefore, the expression of the total transmission is derived to explain the effect. The total transmission is the case for which the transmission coefficient is equal to one, when attenuation is neglected. In other words, the wave completely passes through a multiple layers. In a real material, the transmission coefficient will reach a maximum at the same frequency when the attenuation is considered for a visco-elastic multilayered structure. From equation (1.34a), the transmission coefficient with respect to energy is expressed as:

$$T = |W|^2 = \frac{4\omega^2 Z^2{}_1}{\left(M_{32} - \omega^2 Z_1^2 M_{23}\right)^2 + \left(\omega Z_1 \left(M_{33} + M_{22}\right)\right)^2} \tag{1.63}$$

the condition of the total transmission is:

$$\min\left(\left(\frac{M_{32}}{\omega Z_1} - \omega Z_1 M_{23}\right)^2 + \left(M_{33} + M_{22}\right)^2\right) \tag{1.64}$$

from expression (1.64), the incident angle which produces the total transmission can be obtained for a particular multi-layer structure. When the multi-layer structure is considered as an elastic material, the transmission coefficient equals to one. It will reach the maximum at the incident angle found from expression (1.64). The numerical solutions shown in Figure 1.6 show peaks, which are of the expected total transmissions for a visco-elastic multi-layer at a range of different frequencies.

1.5 References

Ainslie, M. A., 1995, 'Plane-wave reflection and transmission coefficient for a three layered elastic media', J. Acoust. Soc. Am., 97(2), 954-961.

Aristegui, C. and Baste, S., 1997, ' Optimal Recovery Of The Elasticity Tensor Of General Anisotropic Materials From Ultrasonic Velocity Data', J. Acoust. Soc. Am. 101(2), 813-833.

Barnard, G. R., Bardin, J. L. and Whiteley, J. W., 1975, 'Acoustic Reflection and Transmission Characteristics For Thin Plates', J. Acoust. Soc. Am. 57(3), 577-584.

Brekhovkikh, L. M., 1960, *Waves In Layered Media,* Academic Press, New York.

Brekhovkikh, L. M., 1980, *Waves In Layered Media,* 2nd. Ed, Academic Press, New York.

Brekhovskikh, L. M. And. Godin, O.A, 1990, *Acoustics Of Layered Media I*, Springer-Verlag, New York.

Cervenka, Pierre and Challande, Pascal, 1991, ' A New Efficient Algorithm To Compute The Exact Reflection and Transmission Factors For Plane Waves In Layered Absorbing Media (Liquid and Solid)', J. Acoust. Soc. Am, 89(4), Pt.1, 1579-1589.

Cheng, A and Achenbach, J. D. 1996, 'Self-Compensating Technique For The Characterization Of A Layered Structure', Review Of Progress In Quantitative Evaluation, 16, 1815-1822.

Cheng, A, 1997, ' Material Parameter Determination From Time- Domain Signals Transmitted and Reflected By A Layered Structure', Review Of Progress In Quantitative Evaluation, 17.

Claeys, J. M. and Leroy, O., 1982, ' Reflection and Transmission Of Bounded Sound Beams On Half-Space and Through Plates', J. Acoust. Soc. Am. 72(2), 585-590.

Cooper, Henry F. Jr., 1967, 'Reflection and Transmission Of Oblique Plane Waves At A Plane Interface Between Viscoelastic Media', J. Acoust. Soc. Am. 42(5), 1064-1069.

Dayal, Vinay, 1992, 'An Automated Simultaneous Measurement Of Thickness and Wave Velocity By Ultrasound', Experimental Mechanics, 197-202.

Downs, J. III, P. Zhang, and M. L. Peterson, 1999, 'A High-Speed, High-Resolution Ultrasonic Tire Inspection Machine', IEEE/ASME Transactions on Mechatronics to appear, Vol. 3.

Dunkin, J. W., 1965, 'Computation Of Model Solutions In Layered, Elastic Media At High Frequencies', Bull. Seism. Soc. Am. 55, 335- 358.

Ewing, W. M. and Jardetzky, W. S., 1957, *Elastic Waves In Layered Media*, McGraw-Hill, New York.

Folds, D. L. and Loggins, C. D., 1977, 'Transmission and Reflection Of Ultrasonic Waves In Layered Media'. J. Acoust. Soc. Am. 62, 1102-1109.

Hanneman, S. E. and Kinra, V. K., 1992, ' A New Technique For Ultrasonic Nondestructive Evaluation Of Adhesive Joints: Part I Theory', Experimental Mechanics, 32(4), 323-39.

Hanneman, S. E. and Kinra, V. K., 1992, ' A New Technique For Ultrasonic Nondestructive Evaluation Of Adhesive Joints: Part II ', Experimental Mechanics, 32(4), 332-39.

Haskell, N. A., 1953, 'The Dispersion Of Surface Wave On Multilayered Media', Bull. Seism. Soc. Am. 43, 17-34.

Hsiu, D. K. and Patton, T. C., 1993, 'Development of Ultrasonic Inspection for Adhesive Bonds in Aging Aircraft,' Materials Evaluation, Vol. 15, No. 12.

Kantimathi and Sam, Fatigue Concepts Aging Aircraft Course, (916) 933-3360.

Kinra, V. K., Wang, Y. Zhu, C. and Rawal S. P., 1995, ' Simultaneous Reconstruction Of The Acoustic Properties Of A Layered Medium: The Inverse Problem', Review Of Progress In Quantitative Nondestructive Evaluation, 14, 1433-1440.

Kinra, V. K., Jaminet, P. and Zhu, C. and Iyer, V., 1994, ' Ultrasonic Nondestructive Evaluation Of A Three-Layered Medium', Material Evaluation, 52(8), 948-953.

Kinra, V. K., Jaminet, P. T., Zhu, C. and Iyer, V. R., 1994, ' Simultaneous Measurement Of The Acoustical Properties Thin Layered Medium: The Inverse Problem', J. Acoust. Soc. Am., 95(6), 3059-74.

Kinra, V. K. and Zhu, C., 1993, 'Time-Domain Ultrasonic NDE Of The Wave Velocity Of A Sub- Half-Wavelength Elastic Layer', The America Society Of Testing and Materials, 21(1), 29-35.

Kinra, V. K. and Dayal, V., 1988, ' A New Technique For Ultrasonic-Nondestructive Evaluation Of Thin Specimens', Experimental Mechanics, 28(3), 288-297.

Kinra, V. K, Petraitis, M. S. and Datta, S. K., 1980, ' Ultrasonic Wave Propagation In A Random Particulate Composite', Int. J. Solids Struct. 16, 301-312.

Kolsky, H., 1953, *Stress Waves In Solids*, Oxford, Larendon Press.

Kolsky, H., 1958, 'The propagation of stress waves in viscoelastic solids', Applied Mechanics Reviews, 465-468.

Krautkramer, J. and Krautkramer, H., 1977, *Ultrasonic Testing of Materials*, Springer-Verlag, New York.

Levesque, Daniel and Piche, Luc, 1992, 'A Robust Transfer Matrix Formulation For The Ultrasonic Response Of Multilayered Absorbing Media', J. Acoust. Soc. Am. 92(1), 452-467.

Ngoc, T. D. K. and Mayer, W. G., 1980, 'Numerical Integration Method For Reflected Beam Profiles Near Rayleigh Angle', J. Acoust. Soc. Am. 67(4), 1149-1152.

Nichols, Rudolph H., 1973, 'Acoustic Properties Of Rho-C Rubber and ABS In The Frequency Range 100khz-2 MHz', J. Acoust. Soc. Am. 54(6), 1763-1768.

Nolle, A. W. and Mowry, S. C., 1948, 'Measurment Of Ultrasonic Bulk-Wave Propagation In High Polymers', J. Acoust. Soc. Am. 20(4), 432-439.

Nolle, A. W. and Sieck, P.W., 1952, ' Longitudinal and Transverse Waves In A Synthetic Rubber', J. Appl. Phys. 23(8), 888-894.

Papadakis, E. P. Patton, T. Tsai, Y.M. Thompson, D. O. and Thompson R. B., 1991, 'The Elastic Moduli Of A Thick Composite As Measured By Ultrasonic Bulk Wave Pulse Velocity', J. Acoust. Soc. Am. 89, 2753-2757.

Shaw, R. P. and Bugl, P., 1968, 'Transmission Of Plane Waves Through Layered Linear Visco-elastic Media', J. Acoust. Soc. Am. 46(3), 649-654.

Snowdon, J. C., 1963, 'Representation Of The Mechanical Damping Possessed By Rubber Materials and Structures', J. Acoust. Soc. Am. 35(6), 821-829.

Snowdon, J. C. 1968, *Vibration Shock In Damped Mechanical Systems*, J. Wiley, New York.

Spies, M., 1994, 'Elastic Waves In Homogeneous and Layered Transversely Isotropic Media', J. Acoust. Soc. Am. 95(4), 1748-1760.

Taylor, Timothy W. and Nayfeh, Adnan H., 1996, 'Damping Characteristics Of Thick Rectangular Laminates', J. Acoust. Soc. Am.100 (3).

Thomson, William T., 1949, 'Transmission Of Elastic Waves Through A Stratified Solid Medium', J. Appl. Phys. 21, 89-93.

Ting, T. C. T., 1996, *Anisotropic Elasticity*, Oxford University Press, New York.

Tschoegl, Nichols W. 1989, *The Phenomenological Theory Of Linear Viscoelastic Behavior,* Springer-Verlag, New York.

Ursin, B., 1983, 'Review Of Elastic and Electromagnetic Wave Propagation In Horizontally Layered Media', Geophysics, 48(8), 1063-1081.

Ursin, B. and Berteussen, 1986, 'Comparison Of Some Inverse Methods For Wave Propagation In Layered Media', Proceedings Of The IEEE, 74(3) 389-400.

Zhang, P. and Peterson, M. L., 1998, 'Transmission coefficient for multi-layered structures at arbitrary incident angle', v18, Review of Progress in Quantitative Evaluation

Chapter 2

Automatic Gain Correction for Reduced Axis Scanning for Elastic Composite Materials

2.1 Motivation

More widespread adoption of in-process and in-service inspection is dependent on reduction in cost and an increase in inspection reliability. Automation of the inspection process is a key to meeting the required reliability needs and can make inspection a viable alternative for cost sensitive applications. Manual inspection is typically too costly except in critical applications. However, in those applications where cost is less of an issue, reliability of manual inspections is more of a concern. As a result automatic inspection is increasingly becoming the norm in both critical and non-critical applications. Fortunately many NDE processes lend themselves well to automation. In particular, ultrasonic inspection can often be performed for large parts at a reasonable cost using an automatic scanning apparatus.

A number of applications exist in which this situation arises. Reduced axis ultrasonic scanning of tire casings is one example where the use of a simpler scanning system has made the scanning system sufficiently simple that a cost-effective system has been produced [Downs et. al. 1999]. Additional examples of such systems are scanning aircraft structures using open-architecture robotic crawlers as platforms with NDT boards and sensors [Bar-Cohen and Backes, 1999].

One of the challenges facing automatic scanning systems is that in many cases the part geometry may not be known precisely. In other applications the geometry may be sufficiently complex that it requires a scanning system with a large number of degrees of freedom to follow the part contours during the inspection process. For ultrasonic inspection of an obliquely incident wave, refraction of the wave front occurs across the interface between the coupling fluid and the part. However, in cases where the acoustic impedance of the coupling fluid and the part is closely matched, refraction of the wave is low. With closely matched acoustic impedance, relatively complex parts may be scanned without precisely following the part contours. It is possible in those cases to scan a complex part and to be less exact in following the profile. Alternatively, a reduced number of degrees of freedom may be used in the scanning system. Thus a close acoustic impedance match between the part and the coupling fluid can make reduced axis scanning possible for higher efficiency and lower cost. The reduction in the number of degrees of freedom in scanning system can also result in a more reliable scanning system. The use of non-normal incidence scanning is not widespread, however. The approach has become more attractive as significant computational resources have become available at reasonable cost while the cost of scanning hardware has remained high. While reasonable ultrasonic signal amplitude may be obtained when scanning a part using this approach, the refraction and attenuation of the wave in the material may be sufficiently high that amplitude correction of the received signal may be required.

Thus an analytical method or efficient numerical model is needed which can be used to correct the received signal to account for refraction and loss of amplitude which occurs in the part. Without such a correction it is possible to have both false positives and false negatives (detecting a flaw when none exists) depending on the part curvature. In a number of parts such as composites, the component may be modeled as a layered material.

Matrix propagator methods are attractive for the creation of a model that will allow the effect of amplitude variation on the received signal to be corrected for the non-normal wave incidence. The magnitude of the received signal can be adjusted so that it is consistent regardless of the angle of incidence. This approach is well established in the literature [Nayfeh, A. H., 1995], and the interest here is in the application of this technique to a part with a complex curvature that can be inspected in a reduced axis scanning system. Because this is normally a single frequency calculation, the results are often given in terms of the transmission coefficient versus angle for a single frequency. This is a reasonable curve from a theoretical perspective, however for experimental applications, single frequency excitation is rarely used. The standard method of ultrasonic imaging is to extract the peak value from the transmitted signal using an analog circuit [Krautkramer and Krautkramer, 1990]. As a result the curve of interest is the peak of a broadband transmitted signal versus angle. This type of result is much less general being dependent on the particular transducer used for the problem. However, the curve actually indicates the type of signal that is seen in practice. This curve is then directly comparable to the experimental data.

2.2 Theoretical formulation

Automatic gain correction is intended for the calculation of transmission coefficients of orthotropic layered materials at arbitrary incident angles. By necessity though, lower effective material symmetries result when the orthotropic case is considered for angles of incidence that do not correspond to material symmetry axes. Thus, the formulation will consider more general material symmetry in order to treat the orthotropic case for a general angle of incidence. The transfer matrix method is then applied to the calculation of transmission coefficients for use in the automatic gain correction algorithm. The visco-elastic characteristic of the composites are neglected in this chapter since the primary focus of the work is on the variation in the transmission coefficient relative to location in the material. Material attenuation due to a visco-elasticity of matrix material property will be discussed in chapter 3.

2.2.1 Elastic composite material layer immersed in water

In the matrix transfer method, the general solution equations and boundary conditions are expressed in a simplified matrix form and the transmission coefficients are obtained by matrix operations [Brekhovskikh and Godin, 1990, Nayfeh, 1995]. Generally, the solutions are derived from the equations of motion, the constitutive relations and the strain-displacement relations. The general form of calculated matrix is expressed in terms of stresses and displacements, as a 6^{th} order matrix, in which propagation of three coupled waves, two shear waves and one longitudinal wave, are considered.

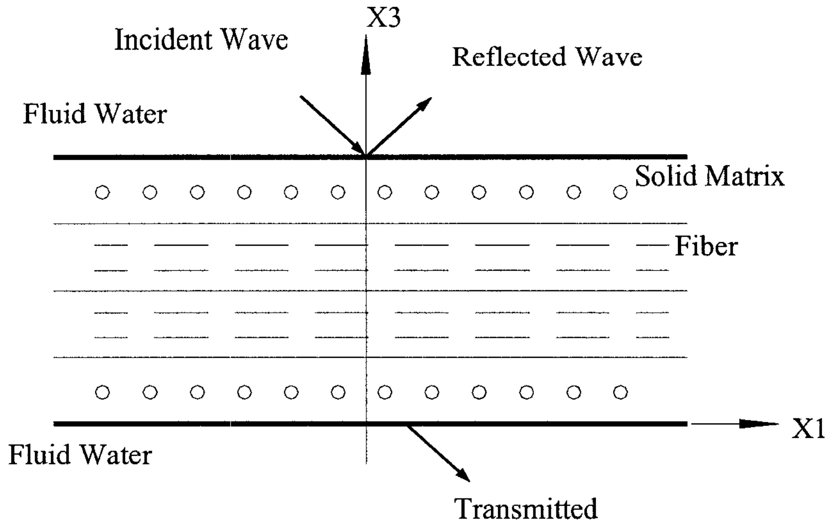

Figure 2.1 A laminated composite plate immersed in water

A composite plate shown in Figure 2.1 is a 4-ply orthotropic structure, for example, the plate could be an epoxy matrix material with carbon fiber, immersed in water. The transmission coefficients are calculated based on two different physical situations: the orthotropic case and the monoclinic case. When an incident beam plane is in a principal material axis for the laminate, a horizontally polarized shear wave SH wave propagating in the $x_1 - x_3$ plane at an arbitrary angle from the normal is uncoupled. The SH wave is independent of a vertical quasi-shear wave, SV, and a quasi-longitudinal wave, L. Only a vertically polarized quasi-shear wave and a quasi-longitudinal wave are produced in the orthotropic case because it is assumed that the incident wave is a longitudinal wave that propagates in the water. Thus, only the coupled vertically polarized shear wave and longitudinal wave need to be considered in the following section. Corresponding to orthotropic material and incident beam plane in fiber direction plane, the 6^{th} order transfer matrix degenerates into a 4^{th} order transfer matrix which includes 2 coupled waves. The transmission coefficient is derived based on Nayfeh and Chimenti [1989] and Nayfeh [1995]. The additional details are given in Appendix B.

$$T = \frac{2\rho_w v^2 \alpha_w}{(M_{11} + M_{22})\rho_w v^2 \alpha_w - (M_{21}\alpha_w^{\ 2} + M_{12}(\rho_w v^2)^2)} \tag{2.1}$$

where:

$$M_{11} = -A_{41}^{\ -1}\begin{vmatrix} A_{21} & A_{22} \\ A_{41} & A_{42} \end{vmatrix},\ M_{12} = -A_{41}^{\ -1}\begin{vmatrix} A_{21} & A_{23} \\ A_{41} & A_{43} \end{vmatrix} \tag{2.2}$$

$$M_{21} = -A_{41}^{\ -1}\begin{vmatrix} A_{31} & A_{32} \\ A_{41} & A_{42} \end{vmatrix},\ M_{22} = -A_{41}^{\ -1}\begin{vmatrix} A_{31} & A_{33} \\ A_{41} & A_{43} \end{vmatrix} \tag{2.3}$$

$[A]$ is the global transfer matrix, ρ_w is the water density, v is the phase velocity of the ultrasonic wave and α_w is the X_3-component of wave vector in water.

However, when the propagation vector of the incident beam deviates from the principal material axis direction, the axis of symmetry is changed. The propagation of the wave is more complicated and the orthotropic material symmetry becomes effectively a monoclinic material. The horizontally polarized quasi-shear wave (SH), the vertically polarized quasi-shear wave (SV) and the quasi-longitudinal wave (L) are all coupled. Then a 6th order matrix expression is used in the calculation of the transmission coefficient. The form of equation (2.1) remains the same, but, the coefficients M_{11}, M_{12}, M_{21}, M_{22} become 3rd order determinant with a complex dependence on the material properties in the general orientation of the composite. Based on the works of Nayfeh and Chimenti [1991], which are presented in monograph by Brekhovskikh and Godin

[1990] and Nayfeh [1995], the coefficients M_{11}, M_{12}, M_{21}, M_{22} may be derived and expressed in the following form (more details are shown in Appendix B):

$$M_{11} = |A|^{-1} \begin{vmatrix} A_{31} & A_{32} & A_{33} \\ A_{51} & A_{52} & A_{53} \\ A_{61} & A_{62} & A_{63} \end{vmatrix}, \; M_{12} = |A|^{-1} \begin{vmatrix} A_{31} & A_{32} & A_{34} \\ A_{51} & A_{52} & A_{54} \\ A_{61} & A_{62} & A_{64} \end{vmatrix} \tag{2.4}$$

$$M_{21} = |A|^{-1} \begin{vmatrix} A_{41} & A_{42} & A_{43} \\ A_{51} & A_{52} & A_{53} \\ A_{61} & A_{62} & A_{63} \end{vmatrix}, \; M_{22} = |A|^{-1} \begin{vmatrix} A_{41} & A_{42} & A_{44} \\ A_{51} & A_{52} & A_{54} \\ A_{61} & A_{62} & A_{64} \end{vmatrix} \tag{2.5}$$

$$|A| = \begin{vmatrix} A_{51} & A_{52} \\ A_{61} & A_{62} \end{vmatrix}$$

2.2.2 Implementation

Since the program is intended to serve as a correction for a reduced axis scanning system, near real-time computation is required. Alternatively a data table style look up function would be is required for each configuration. Figure 2.2 shows a flow chart for the calculation of transmission coefficient programmed in C++. The program as currently implemented runs on a UNIX workstation as a complex, double precision program in ANSI C++. The program runs in less than 3 minutes to find 100 points. The computational throughput on the machine is roughly equivalent to a typical personal computer, which would allow the program to be run on a personal computer in a sufficiently small amount of time to allow on-the-fly correction of the signal amplitude.

The inputs to the model are the angle of incidence of the signal and the material properties of an undamaged layer of the material. For the example problem described below, the required material properties are for individual layers of carbon fiber epoxy.

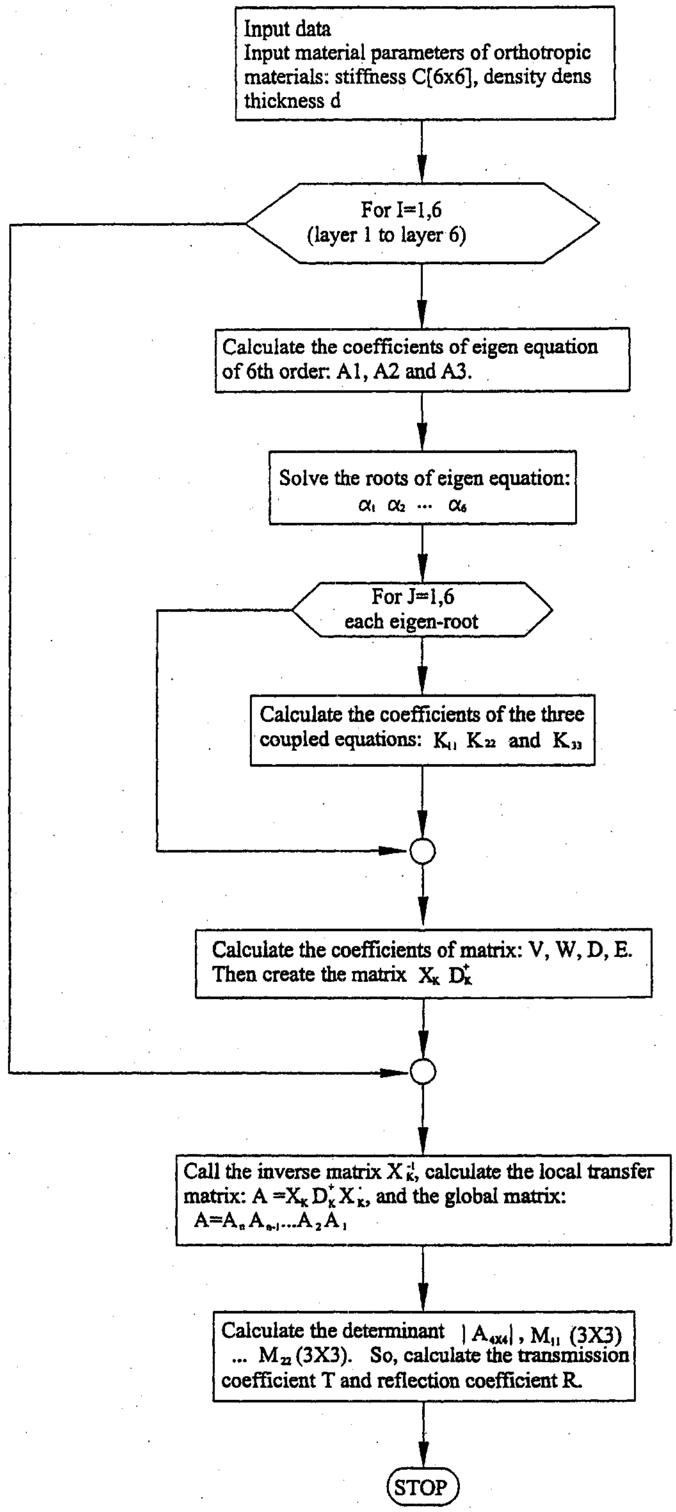

Figure 2.2 Flow chart for the calculation of transmission coefficients through a multi-layered solid

The single layer properties are then assembled into the laminate within the program. The moduli used in the calculations are shown in Table 2.1. Poisson's ratio ν_{12} and Poisson's ratio ν_{13} are 0.340 and 0.502, respectively. The tensor material properties shown in Table 2.2 are calculated from the engineering constants [Bodig and Jayne, 1993]. Nine-independent elastic stiffness material parameters are required to describe the orthotropic materials.

In addition to the elastic property data, the input data for the calculations includes material density, fiber lay-up direction angles and the thickness of each of the lamina. Three carbon fiber/epoxy composite plates are used as samples with different lay-up sequences. The lamina properties used in all cases are the same with 4 plies. The lay-up sequences are $[0]_{4T}$, $[0, 90]_s$ and $[90, 0]_s$, where the subscript T indicates that all layers are described notationally and a subscript of S indicates a symmetric lay-up with only half of the layers shown. Thus all 3 samples consist of 4 total layers. The density of the material used is 1.5 g/cm^3.

2.2.3 Theoretical results for orthotropic layered samples

Based on the formulation described, the newly developed program is used to perform the calculations for each of the different cases. To verify the program, a comparison to previous results is made [Chimenti and Nayfeh, 1990]. The calculated results are very close with at least some of the difference caused by the manual digitizing of points from the paper. The remainder of the difference appears to be scaling that appears to place the calculations performed in this work closer to the experiments reported by Cimenti and Nayfeh (see Appendix F). The transmission coefficient is

Table 2.1 Young's moduli and shear moduli for each layer of carbon fiber epoxy materials

E_1 (Gpa)	E_2 (GPa)	E_3 (GPa)	G_{12} (GPa)	G_{13} (GPa)	G_{23} (GPa)
137.3	8.4	8.4	4.36	4.36	2.27

Table 2.2 Elastic constants [C] (GPa) and density (kg/m^3) for each layer of carbon fiber epoxy materials

C_{ij}	1	2	3	4	5	6
1	141.3	5.90	5.90	0.	0.	0.
2	5.90	11.47	5.88	0.	0.	0.
3	5.90	5.88	11.47	0.	0.	0.
4	0.	0.	0.	2.27	0.	0.
5	0.	0.	0.	0.	4.36	0.
6	0.	0.	0.	0.	0.	4.36
Density ρ		1500.				

calculated as a function of frequency and incident angle for all three samples. The sensitivity of the transmission coefficient to the incident angle and frequency is particularly important to determine the inspection accuracy.

Figure 2.3 shows the reflection coefficients versus frequency curves that are compared to previous work by Nayfeh and Chimenti [1989]. The figures show the reflection coefficient for the $[0_2, 90_2]_s$ laminate with an incident angle of 16 degree and with the fiber direction of the uppermost ply in the incident plane, and perpendicular to the incident plane. Further details of material properties are given by Chimenti and Nayfeh [1990]. The figure shows reasonable agreement with the implementation in the application.

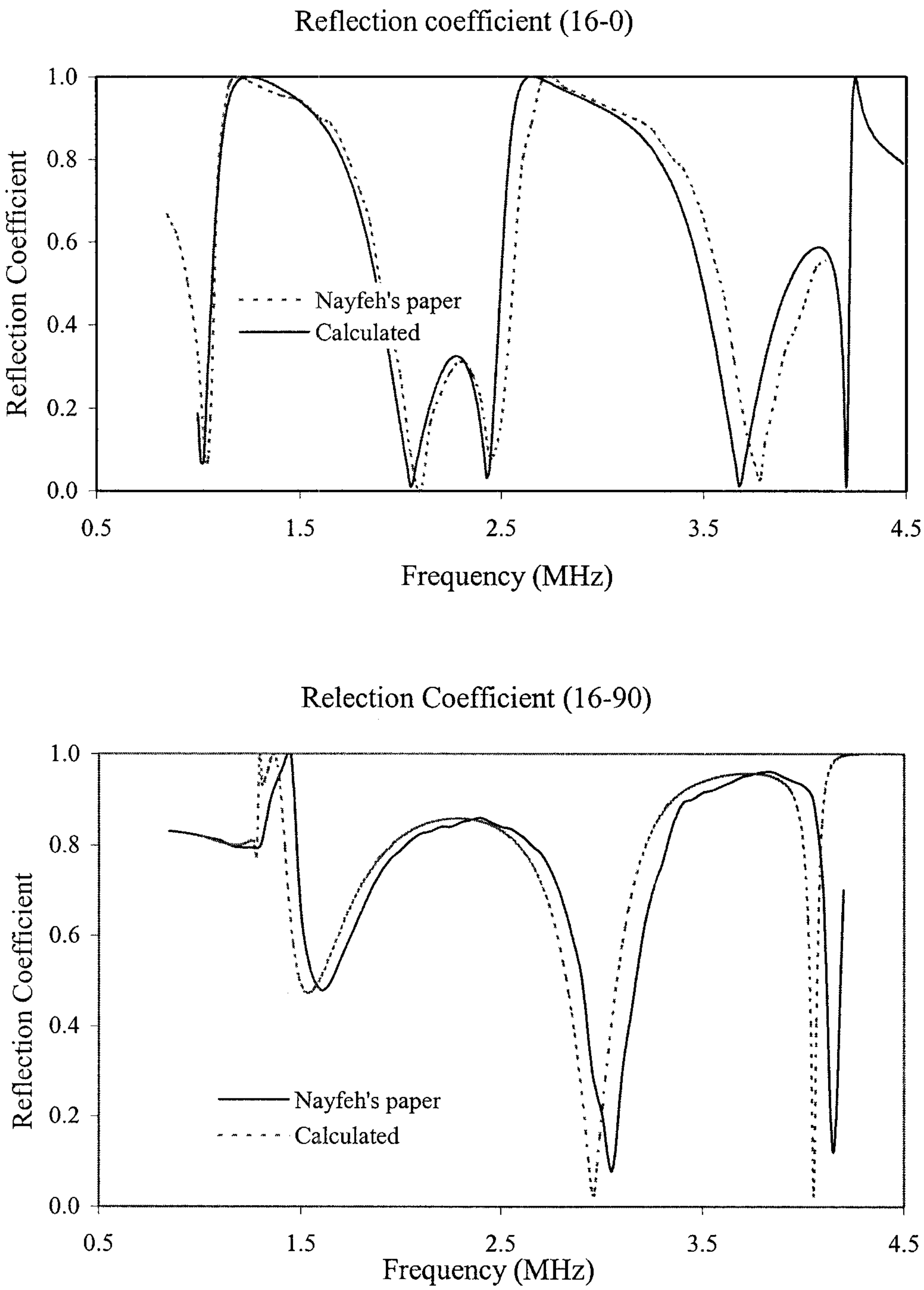

Figure 2.3 Comparison of calculated results to previous paper (reference Chimenti and Nayfeh, 1990)

Figures 2.4, 2.5 and 2.6 show the dependence of the transmission coefficient on frequency for the three different lay-up sequences considered in this work. These figures show the dependence of the transmission coefficient on not only the orientation of the lamina, but also on the angle of incidence of the ultrasonic wave for the three example cases. The ranges of frequencies shown in the calculations are selected to match the usable bandwidth of the 2.25 MHz transducer which is used in the experimental portion of the work. The thicknesses of each lamina in these cases for lay-up sequences of $[0]_{4T}$, $[0,90]_s$, $[90,0]_s$ were based on measurement and found to be 0.127mm, 0.130 mm, 0.159 mm, respectively, which are consistent with the nominal thickness of the lamina used in the experimental results below. The laminae are assumed to have the same thickness in each sample

2.3 Experiments

2.3.1 Experimental setup

The experimental set-up is configured as shown in Figure 2.7. The experimental equipment includes an ultrasonic pulser-receiver, a digitizing oscilloscope, two piezoelectric transducers, a motion control system and a personal computer. The system is configured so that the angle of the sample between the two transducers can be adjusted precisely using optical positioners. The digital signal is acquired at a range of angles both through the sample and without the sample as a reference signal that is transmitted through water.

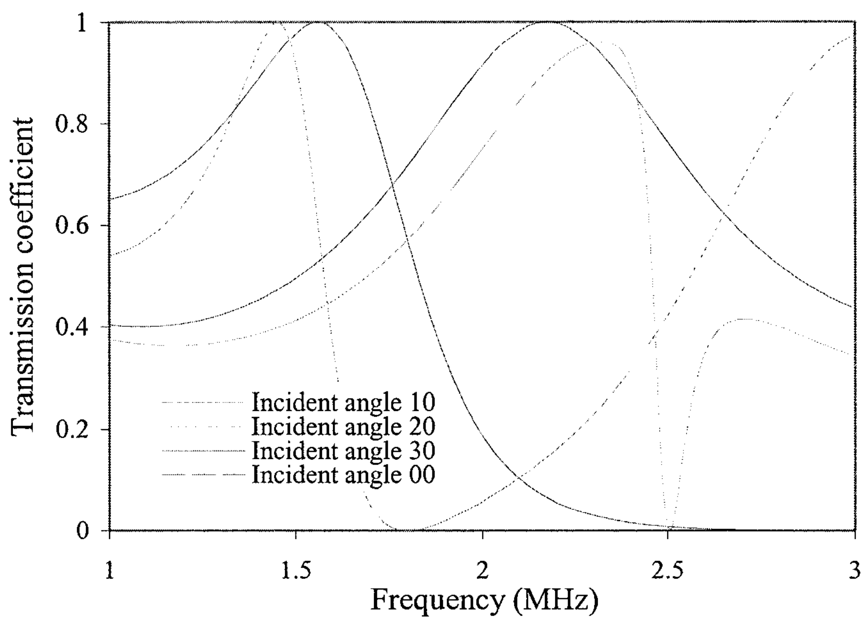

Figure 2.4 Calculated curves of transmission coefficient versus frequency for the carbon fiber composite of $[0, 90]_s$ lay up, at different incident angles

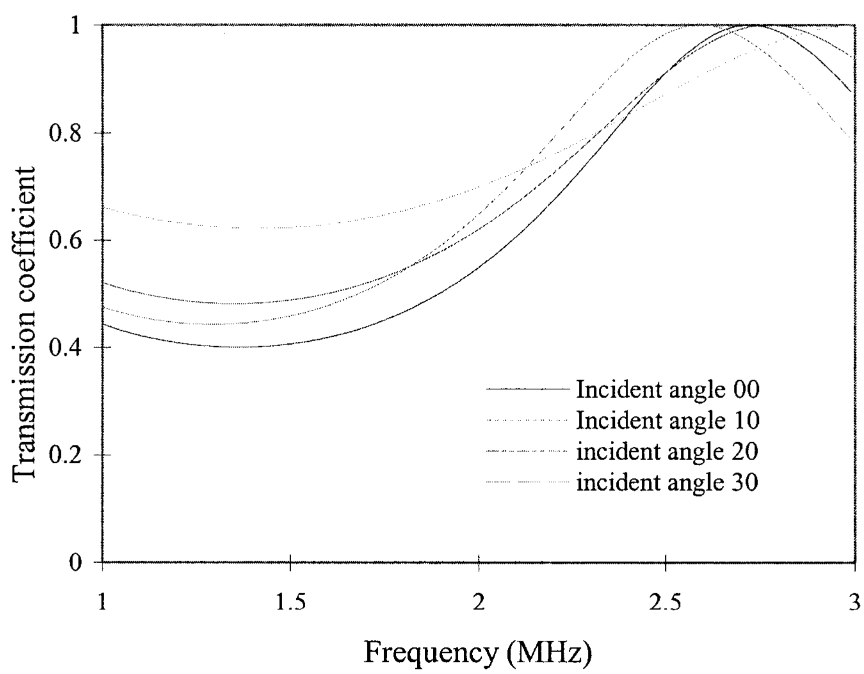

Figure 2.5 Calculated curves of transmission coefficient versus frequency for the carbon fiber composite of $[0]_{4T}$ lay up, at different incident angles

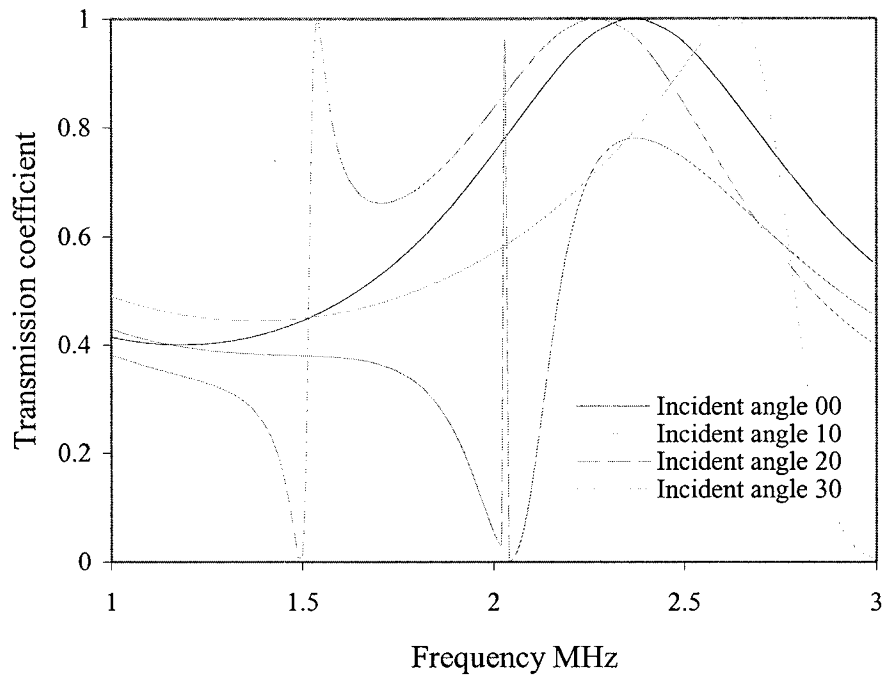

Figure 2.6 Calculated curves of transmission coefficient versus frequency for the carbon fiber composite of $[90, 0]_s$ lay up at different incident angles

All of the experiments were carried out in this water immersion apparatus using the through-transmission configuration. The matched pair of piezoelectric transducers used have a nominal center frequency of 2.25 MHz. A focussed transmitter and a flat receiver with a 12 mm element diameter were used. The useable bandwidth of the transducers was chosen to be the frequency ranges over which the magnitude of the spectrum was greater than 75 percent of the peak value. The transducers were excited using a short duration pulse from the pulser-receiver (Panametrics, Waltham MA, 5052PR). The signal was oversampled, at 250 M samples/sec. using a digital storage oscilloscope (Tektronix TDS 520A) and the signal was transferred to a personal computer using a general purpose interface bus connection (GPIB).

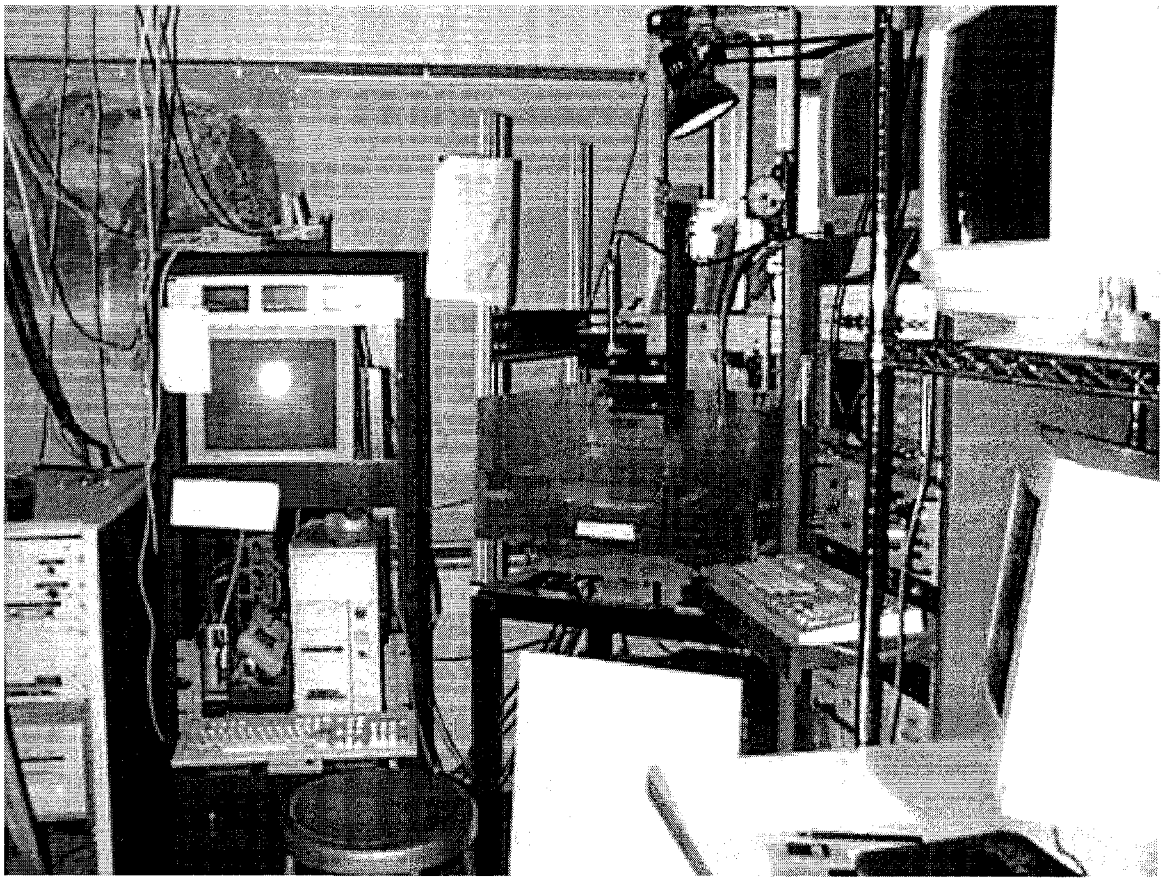

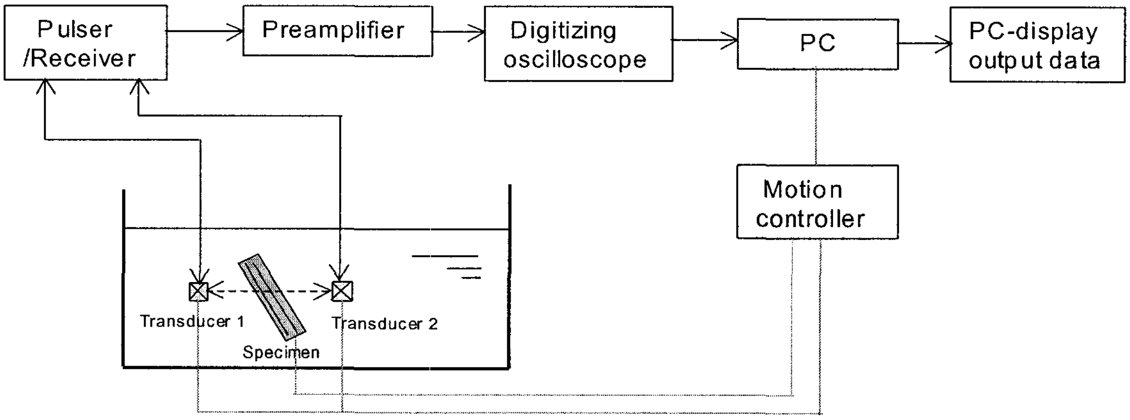

Figure 2.7 System configuration for the experimental data acquisition

Three composite plate samples of carbon fiber reinforced, epoxy matrix, were fabricated from fiber CYCOM 950-1 and T650-35 epoxy. The three samples all used the same matrix and fibers (CYCOM 950-1/T650-35). Measured sample thickness varies between the three samples slightly, with the thicknesses of the $[0]_{4T}$, $[0,90]_s$ and $[90,0]_s$ measured as 0.508 mm, 0.635 mm and 0.520 mm, respectively. The density of material was measured to be approximately 1.5 g/cm^3.

2.3.2 Results

2.3.2.1 Experimental records

Experiments were performed in the experimental apparatus shown in Figure 2.7 the samples were immersed in water and were fixed by the special apparatus. The samples were rotated at 5 degree increment, the transmission signals were recorded by a personal computer at 00, 05, 10, 15, 20, 25, 30 incident angles. The original signal records for the samples and water are shown in Figures 2.8, 2.9, 2.10.

2.3.2.2 Comparison of experimental and theoretical results in frequency domain

The Figures 2.11, 12 and 13 are comparisons between theoretical curves and experimental curves in a frequency domain. Theoretical results are calculated from the programs which follow the flow chart in Figure 2.2. Experimental data in the time domain in Figures 2.8, 2.9 and 2.10 were transferred into the experimental transmission amplitudes in the frequency domain by discrete Fourier transform. Theoretical transmission amplitudes were obtained by convolving the Fourier transforms of a signal passing through a water path without the sample with the theoretically calculated

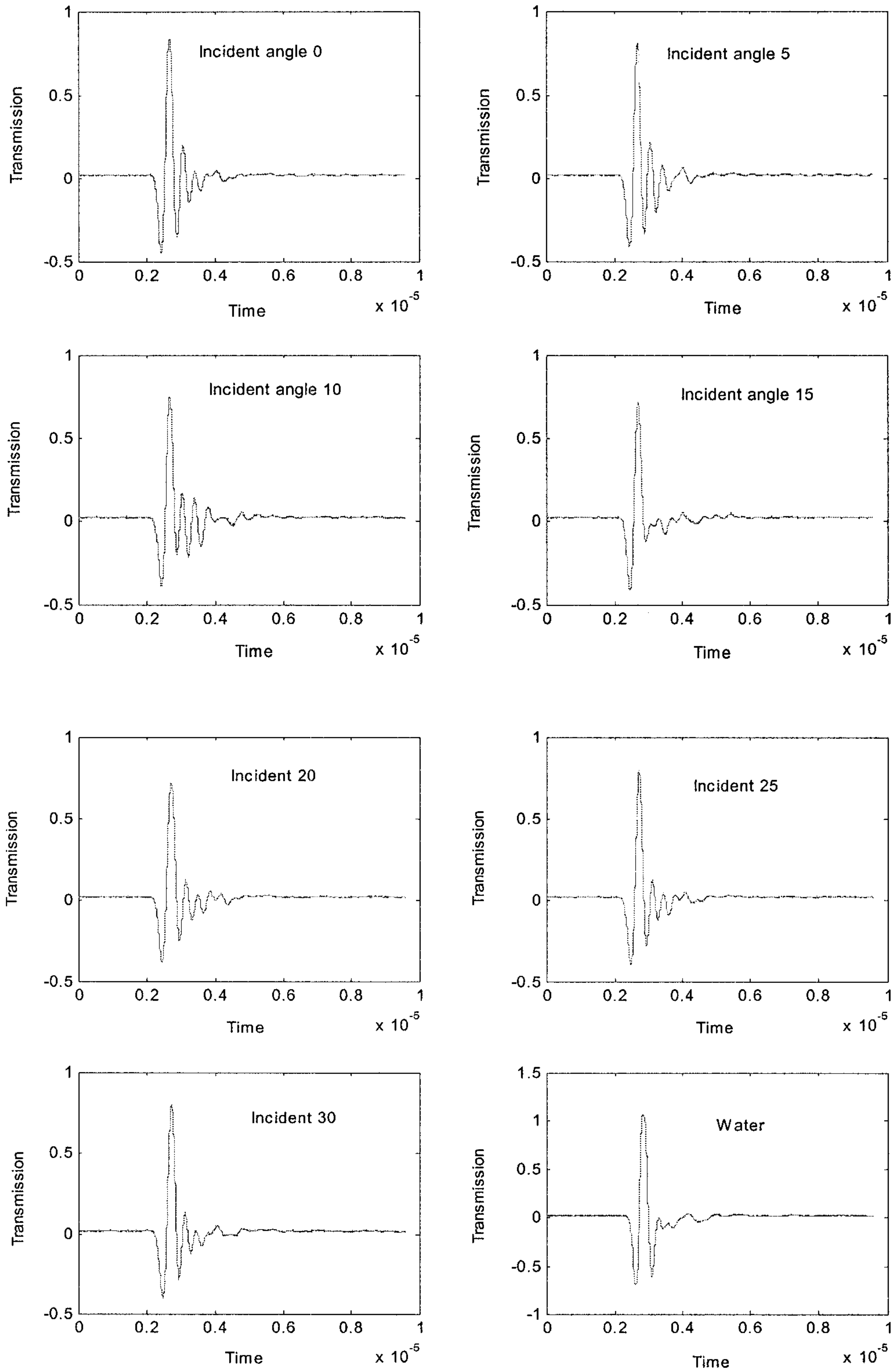

Figure 2.8 Experimental curves for carbon fiber/epoxy composite plate $[0,90]_S$ at different incident angles and reference water transmission signal

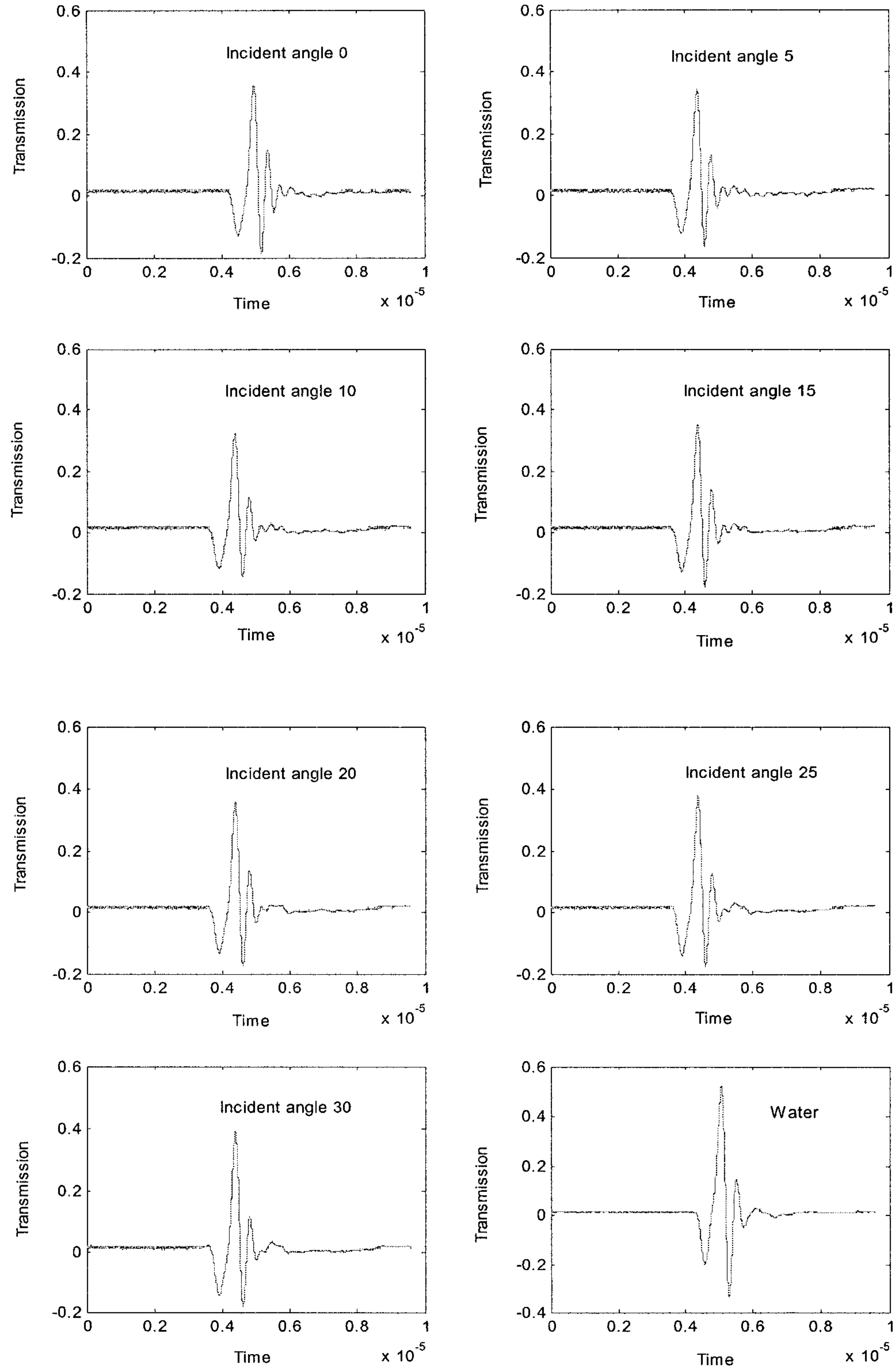

Figure 2.9 Experimental curves for carbon fiber/epoxy composite plate $[0]_{4T}$ at different incident angles and reference water transmission signal

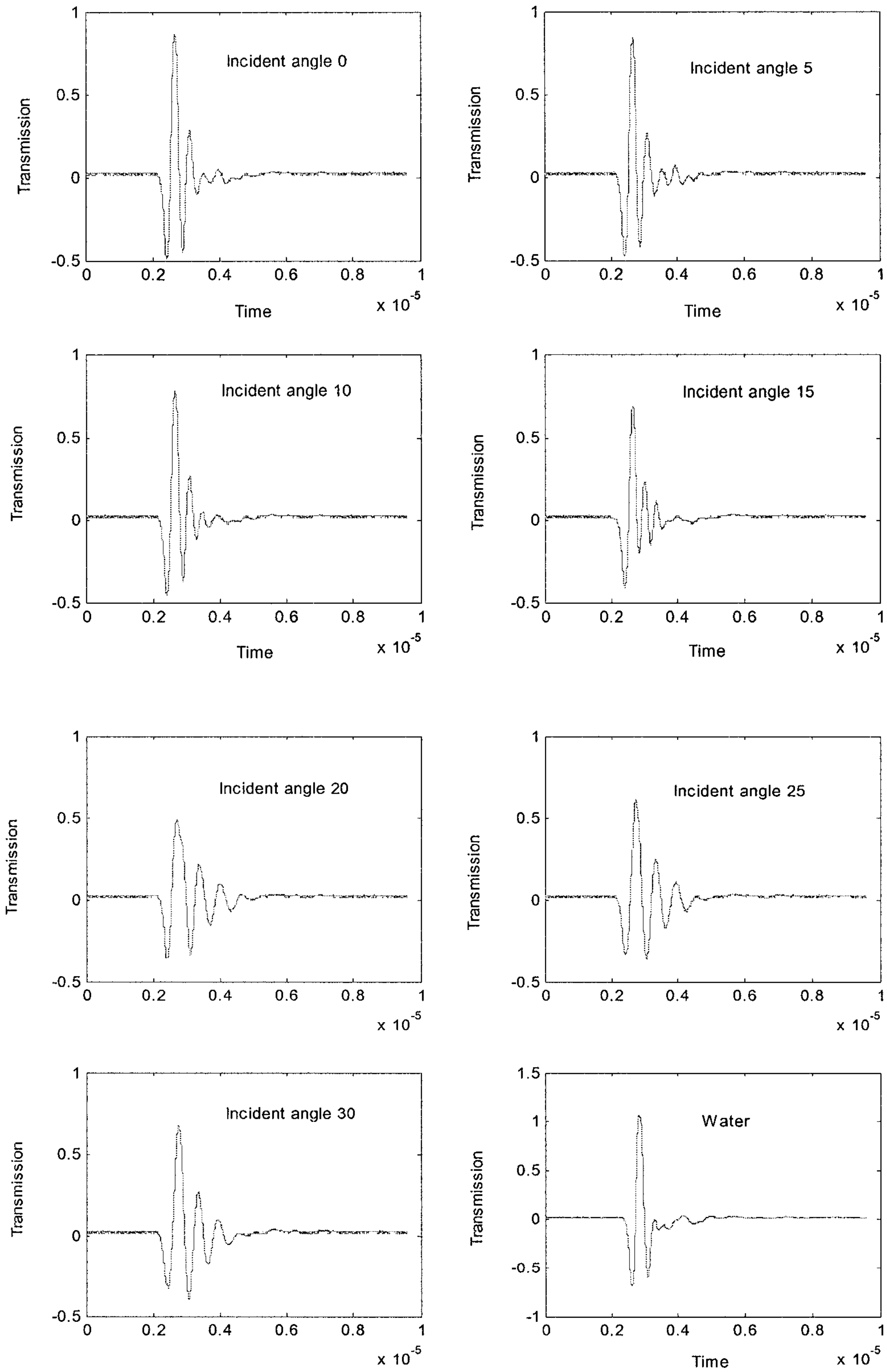

Figure 2.10 Experimental curves for carbon fiber/epoxy composite plate $[90,0]_S$ at different incident angles and reference water transmission signal

transmission coefficients. Their transmission amplitude formula is expressed as the following:

$$A(\omega) = T(\omega)W(\omega) \tag{2.6}$$

where $A(\omega)$ is the theoretical reconstructed transmission in the frequency domain, $T(\omega)$ is the theoretical transmission coefficient, $W(\omega)$ is the Fourier transform of transmitted signal through water path without sample.

The theoretical reconstructed transmission amplitude versus frequency is acquired with equation (2.6) at the different incident angles. The signal is computed at frequencies from 0 to 10 MHz. Experimental transmission amplitude is the discrete Fourier transfer of the experimental data in the range of 0-10 MHz in Figures 2.8, 2.9 and 2.10. The transmission amplitudes of theoretical and experimental results are very close in a range of angles in Figures 2.11, 12 and 13. It is evident that matrix transfer theory of multi-layered composite plate is applicable as a gain correction algorithm for reduced axis scanning. The real time gain correction algorithm for reduced axis scanning system will be discussed in the next section.

2.3.2.3 Comparison of experimental and reconstructed curves in time domain

Theoretical curves were obtained from equation (2.1) using a computer program. When the theoretical curves calculated from the program are convolved with a reference incident signal. The transmission coefficients for experimental incident wave profiles are obtained, the reference signal is acquired from the transmitted signal through water without sample, The transmitted signals in the time domain are reconstructed through the product of theoretical and transmitted coefficient in water path by taking inverse Fourier

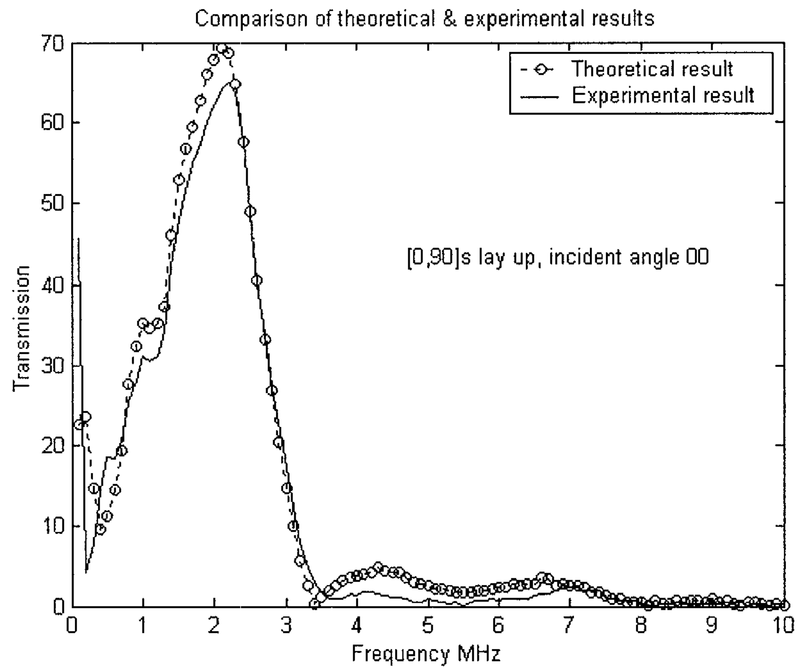

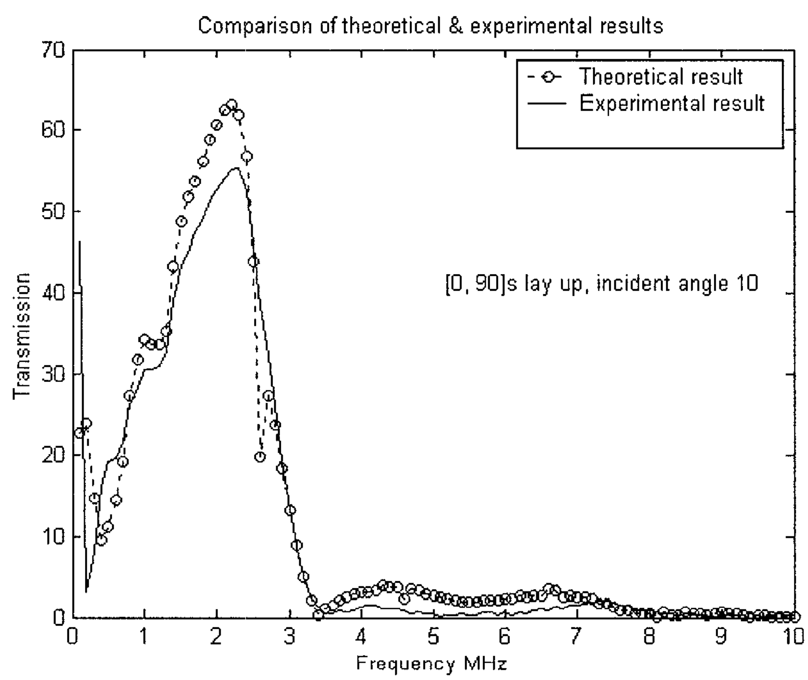

Figure 2.11a Comparison of theoretical and experimental spectral results of transmission amplitude versus frequency for $[0, 90]_S$ carbon fiber, at incident angles 0 and 10 degrees

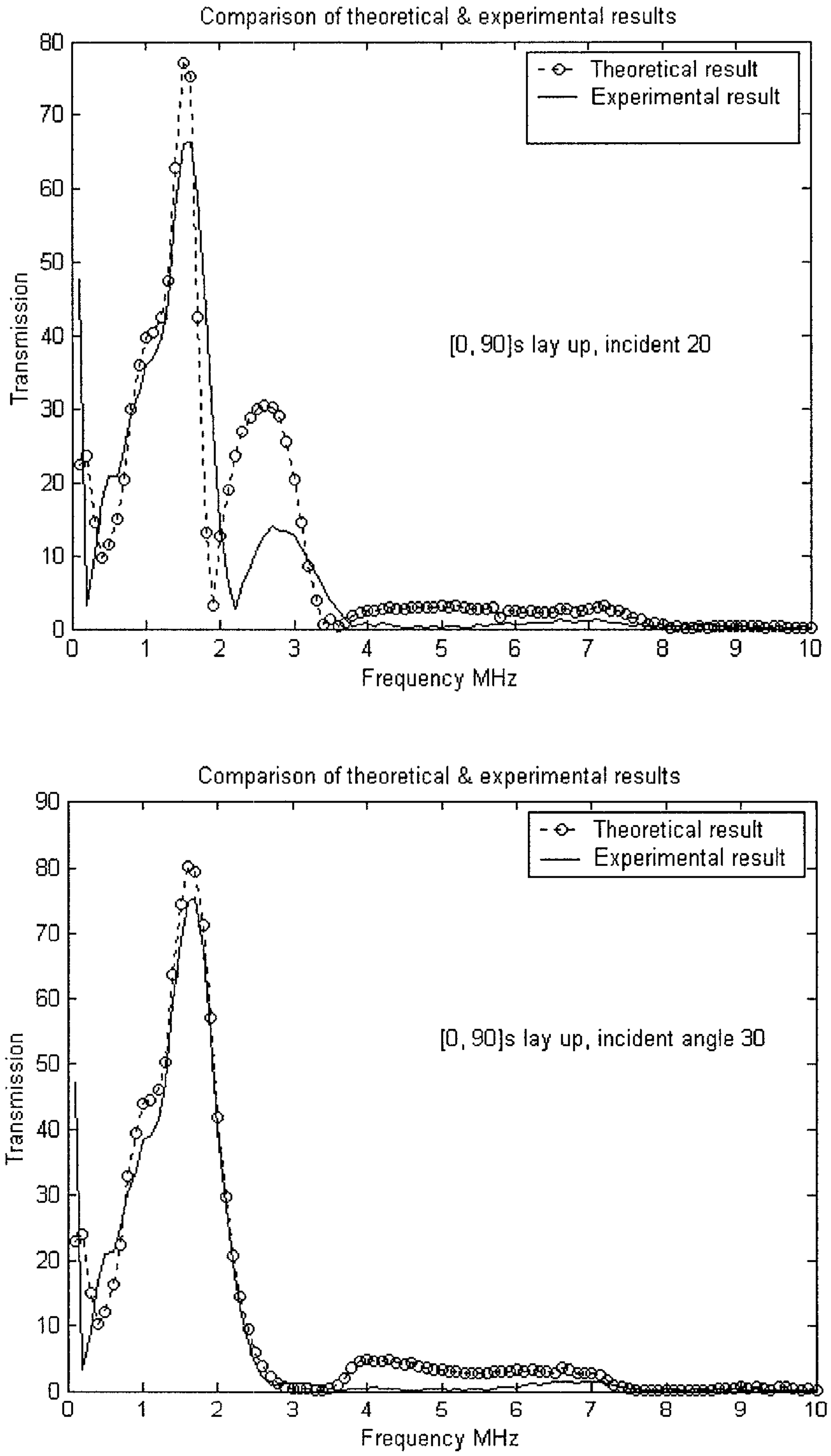

Figure 2.11b Comparison of theoretical and experimental spectral results of transmission amplitude versus frequency for $[0, 90]_S$ carbon fiber, at incident angles 20 and 30 degrees

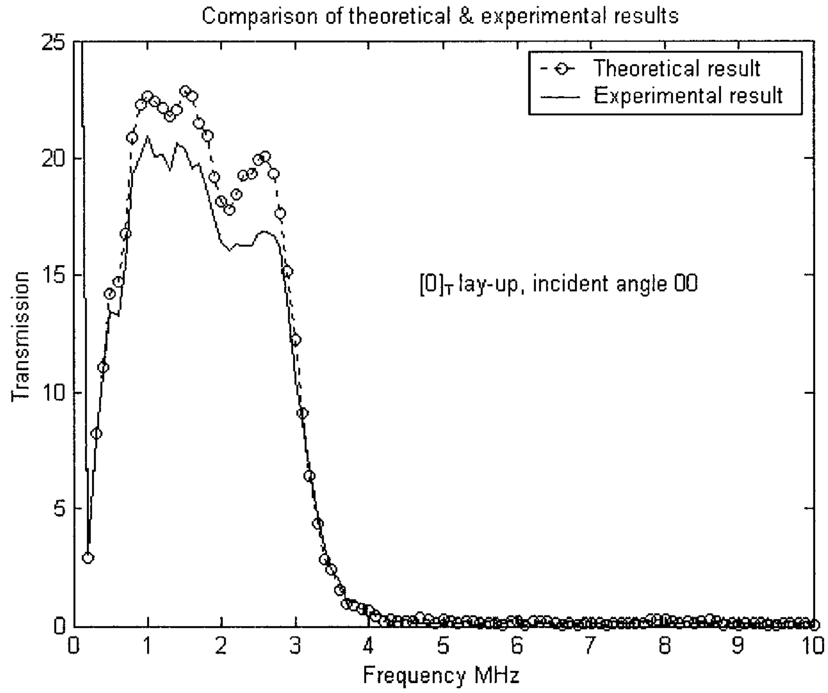

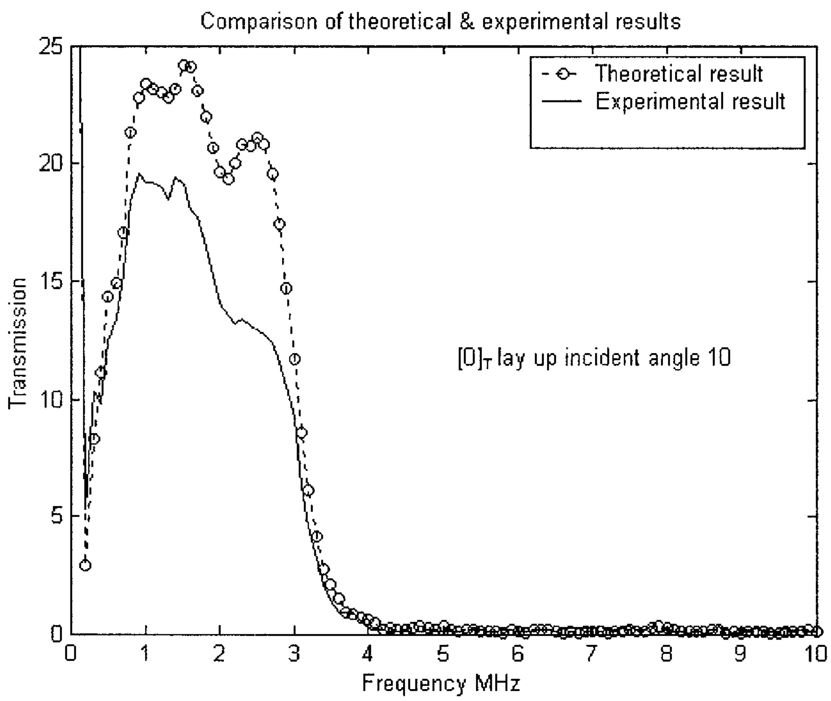

Figure 2.12a Comparison of theoretical and experimental spectral results of transmission amplitude versus frequency for $[0]_{4T}$ carbon fiber, at incident angles 0 and 10 degrees

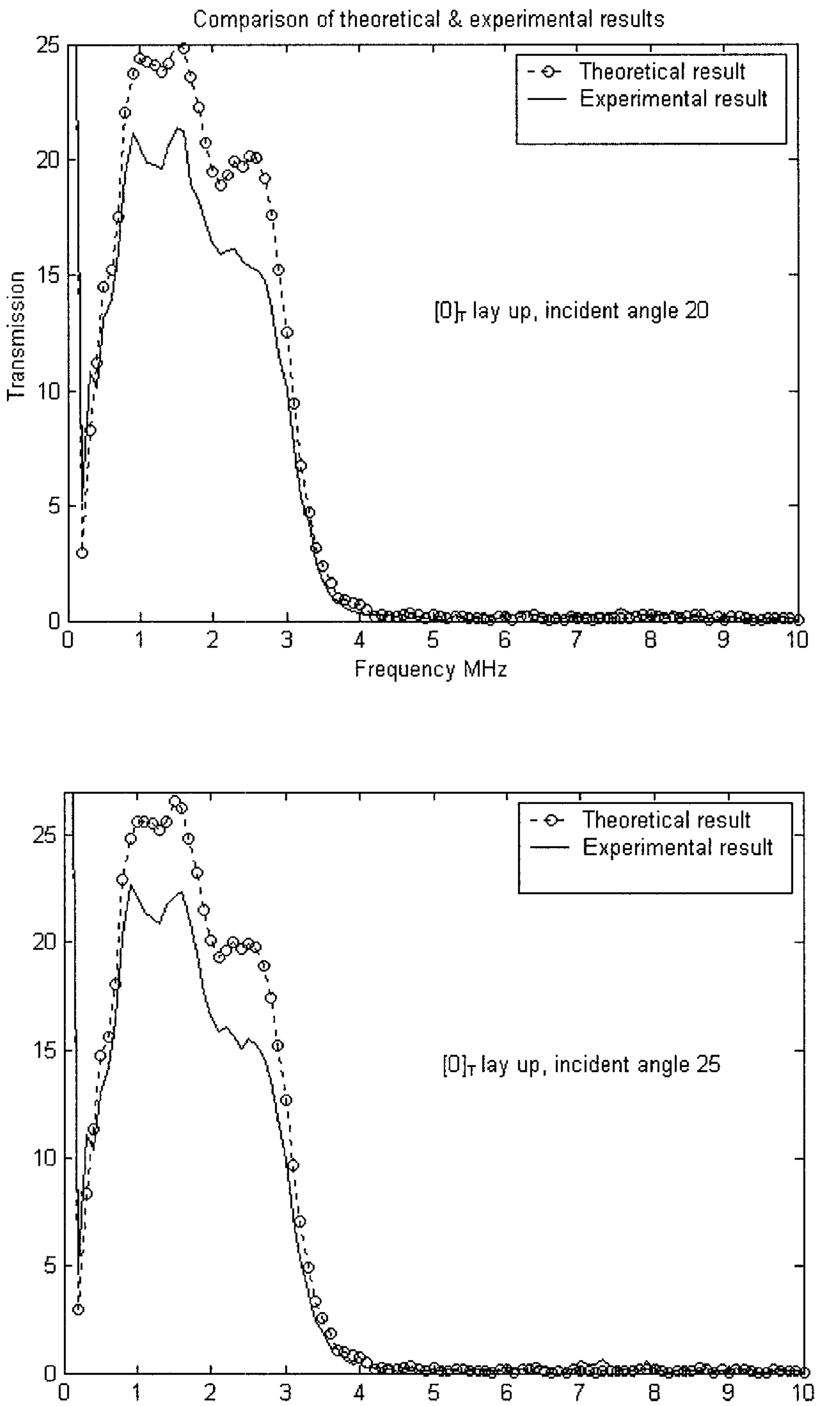

Figure 2.12b Comparison of theoretical and experimental spectral results of transmission amplitude versus frequency for $[0]_{4T}$ carbon fiber, at incident angles 20 and 25 degrees

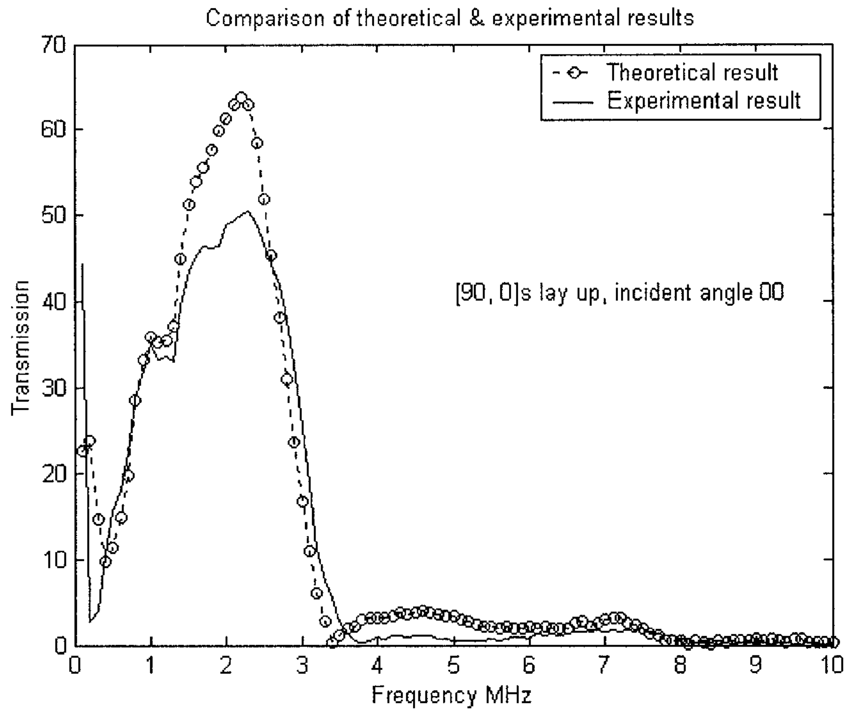

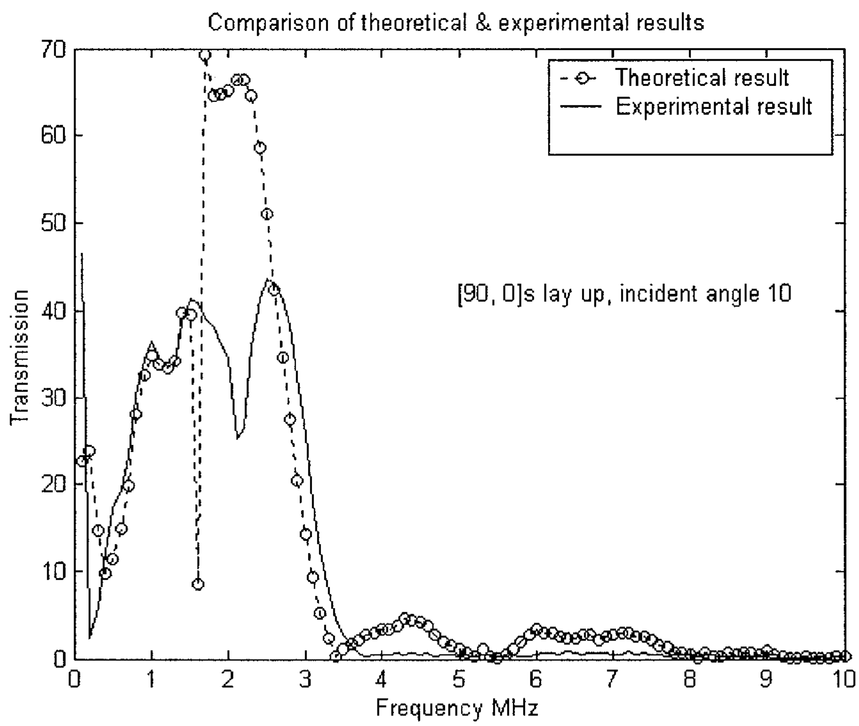

Figure 2.13a Comparison of theoretical and experimental spectral results of transmission amplitude versus frequency for $[90, 0]_S$ carbon fiber, at incident angles 0 and 10 degrees

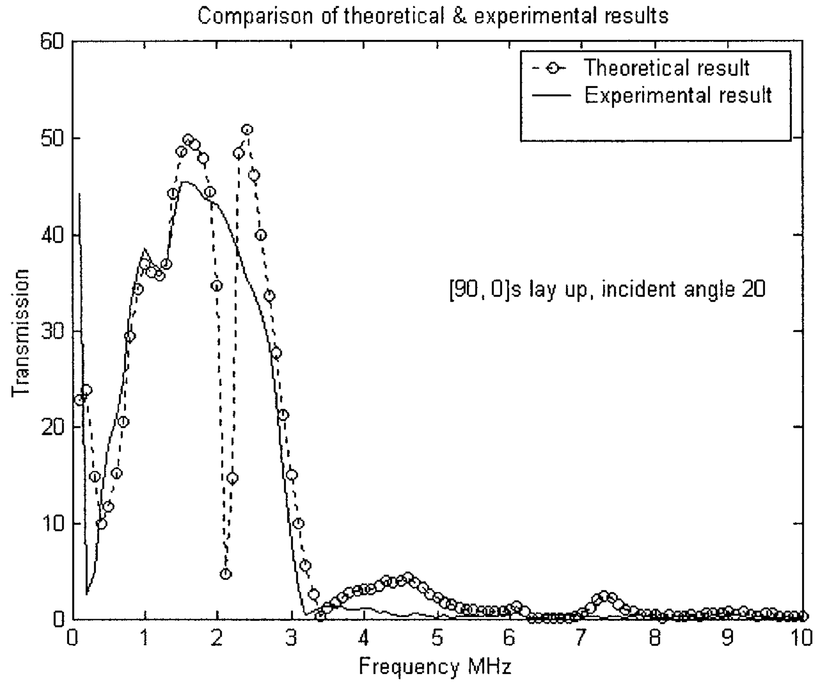

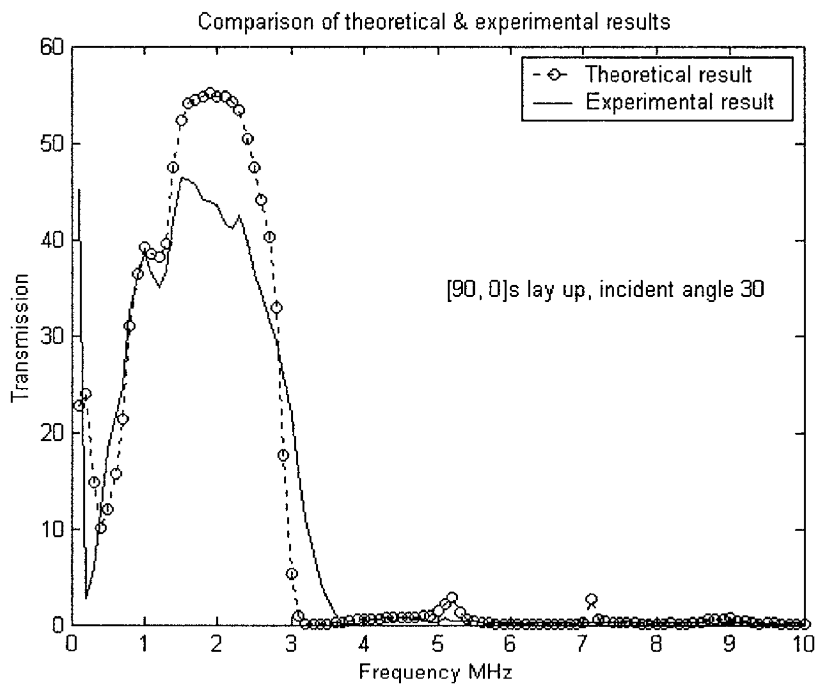

Figure 2.13b Comparison of theoretical and experimental spectral results of transmission amplitude versus frequency for $[90, 0]_S$ carbon fiber, at incident angles 20 and 30 degrees

transform. Reconstructed signals are expressed as:

$$a(t) = t(t) \otimes w(t) \tag{2.7}$$

where a(t) is the reconstructed transmitted signal in time domain, t(t) theoretical transmission coefficient in time domain, which is convolved with w(t) the transmitted signal passing through water.

For a range of the different incident angles, the transmitted signals are reconstructed and compared with experimental curves in Figures 2.14, 2.15 and 2.16. The figures correspond to the transmitted signal versus time. The signals are reconstructed using equation (2.7) that is implemented by programs in Matlab. For the reduced axis scanning system, the changes of transmission coefficient are required with respect to the incident angle. The figures for transmission coefficient versus incident angle are shown. The maximum value of the time domain signal is found for the reconstructed signal at incident angles 00, 05, 10, 15, 20, 25 and 30. It is the peaks of the time domain signal from experiments that are shown in figure 2.14, 2.15 and 2.16 for the three $[0,90]_s$ $[0]_{4T}$ and $[90,0]_s$ lay-ups for the carbon fiber/epoxy composite plates. The comparisons are reasonable, showing nearly all features of the transition. The applications of the program to reduced axis scanning system can thus be performed in the type of real time processing. The application is direct since comparisons of the peaks of the experimental signal are used in the scanning system. The results between the theoretical and experimental curves are different because the theoretical model assumes a fully elastic matrix, the materials used in this work all exhibit significant visco-elasticity.

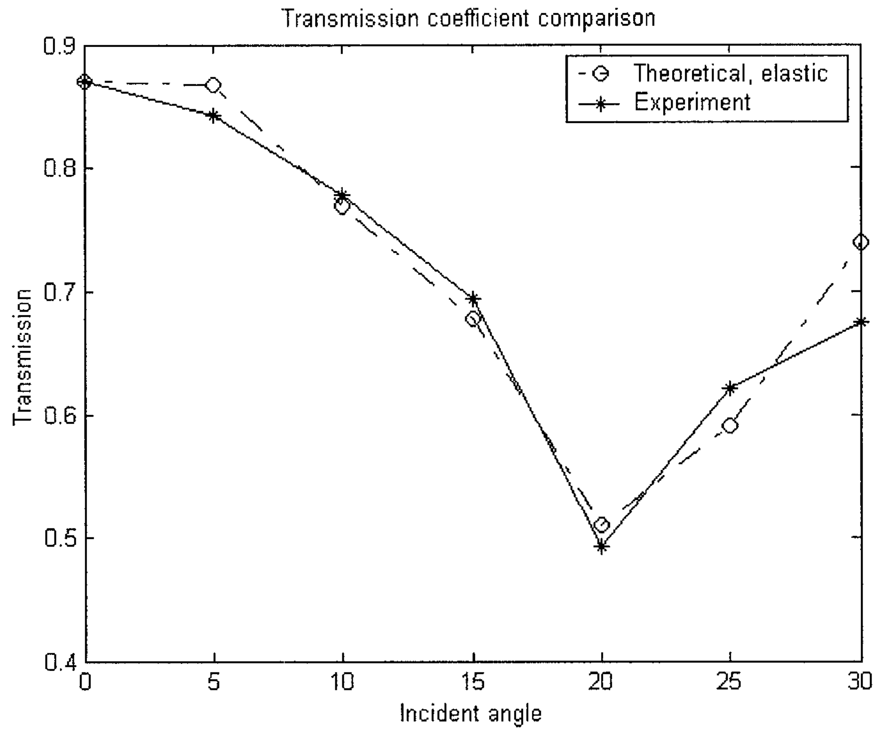

Figure 2.14 Comparison of reconstructed curve and experimental curve of transmission coefficient versus incident angle for $[0, 90]_S$ carbon fiber composite at real time processing

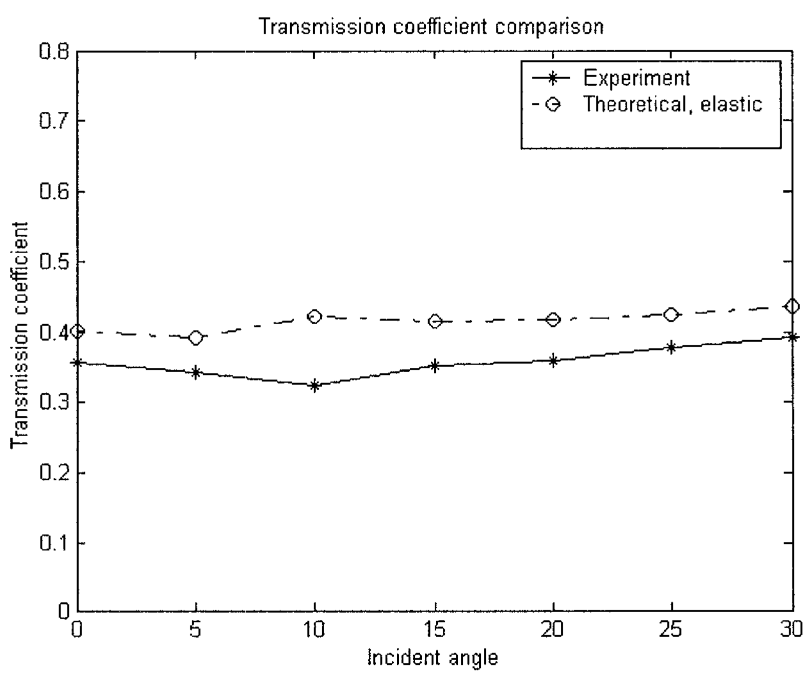

Figure 2.15 Comparison of reconstructed curve and experimental curve of transmission coefficient versus incident angle for $[0]_{4T}$ carbon fiber composite at real time processing

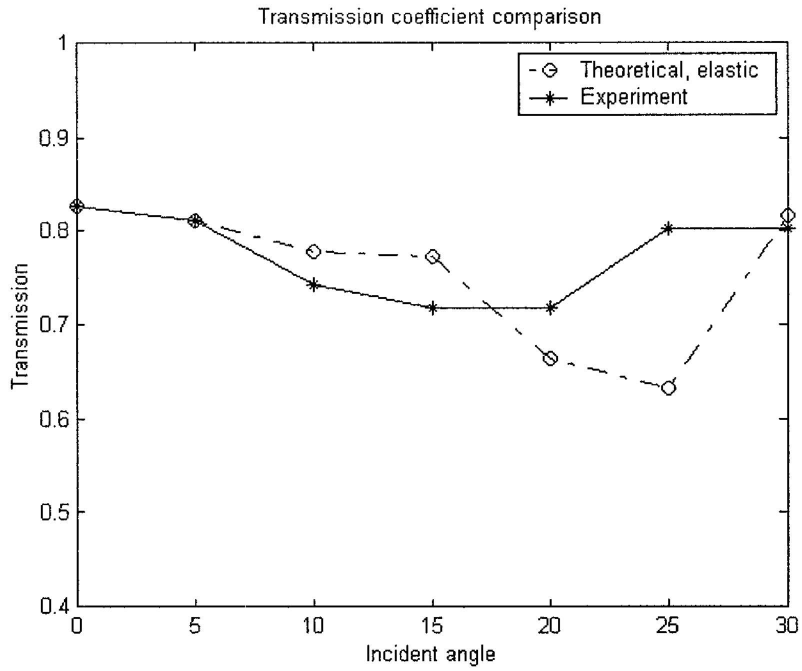

Figure 2.16 Comparison of reconstructed curve and experimental curve of transmission coefficient versus incident angle for $[90,0]_S$ carbon fiber composite at real time processing

2.4 References

Bar-Cohen, Y and Backes, P. G, 1999, 'Scanning aircraft structures using open-architecture robotic crawlers as platforms with NDT Boards and sensors', Materials evaluation.

Brekhovskikh, L. M. And. Godin, O.A, 1990, *Acoustics Of Layered Media I*, Springer-Verlag, New York.

Bodig, Jozsef and Jayne, Benjamin A, 1993, *Mechanics of Wood and Wood Composites*, Krieger Publishing Company, Malabar, Florida.

Chimenti, D.E. and Nayfeh, Adnan H., 1990, 'Ultrasonic Reflection And Guided Wave Propagation In Biaxially Laminated Composite Plates', J. Acoust. Soc. Am. 87(4), 1409-1415.

Downs, J., P. Zhang and M. L. Peterson, 1999, 'A High-Speed High-Resolution Ultrasonic Inspection Machine', IEEE/ASME Transactions on Mechatronics Vol. 4, no. 1, 301-311.

Krautkramer, J and Krautkramer, H., 1990, *Ultrasonc testing of materials*. Springer-Verlag, New York.

Nayfeh, Adnan H., 1995, *Wave propagation in layered anisotropic media*, Elsvier, New York.

Nayfeh, Adnan H. and Chimenti, D. E., 1991, 'Elastic wave propagation in fluid-loaded multiaxial anisotropic media' J. Acoust. Soc. Am. 89 (2), 542-549.

Nayfeh, Adnan H. and Chimenti, D. E., 1989, 'Free Wave Propagation in Plates of General Anisotropic Media', J. Applied Mechanics, 56, 881-886.

Chapter 3

Automatic Gain Correction for Reduced Axis Scanning for Orthotropic Visco-Elastic Composite Materials

3.1 Introduction

The purpose of this investigation in this chapter is to extend previous studies of ultrasonic-wave propagation in carbon fiber/epoxy composite to a visco-elastic model. This will extend the previous studies to accommodate the material attenuation of the ultrasonic wave in the carbon fiber/epoxy matrix or steel fiber/rubber matrix composite. Because of practical considerations regarding baseline knowledge of material properties, the transmission of the wave through the visco-elastic model in carbon fiber/epoxy composite is emphasized. However, the change in complex impedance also impacts the reflection in the material. Comparisons of experimental curves with theoretical curves are shown for both visco-elastic and elastic models. Experimental verification is also provided to give a reasonable theoretical foundation for auto gain correction which is implemented for the reduced axis scanning. The samples used for experiments are carbon fiber reinforced, epoxy matrix, composite plates with lay-ups of $[0, 90]_S$, $[90, 0]_S$

and $[0]_{4T}$. The elastic matrix model is extended to a visco-elastic matrix model by using complex elastic material constants in the formulation of the wave transmission.

The calculation of transmission coefficient of a multi-layered structure is used for reduced axis scanning as described above. Previous calculations for elastic, isotropic and orthotropic materials had good qualitative agreement with the experimental data. It is expected that the extension in this chapter to visco-elastic plates will better match the material attenuation observed experimentally. The material attenuation observed in experiments is mostly simply represented by a linear visco-elastic material. This extension to the elastic case should increase the similarity to the experimental data.

3.2 Theoretical Formulation

Automatic gain correction is primarily intended for the calculation of transmission coefficients of orthotropic layered materials at arbitrary incident angles. The transfer matrix method is then applied to the calculation of transmission coefficients for use in the automatic gain correction algorithm. Because of the significant degree of visco-elastic behavior of the matrix properties of most composites, the need for this extension is predicable. Because of the orientation of the fibers, the composite materials are modeled as orthotropic models, as discussed in Chapter 2.

3.2.1 Wave propagation in a visco-elastic composite material plate immersed in water - by matrix transfer method

In the matrix transfer method, general solution equations and boundary conditions are expressed in a simplified matrix form. Transmission coefficients are obtained by matrix operations along satisfying boundary conditions [Brekhovskikh and Godin, 1990, Nayfeh, 1995]. Generally, the solutions are derived from the equations of motion, the constitutive (stress and strain) relations and the strain-displacement relations. The form of calculated matrix is expressed in term of stresses and displacements, as a 6^{th} order matrix, in which propagation of three coupled waves, two shear waves and one longitudinal wave, are considered.

For the sample shown in Figure 2.1, the layers of composite material are assumed to be visco-elastic and orthotropic. The composite plate is immersed in water. The transmission coefficients are calculated for the orthotropic case and the monoclinic case. The monoclinic case must be considered to accommodate coupling of waves when the sample is oriented out of a principal material axis. Similar to Chapter 2, transmission coefficients are exactly expressed as Equation (2.1). However, all of the material constants are in the form of a complex modulus which results in a combination of the oscillating character of wave propagation with attenuation due to the imagery portion on the constant.

Many materials used in many application have a significant level of material visco-elasticity. This is particularly true of many of the matrix materials which are commonly used in composites. Previous work has considered the effects of visco-elasticity on the propagation of an ultrasonic signal through a layered sample using an isotropic model [Zhang and Peterson, 1998]. These effects should be considered in a practical application like the automatic gain correction because of the similar effects that change in thickness of the sample would have to change in the curvature of the sample. As a result, the completed model includes those effects as well as the effect of curvature. A simple linear viso-elastic model is used with both a Voight and a 3-element material model. The elastic and visco-elastic properties are included in the material constants of the standard formulation in terms of a complex modulus [Hosten, 1991, Shaw and Bugl, 1968]. The visco-elastic properties of the composites are then directly expanded into the transfer matrix method for the calculation of transmission coefficients, the complex moduli replaces the real moduli, which in turn create a complex value for the transmission and reflection coefficients. The material constants in terms of the complex modulus result in wave behavior which shows both attenuation and propagation. The transfer matrix method still is applicable to the visco-elastic case.

3.2.2 Visco-elastic models and input material constants

Generally, materials, such as rubber, plastic and most matrix materials, are most reasonably characterized as a linear visco-elastic material for linear wave propagation. A Voigt model and a 3-element mechanical model are used to describe the properties of the linear visco-elastic materials. The 3-element model represents a frequency dependent visco-elasticity which is most realistic. Polymer matrix composites are generally composed of visco-elastic matrix and fibers that introduce the anisotropy. Wave propagation in a composite material along an axis that is not contained in a plane of symmetry will cause coupling of the modes that propagate as with elastic materials. Damping and thus attenuation as well as velocity of the propagating waves in general varies with the direction in material. Typically, the attenuation along a fiber direction is less than in the other material axes because of the high relative value of damping behavior in the matrix relative to the fiber properties. However, because the waves propagate in the matrix as well as the fibers, it may be reasonable to simplify the problem to assume that the attenuation in all directions is approximately equivalent. This is clearly not true for a unidirectional laminate, but is reasonable for some more complex lay-ups. This assumption will simplify the measurement of attenuation in the composite materials. As will be discussed below. However, this does not result in any angle dependent attenuation variation from the model. Therefore, the simplest situation, isotropic damping is initially used to describ an orthotropic material with the attenuation as a function of frequency.

For an isotropic material, Lame's constants are expressed as complex material constants. Visco-elastic stiffness coefficients in composite materials are consisted of a real part, which characterizes the propagating elastic wave, and the imaginary part, which damps propagating wave. The complex Lame's modulus and shear modulus are expressed for linear viscoelasticity as [Brekhovskikh and Godin in 1990]:

$$\lambda * = \lambda + i\omega\ (2\eta/3-\varsigma) \tag{3.1}$$

$$\mu * = \mu - i\omega\eta \tag{3.2}$$

where μ, λ are the elastic coefficients, η is the viscosity coefficient for the shear viscosity and ς is the dissipation coefficient for the bulk viscosity. When ς is neglected, the expression reduces to a Voigt model. In practical engineering applications, the attention coefficient is more commonly used to describe the damping properties of a composite. From experiments, attenuation coefficients of materials are easier to measure than Lame's and shear modulus. The relation between the attenuation coefficient and Lame's and shear Moduli both is:

$$k_l^* = \omega\sqrt{\frac{\rho}{2\mu^* + \lambda^*}} \tag{3.3}$$

$$k_s^* = \omega\sqrt{\frac{\rho}{\mu^*}} \tag{3.4}$$

where the wave numbers k can be expressed as a real part and a imaginary part in terms of the wave propagation and the wave attenuation:

$$k_l^* = k_l + \alpha_l i \tag{3.5}$$

$$k_s^* = k_s + \alpha_s i \tag{3.6}$$

where α is the material attenuation coefficient, where subscript l is the longitudinal wave and subscript s is the shear wave. Replacing λ^*, μ^* in the equations (3.3) and (3.4) by the equations (3.3) and (3.4), the equations are expanded by the binomial theorem. Because the viscosity coefficient η and the dissipation coefficient ζ are much less than the Lame's modulus and shear modulus, respectively, the higher order terms are ignored.

$$k_l^* = \omega\sqrt{\frac{\rho}{2\mu+\lambda}}\left(1 + i\omega\left(\frac{\zeta + \frac{4}{3}\eta}{2(\lambda+2\mu)}\right)\right) \tag{3.7}$$

$$k_s^* = \omega\sqrt{\frac{\rho}{\mu}}\left(1 + i\omega\frac{i\omega\eta}{2\mu}\right) \tag{3.8}$$

Comparing the equations (3.7) and (3.8) with the equations (3.5) and (3.6), thus, we have the following expressions.

$$\alpha_l = \omega\sqrt{\frac{\rho}{2\mu+\lambda}}\,\omega\frac{\zeta + \frac{4}{3}\eta}{2(\lambda+2\mu)} \tag{3.9}$$

$$\alpha_s = \omega\sqrt{\frac{\rho}{\mu}}\frac{\omega\eta}{2\mu} \tag{3.10}$$

substituting $c_l = \sqrt{\dfrac{\lambda + 2\mu}{\rho}}$ and $\alpha_s = \sqrt{\dfrac{\mu}{\rho}}$ into the equations (3.9) and (3.10), then we have:

$$\alpha_l = \frac{\omega}{c_l} \frac{\omega\left(\varsigma + \frac{4}{3}\eta\right)}{2(\lambda + 2\mu)} \tag{3.11}$$

and

$$\alpha_s = \frac{\omega}{c_s} \frac{\omega\eta}{2\mu} \tag{3.12}$$

The attenuation coefficient is expected to be of a smaller order than wave propagation coefficient [Hosten, 1991]. In considering a carbon fiber/epoxy composite (fiber CYCOM 950-1/matrix T65035 epoxy) of 4 layers lay up, the real parts of the constants for each layer are found from Chapter 2, and the imaginary parts of materials constants are assumed as shown in Table 3.1 [Hosten, 1991]. The input data shown in Table 3.1 is then sufficient for transmission coefficient calculations for carbon fiber composite materials, where a complex value will be obtained.

3.3 Results for a Visco-Elastic Composite Material

Transmission coefficients are calculated in a similar fashion as for the previous elastic case (in chapter 2). When the complex moduli material constants are used in place of real moduli material constants, equation (2.2) can be extended to describe the visco-elastic matrix, in the carbon fiber reinforced composite plate. The calculation programs are programmed in the C++ language with double precision complex values moduli and run on an ANSI C++ workstation. The flow chart is shown in Figure 2.2. The input data for the visco-elastic model are used as shown in Table 3.1 except that the complex moduli is used instead of real modulus in Table 2.2 for the elastic model. All of the numerical work had to be performed using methods that were applicable for complex numbers. The calculated results more closely represent the behavior of the actual system as shown in the following sections.

3.3.1 Theoretical results

1. Calculation results for a carbon fiber reinforced composite material using a $[0]_{4T}$ lay up (Figure 3.1)

Calculated results are shown in Figure 3.1 for a composite material plate $[0]_{4T}$ lay up. The input data in the visco-elastic case and the elastic case are shown in Table 3.1 and Table 2.2 for 0.127mm thickness. The curves represent the transmission coefficients

Table 3.1 Visco-elastic constants [C] (GPa) and density (kg/m^3) for each layer of carbon fiber epoxy materials

C_{ij}	1	2	3	4	5	6
1	(141.3, 2.51)	(5.90, 0.1)	(5.90, 0.1)	(0., 0.)	(0., 0.)	(0., 0.)
2	(5.90, 0.1)	(11.47, 0.27)	(5.88, 0.1)	(0., 0.)	(0., 0.)	(0., 0.)
3	(5.90,0.1)	(5.88, 0.1)	(11.47, 0.27)	(0., 0)	(0., 0.)	(0., 0)
4	(0., 0)	(0., 0.)	(0., 0.)	(2.27, 0.094)	(0., 0.)	(0., 0.)
5	(0., 0)	(0., 0.)	(0., 0.)	(0., 0.)	(4.36, 0.094)	(0., 0.)
6	(0., 0)	(0.,0.)	(0., 0.)	(0., 0.)	(0., 0.)	(4.36, 0.094)
Density ρ		1500.				

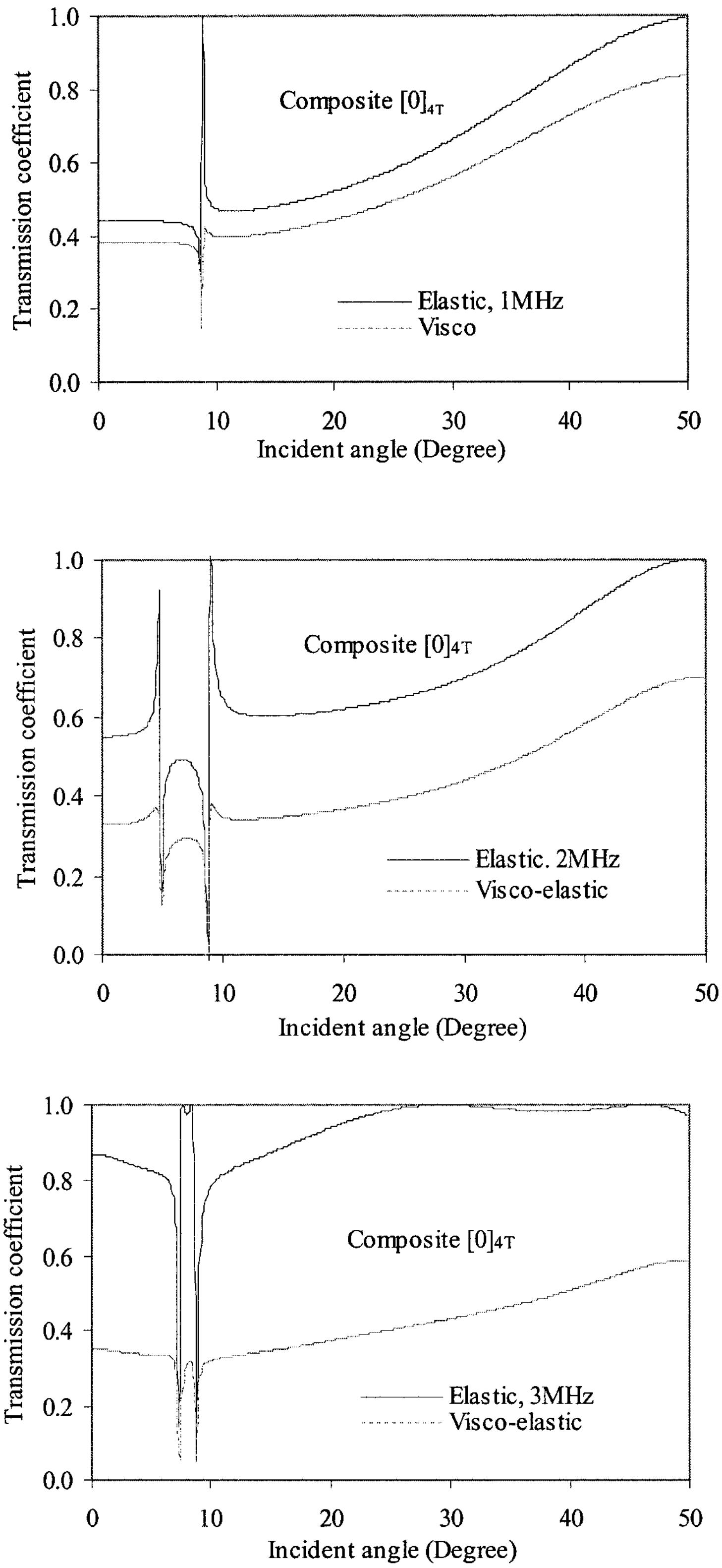

Figure 3.1 Calculated curves for the comparison of elastic and visco-elastic properties of carbon fiber composite $[0]_{4T}$

versus incident angles at frequencies, 1 2 and 3 MHz. Three figures compare the transmission coefficients of the elastic model with transmission coefficients corresponding to visco-elastic model in the carbon fiber/epoxy composite plate. At a single frequency, the transmission coefficient curves including material damping properties results in similar curves to the elastic transmission coefficients, with the exception of showing increased attenuation. The propagation of a wave passing though a composite material plate is a combination of elastic wave propagation and wave attenuation which results from material damping. The material attenuation of the composite material increases with an increase in frequency. When the frequency increases, the wavelength becomes shorter and the material damping increases significantly. This material damping becomes more important at high frequency, which is also used to increase spatial resolution. In addition, change in attenuation at different incident angle is also altered. The changes are particularly notable in some areas, especially, in regions of abrupt change in transmission coefficients. In experiments using composite material plate, the abrupt change in the transmission coefficients seen in the elastic case are not observed. Thus, for any practical application, a composite material is more appropriately modeled as the visco-elastic material.

2. Calculation results for a carbon fiber reinforced composite material using a $[0, 90]_S$ lay up (Figure 3.2)

Results are shown in Figure 3.2 for the calculated transmission coefficient of a visco-elastic model and elastic model in the carbon fiber/epoxy composite material plate $[0, 90]_S$ with the lamina lay up sequence shown in Table 3.1 and Table 2.2 for 0.159 mm thickness. The three curves represent the transmission coefficient versus the incident

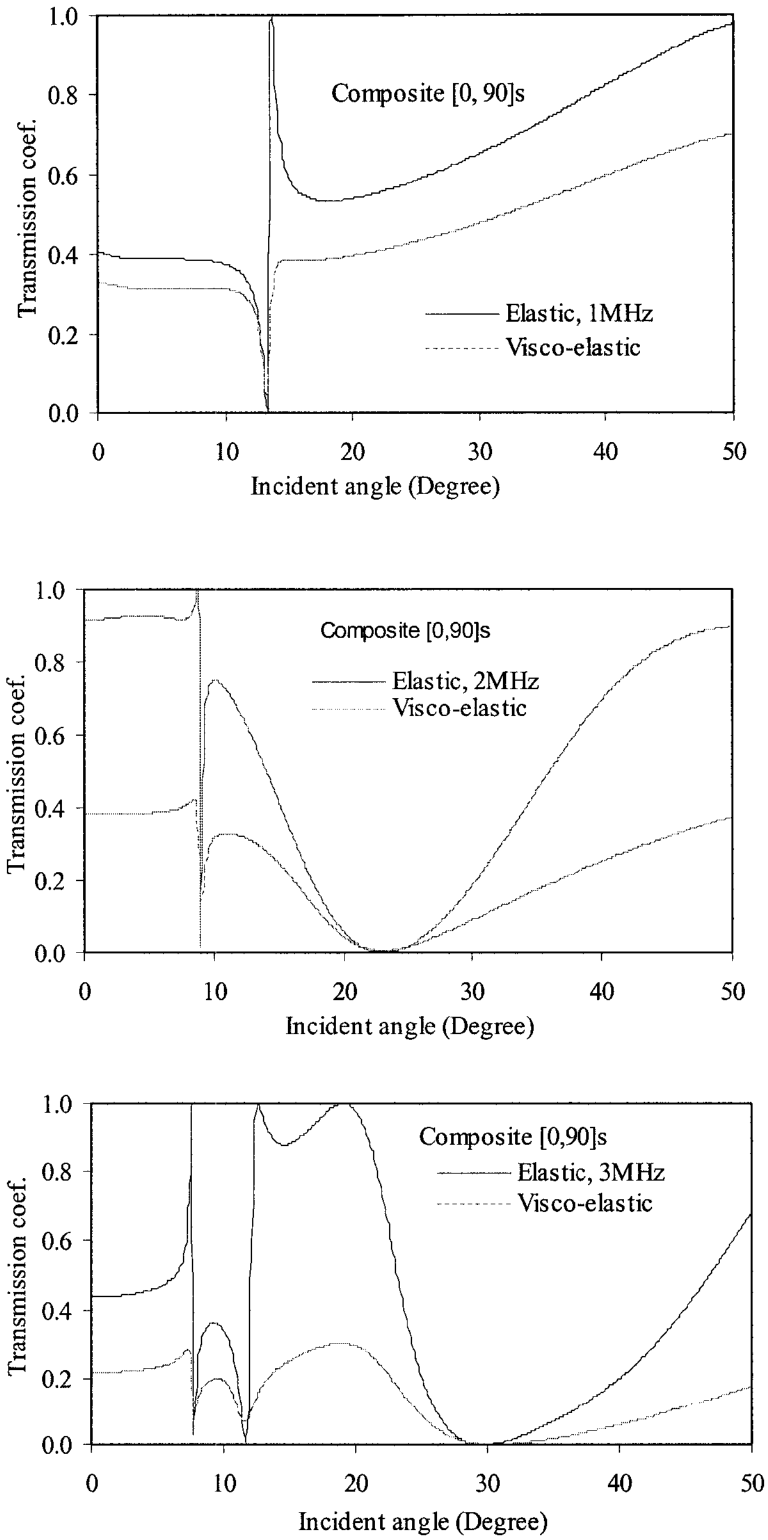

Figure 3.2 Calculated curves for the comparison of elastic and visco-elastic properties of $[0, 90]_s$ carbon fiber composite

angle at 3 different frequencies, 1, 2 and 3 MHz. The transmission coefficients for the elastic model are compared to the transmission coefficients calculated using the visco-elastic model. As in Figure 3.1, at a particular frequency, the transmission coefficients are similar to curves when material damping is not included. The figure differs only in fiber directions. At a low frequency – 1MHz, which corresponds to a longer wavelength, the fiber direction does not significantly affect the transmission coefficients. For the $[0]_{4T}$ lay-up and [0,90]s lay-up, transmission coefficients curves are very similar. When frequency increases, the effect of lay-up increases. Transmission coefficients change significantly with an increase in frequency, and the effect of carbon fiber reinforced increases with a frequency increase. The addition of damping is more closely represents the behavior of a real material than the elastic material model.

3. Calculation results for a carbon fiber reinforced composite material using a $[90, 0]_S$ lay up (Figure 3.3)

Results are shown in Figure 3.3 for the calculated transmission coefficient of a visco-elastic model and elastic model in a carbon fiber/epoxy composite material plate $[90, 0]_S$ with lamina lay-up sequence shown in Table 3.1 and Table 2.2 for 0.146 mm thickness, the three set of curves represent the transmission coefficients versus incident angles at 3 different frequencies, 1 2 and 3 MHz. The transmission coefficients for the elastic model are compared to the transmission coefficients calculated for the visco-elastic model. As in Figures 3.1, 3.2, wave propagation in the visco-elastic material is the combination wave propagation and wave attenuation, the fiber directions significantly change the transmission coefficients. Particularly at higher frequencies, the inspection of composite

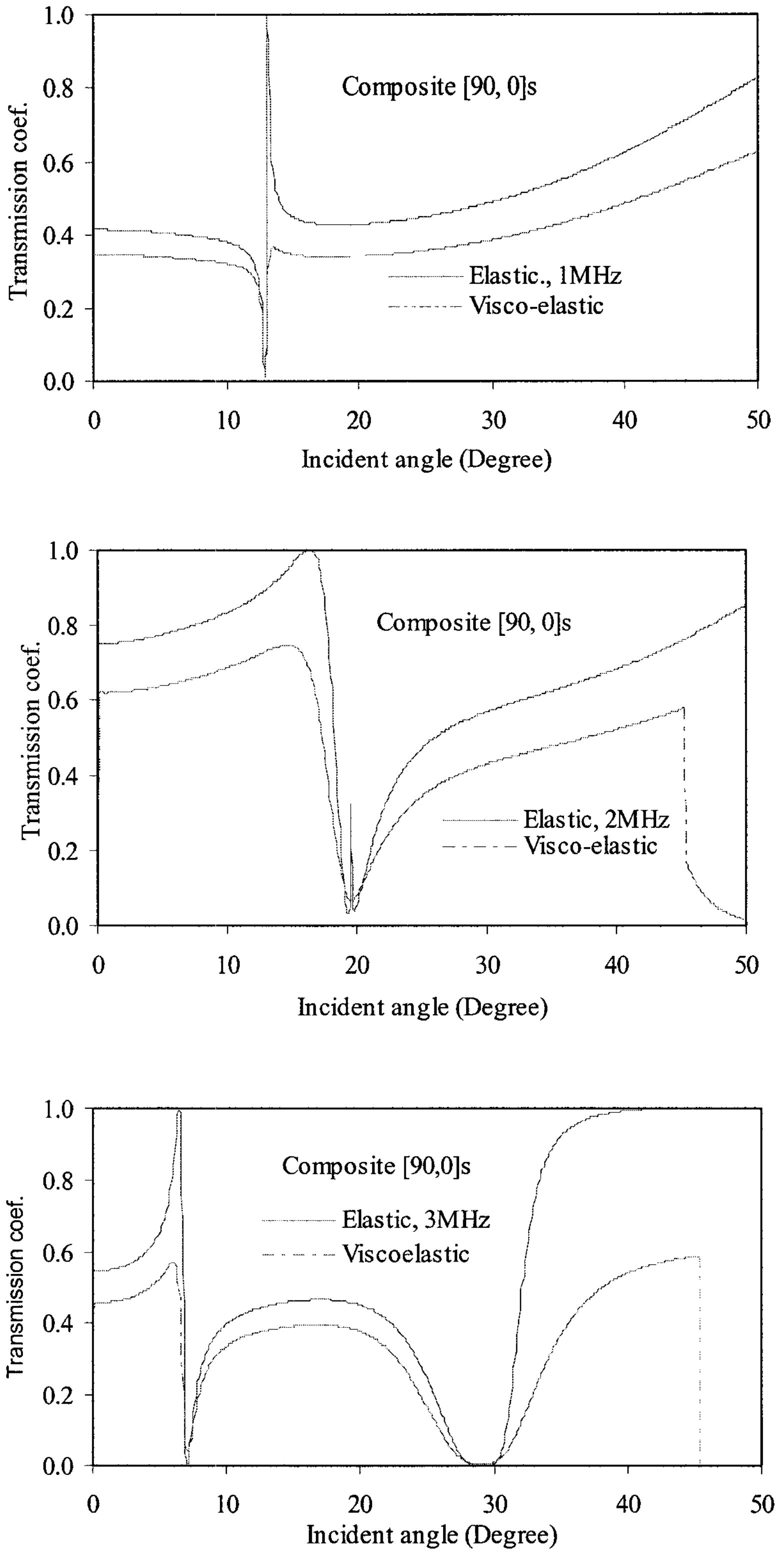

Figure 3.3 Calculated curves for the comparison of elastic and visco-elastic properties of carbon fiber composites $[90, 0]_S$

materials both the frequency of the incident wave and the fiber direction are important for obtaining accurate results.

3.3.2 Analysis and explanation for theoretical results

While at low frequencies the changes are subtle, Figures 3.1, 3.2, 3.3 show results for a visco-elastic material model that is more suitable for description of carbon fiber reinforced composite materials than the elastic material model, previously described, because of the visco-elastic matrix. Fiber direction of composite material is also shown to be an important factor affecting the transmission coefficient. Visco-elastic damping and wave propagation of the matrix material are combined in a single model. Carbon fiber reinforcement also introduces anisotropy in the material properties. The direction of characteristic in the anisotropic propagation relative material axes in the material is clearly the most important in composite materials and nature materials. However, at low frequency, the fiber direction is less significant so that isotropic approximations may be made for the simple cases shown. For a material inspection, comprehensive considerations of frequencies, fiber directions and material models should be applied.

3.3.3 Comparisons of theoretical reconstructed and experimental results

Experimental results are compared with theoretical reconstructed results for a visco-elastic model and an elastic model in Figures 3.4, 3.5 and 3.6. The calculations are completed by C++ and Matlab programs, following the steps in Appendix B and flow chart 2.2. Experiments are performed in a water tank and experimental apparatus shown in Figure 2.7. Experimental procedures and signal processing are similar to the section 2.3 applied in the measurement of a real composite material plate. The carbon fiber l

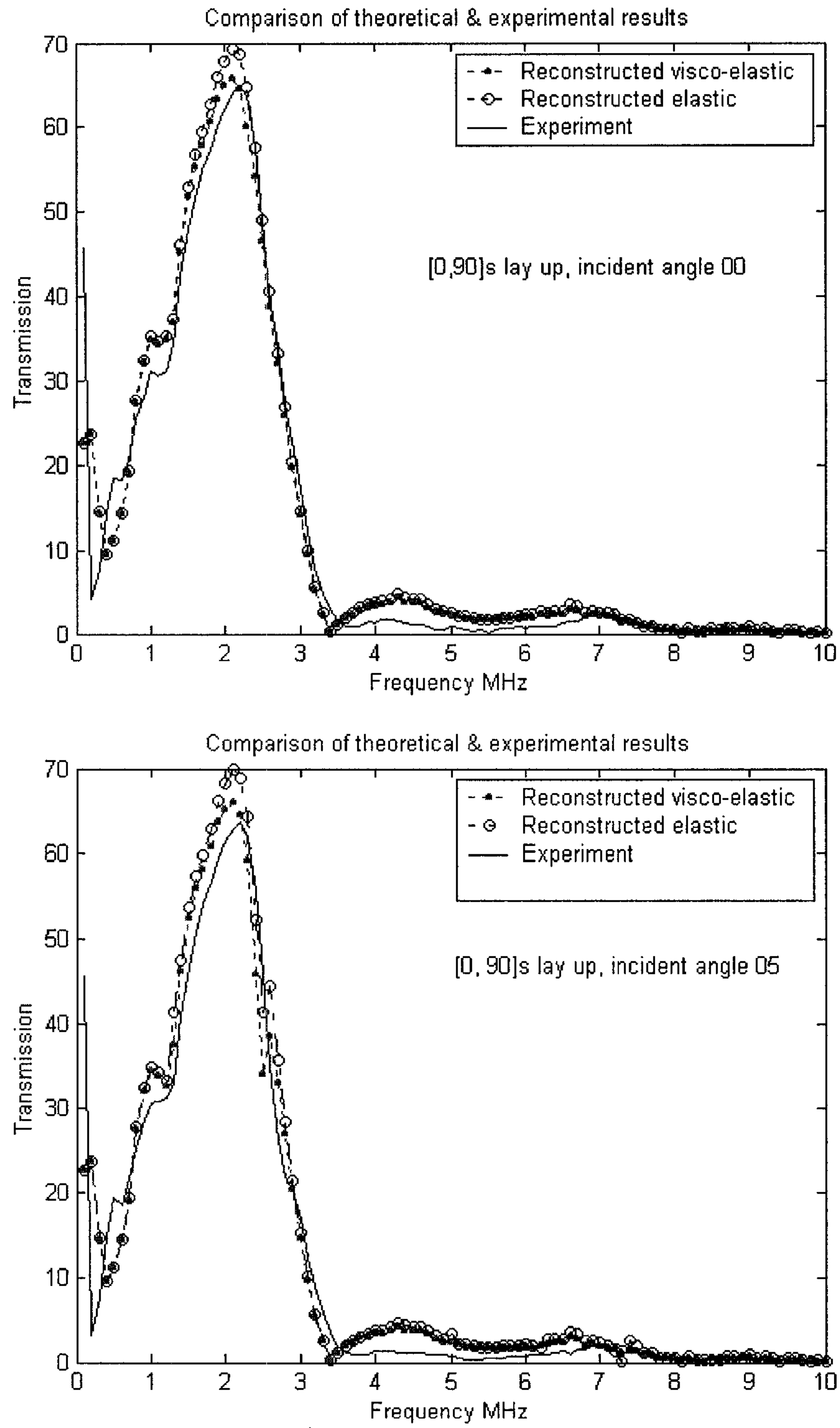

Figure 3.4a Comparison of theoretical reconstructed and experimental results of transmission amplitude versus frequency for $[0, 90]_S$ lay up carbon fiber/epoxy composite plate, at incident angles 0 and 5 degrees

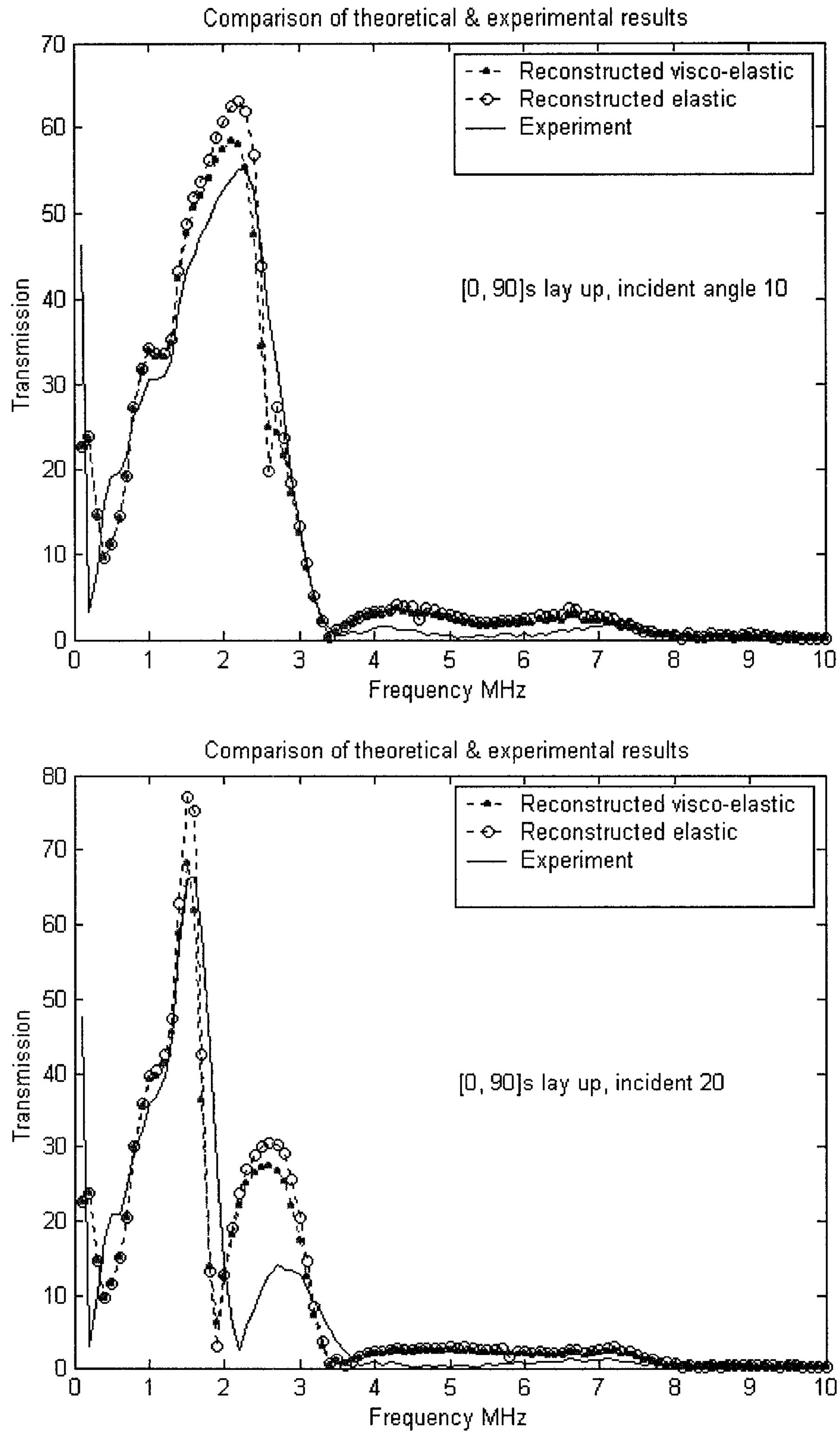

Figure 3.4b Comparison of theoretical reconstructed and experimental results of transmission amplitude versus frequency for $[0, 90]_S$ lay up carbon fiber/epoxy composite plate, at incident angles 10 and 20 degrees

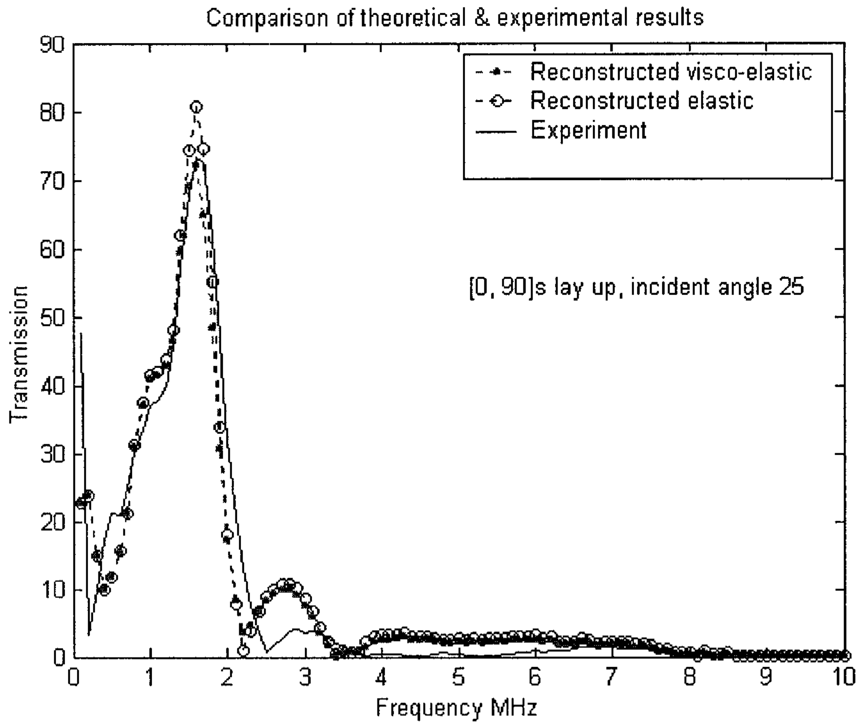

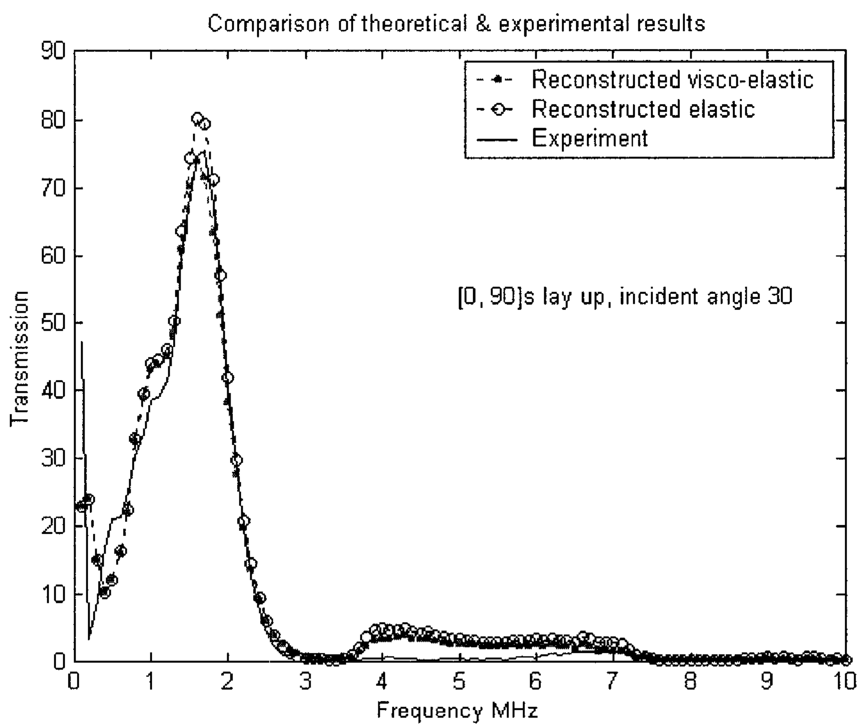

Figure 3.4c Comparison of theoretical reconstructed and experimental results of transmission amplitude versus frequency for $[0, 90]_S$ lay up carbon fiber/epoxy composite plate, at incident angles 25 and 30 degrees

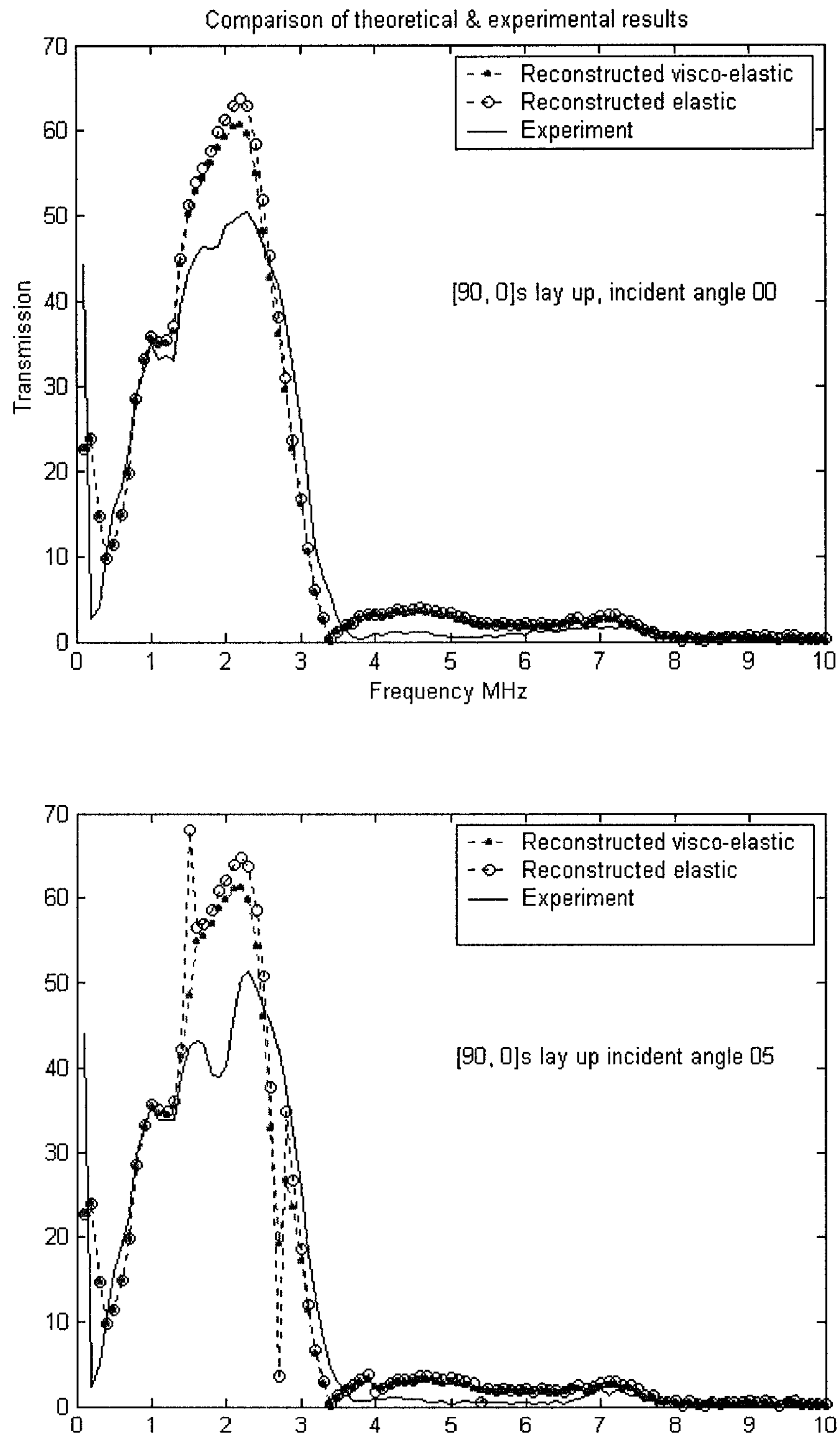

Figure 3.5a Comparison of theoretical reconstructed and experimental results of transmission coefficient versus frequency for $[90, 0]_S$ lay up carbon fiber/epoxy composite plate, at incident angles 0 and 5 degrees

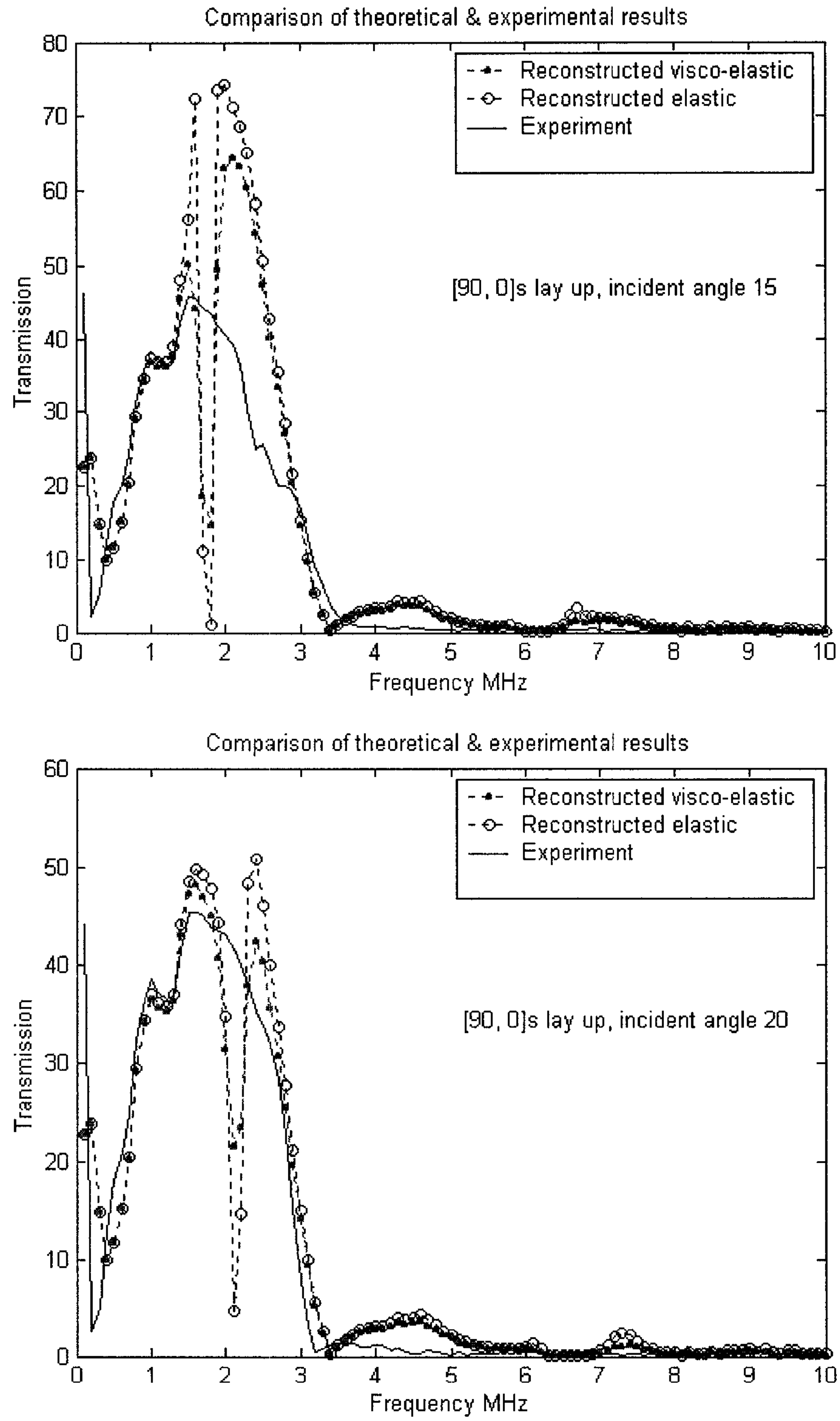

Figure 3.5b Comparison of theoretical reconstructed and experimental results of transmission coefficient versus frequency for $[90, 0]_S$ lay up carbon fiber/epoxy composite plate, at incident angles 15 and 20 degrees

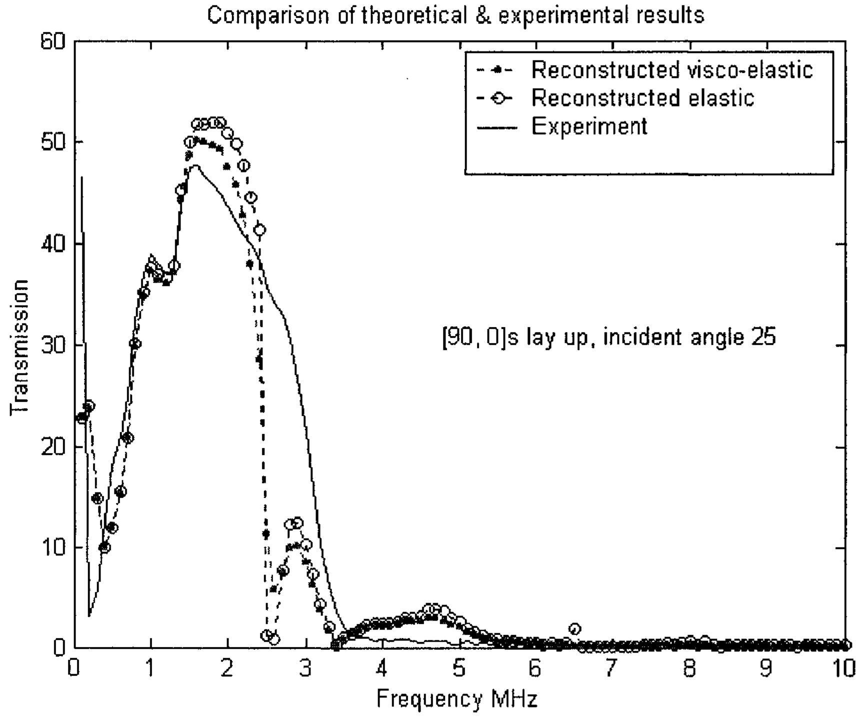

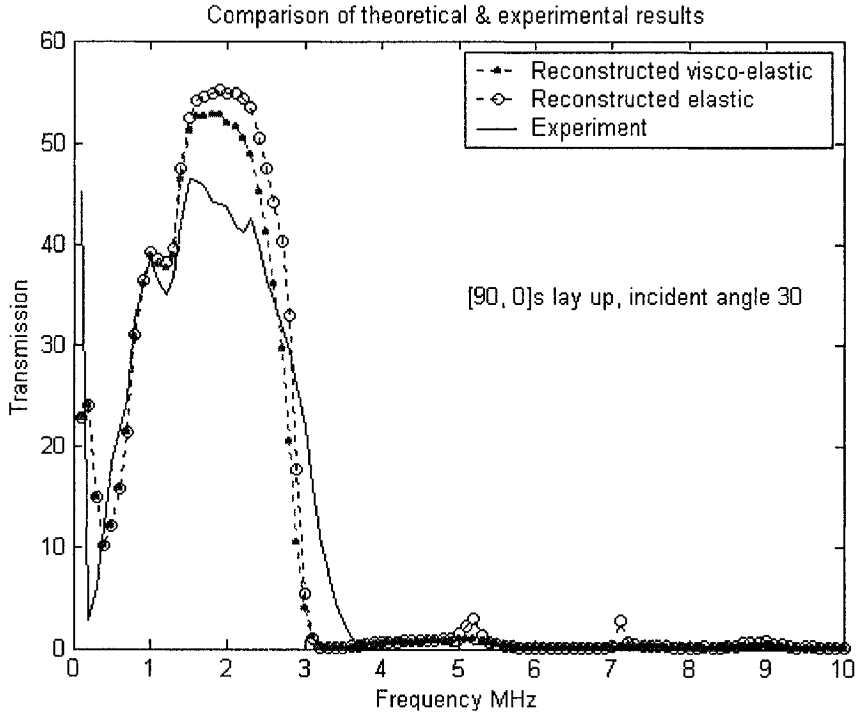

Figure 3.5c Comparison of theoretical reconstructed and experimental results of transmission coefficient versus frequency for $[90, 0]_S$ lay up carbon fiber/epoxy composite plate, at incident angles 25 and 30 degrees

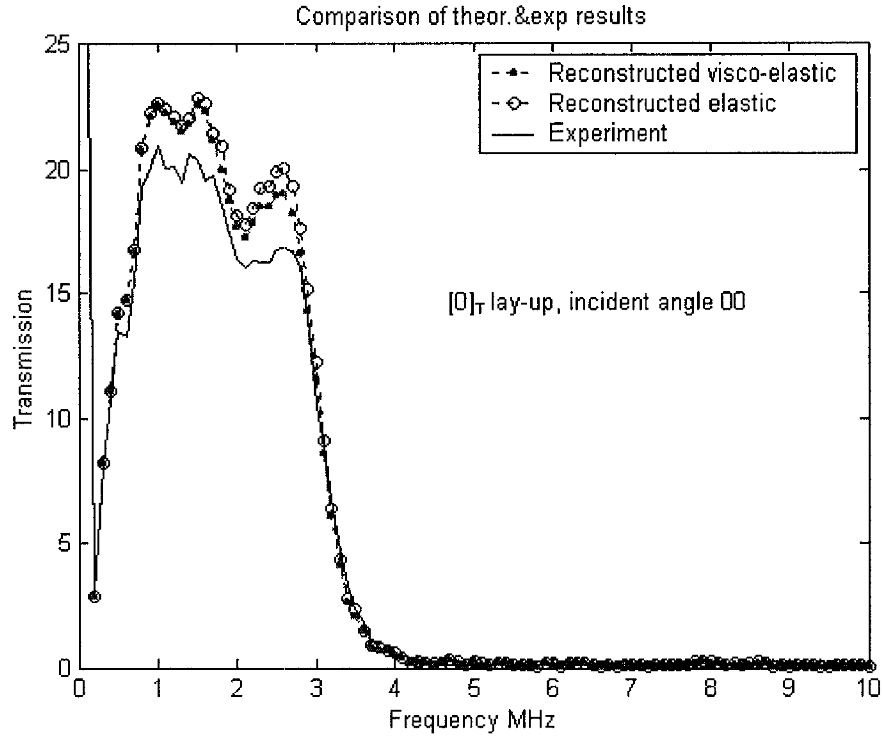

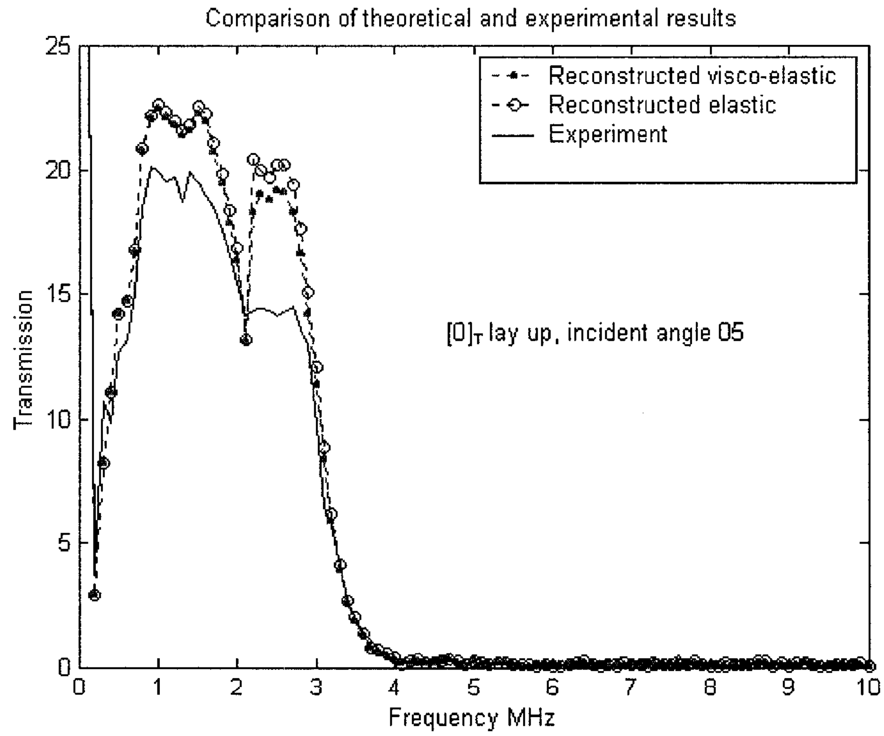

Figure 3.6a Comparison of theoretical reconstructed and experimental results of transmission coefficient versus frequency for $[0]_{4T}$ lay up carbon fiber/epoxy composite, at incident angles 0 and 5 degrees

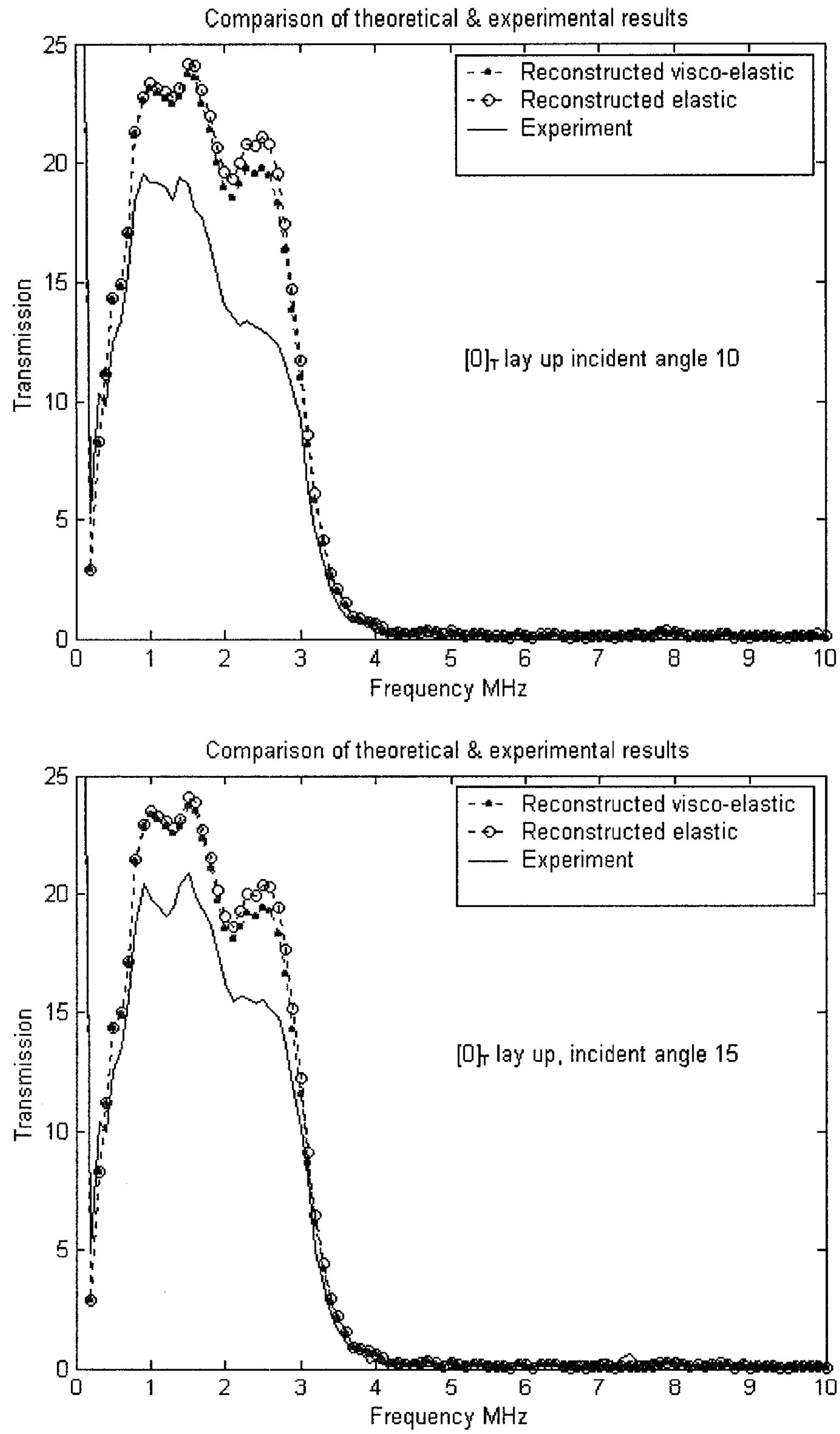

Figure 3.6b Comparison of theoretical reconstructed and experimental results of transmission coefficient versus frequency for $[0]_{4T}$ lay up carbon fiber/epoxy composite, at incident angles 10 and 15 degrees

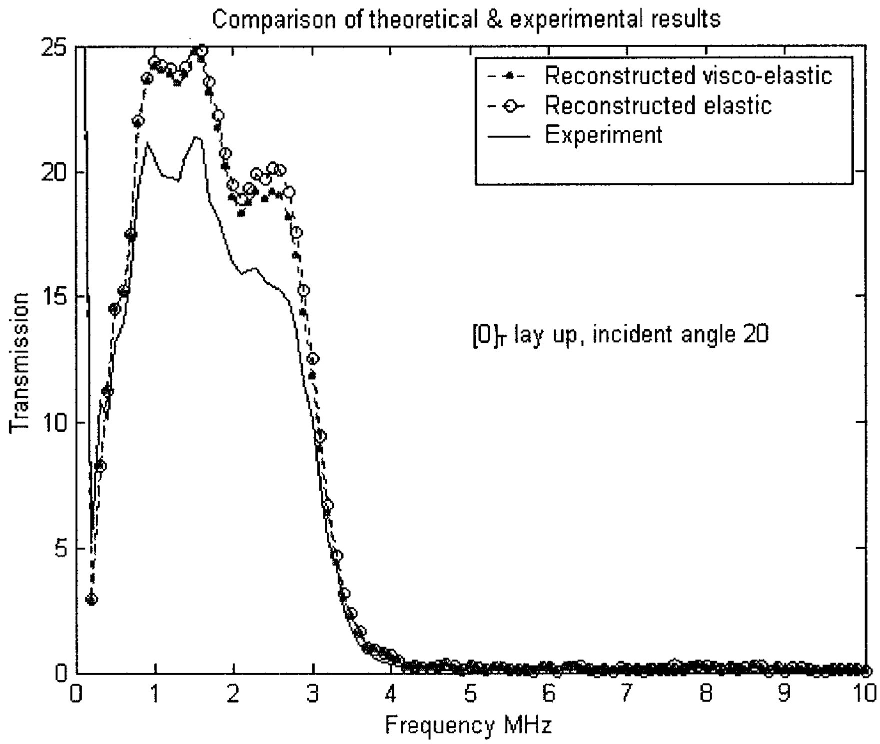

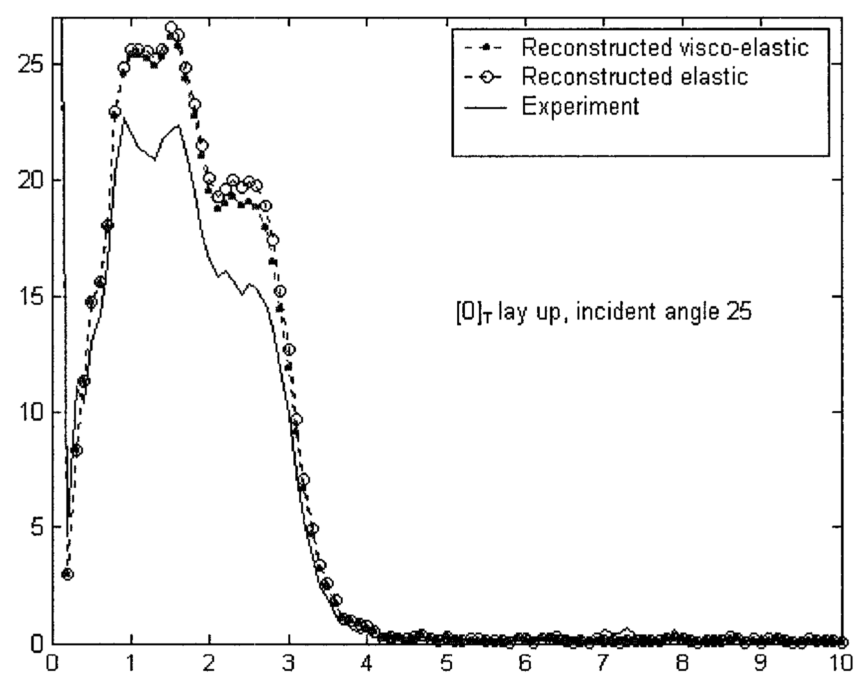

Figure 3.6c Comparison of theoretical reconstructed and experimental results of transmission coefficient versus frequency for $[0]_{4T}$ lay up carbon fiber/epoxy composite, at incident angles 20 and 25 degrees

reinforced, epoxy matrix, composite plates are exactly the same as previous samples in chapter 2, those are: $[0, 90]_S$, $[90, 0]_S$ and $[0]_{4T}$ lay-up composite plates, the measured thicknesses are 0.635mm, 0.584 and 0.508, respectively. The matched pair of piezoelectric transducers used have a nominal center frequency of 2.25 MHz. A focussed transmitter and a flat receiver with a 12 mm element diameter were used. The useable bandwidth of the transducers was chosen to be the frequency ranges over which the magnitude of the spectrum was greater than 75 percent of the peak value. The transducers were excited using a short duration pulse from the pulser-receiver (Panametrics, Waltham MA, 5052PR). The signal was over-sampled, 250 Msamples/sec. using a digital storage oscilloscope (Tektronix TDS 520A) and the signal was transferred to a personal computer using a general purpose interface bus connection (GPIB).

Investigated cases are studied at different incident angles 00, 05, 10, 15, 20, 25, 30. Experimental files were acquired and recorded by a computer as shown in the system diagram. For analysis the acquired data in time domain was transformed into the frequency domain by fast Fourier transform. Reconstructed theoreticaTransmitted signals are reconstructed by convolving the theoretical transmission coefficients with a reference signal. The reference signal is obtained by propagating the wave through a water path without sample. The theoretically reconstructed transmission signal is expressed as the following:

$$A(\omega) = T(\omega)\,W(\omega) \tag{3.5}$$

where $A(\omega)$ is a theoretically reconstructed transmission amplitude, $T(\omega)$ is the theoretical transmission coefficients and $W(\omega)$ is the Fourier transform of transmitted signal through water path without sample.

Figure 3.4 shows the comparison of theoretical reconstructed and experimental results of transmission amplitude versus frequencies 1 – 10 MHz for the $[0, 90]_S$ lay up carbon/epoxy composite plate at different incident angles (0, 5, 10, 15, 20, 25, 30). The theoretical curves match the experimental curves to a reasonable degree, the visco-elastic models are closer to the experimental results than elastic models. At the incident angles 10 and 15, near the critical angle, the experimental curves are significantly different from the theoretical curves. Because of the abrupt changes in transmissions coefficients near the critical angle, this difference is expected. Experimental measurements are much more difficult near the critical area and an averaging occurs due to the finite area of the transducer. Figure 3.5 shows the comparison of theoretical reconstructed and experimental results of the transmission amplitude versus frequencies. Results are shown for frequencies from 1 to 10 MHz for the $[90, 0]_S$ lay up carbon/fiber epoxy composite plate. Results for different incident angles (0, 5, 10, 15, 20, 25, 30) are given. The theoretical curves do not match the experimental curves well. It is easy to have large experimental measurement error when the incident wave beam crossed the fiber direction, especially, near the critical angle. Figure 3.6 shows the comparison of theoretical reconstructed and experimental results of transmission amplitude versus frequencies 1 – 10 MHz for the $[0]_{4T}$ lay up carbon/fiber epoxy composite plate at the different incident angles (0, 5, 10, 15, 20, 25, 30). The theoretical curves match the experimental curves well because the simpler material symmetry resulted in more reasonable experimental complexity.

The transmission coefficients versus incident angles for a center frequency of 2.25 MHz are shown in Figures 3.7. The comparison for the $[0, 90]_S$ lay up carbon fiber composite for the visco-elastic model is shown versus experimental results. The curves of Figures 3.8, 3.9 show the comparisons for the $[0]_{4T}$ lay up and the $[90, 0]_S$ lay up carbon fiber composite in the visco-elastic model. In all of these cases the linear visco-elasticity just slightly decreases the amplitude of the transmitted wave. No significant improvement in reproducing the shape of the amplitude curves is evident. This stems at least in part from the isotropic damping model used in the constant. The actual material damping is quite different in the fiber direction due to lower fiber damping compared to the matrix.

3.3.4 Analysis and conclusion

Theoretically reconstructed results and experimental results for the $[0, 90]_S$ lay up carbon fiber composite show reasonable consistency. The incident wave is in the same plane as the fiber direction. Because the visco-elastic matrix is shown to have an effect that is more important than the reinforced carbon fiber, the damping for the composite $[90, 0]_S$ is more than composite $[0, 90]_S$ when an ultrasonic wave impacts the composite surface. For the $[90, 0]_S$ lay up, the incident wave crosses the fiber direction. The carbon fiber has a particularly large effect on the wave propagation in the composite, especially when it functions as a quarter wave layer. In the experiments, the higher the sensitivity of the incident beam to the fiber direction in the samples, and the more complex the symmetry, the worse the comparison to the experimental becomes. For the $[0]_{4T}$ lay up carbon fiber composite, the theoretical and experimental curves show good comparison. The sensitivity of incident wave to fiber direction is the maximum at cross fiber direction in incident top layer. The visco-elastic properties of the composite plate

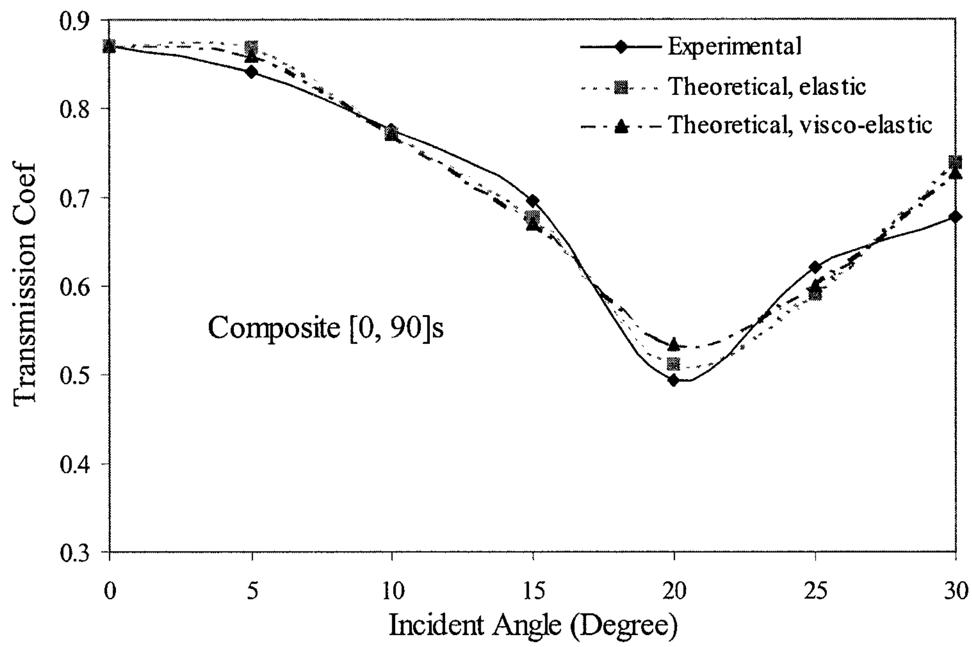

Figure 3.7 Comparison of theoretical reconstructed and experimental results of transmission coefficients versus incident angles for $[0, 90]_S$ lay up carbon fiber composite

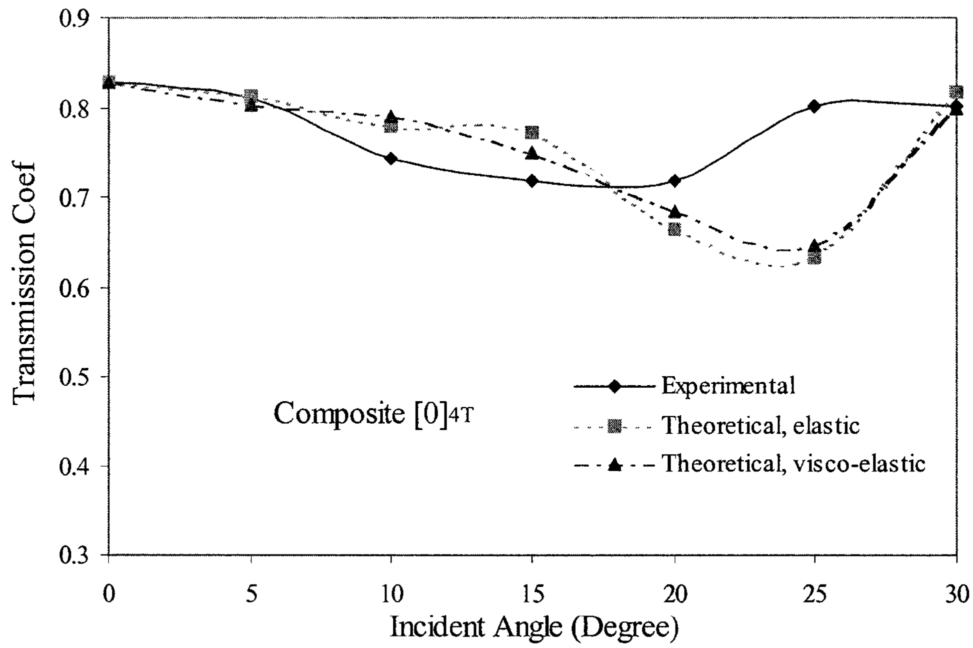

Figure 3.8 Comparison of theoretical reconstructed and experimental results of transmission coefficients versus incident angles for $[0]_{4T}$ lay up carbon fiber composite

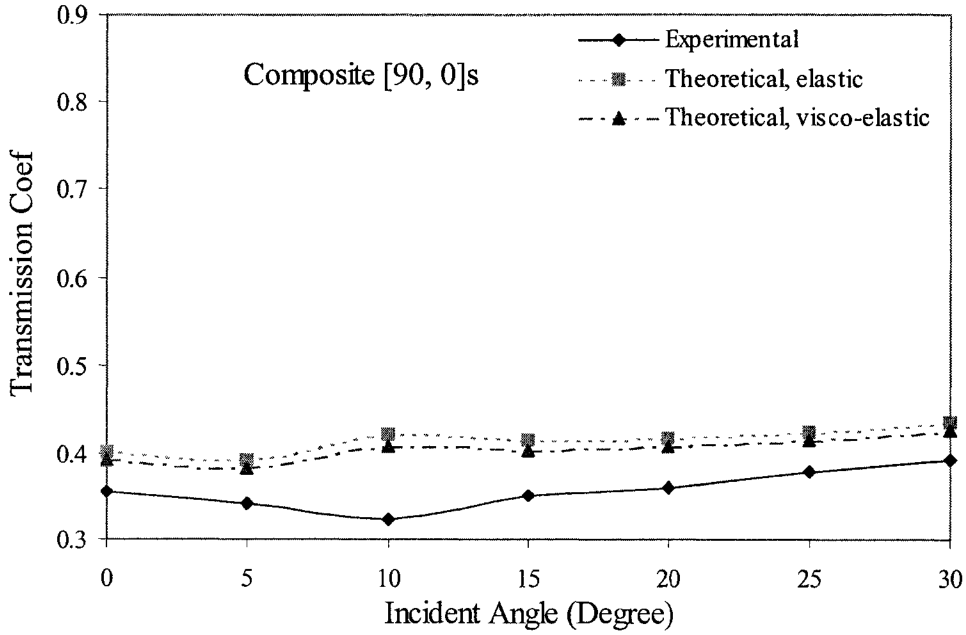

Figure 3.9 Comparison of theoretical reconstructed and experimental results of transmission coefficients versus incident angles for the $[90, 0]_S$ lay up carbon fiber composite

have been studied, theoretically and experimentally. Verification of the model is in good agreement for the simpler cases. For the practical application, the transmission coefficients from theoretical analysis will provide a reasonable gain correction in the reduced axis scanning system configuration.

3.4 References

Brekhovskikh, L. M. And. Godin, O.A, 1990, *Acoustics Of Layered Media I*, Springer-Verlag, New York.

Downs, J., Zhang, P. and Peterson, M. L., 1999, 'A High-Speed High-Resolution Ultrasonic Inspection Machine', IEEE/ASME Transactions on Mechatronics Vol. 4, no. 1, 301-311.

Hosten, Bernard, 1991, 'Reflection and transmission of acoustic plane waves on an immersed orthotropic and visoelastic solid layer', J. Acoust. Soc. Am. 89(6), 2745-2752.

Nayfeh, Adnan H., 1995, *Wave propagation in layered anisotropic media*, Elsvier, New York.

Nayfeh, Adnan H. and Chimenti, D. E., 1989, 'Free Wave Propagation In Plates Of General Anisotropic Media', J. Applied Mechanics, 56, 881-886.

Newell, K. J., Sinclair, A. N. and Fan, Y., 1997, 'Ultrasonic determination of stiffness properties of an orthotropic viscoelastic material', Res. Nondestr. Eval. 9, 25-39.

Shaw, R. P. and Bugl, P., 1968, 'Transmission Of Plane Waves Through Layered Linear Viscoelastic Media', J. Acoust. Soc. Am. 46(3), 649-654.

Zhang, P. and Peterson, M. L., 1998, 'Transmission coefficient for multi-layered structures at arbitrary incident angle', Review of Progress in Quantitative Evaluation, 18.

Appendix A Matrix A Coefficients of Transfer Local Matrix for an Isotropic Material

For isotropic materials, matrix constants are expressed in the solutions of matrix method [Brekhovskih and Godin, 1990]. For each layer, the matrix $A^{(j)}$ coefficients are listed:

$$a_{11} = 2\sin^2\theta_t \cos P + \cos 2\theta_t \sin Q$$

$$a_{12} = i(\tan\theta_l \cos 2\theta_t \sin P - \sin 2\theta_t \sin Q)$$

$$a_{13} = i\sin\theta_t (\cos P - \cos Q)/\omega\rho c_t$$

$$a_{14} = (\tan\theta_l \sin\theta_t \sin P + 2\cos\theta_t \sin Q)/\omega\rho c_t$$

$$a_{21} = i(2\cot\theta_l \sin^2\theta_t \sin P - \tan\theta_t \cos 2\theta_t \sin Q)$$

$$a_{22} = \cos 2\theta_t \cos P + 2\sin^2\theta_t \cos Q$$

$$a_{23} = (\cot\theta_l \sin\theta_t \sin P + \sin\theta_t \tan\theta_t \sin Q)/\omega\rho c_t$$

$$a_{24} = a_{13}$$

$$a_{31} = -2i\omega\rho c_t \sin\theta_t \cos 2\theta_t (\cos Q - \sin P)$$

$$a_{32} = -\omega\rho c_t (\tan\theta_l \cos^2\theta_t \sin P + \sin^2 2\theta_t \tan\theta_t \sin Q)/\sin\theta_t$$

$$a_{33} = a_{22}$$

$$a_{34} = a_{12}$$

$$a_{41} = -\omega\rho c_t [4\cot\theta_l \sin^3\theta_t \sin P + (\cos^2 2\theta_t / \cos\theta_t)\sin Q]$$

$$a_{42} = a_{31}$$

$$a_{43} = a_{21}$$

$a_{44} = a_{11}$

where $P = \alpha\,(z_j - z_{j-1})$, $Q = \beta\,(z_j - z_{j-1})$ and $\alpha = k_l \cos\theta_l$, $\beta = k_t \cos\theta_t$

Appendix B Wave Propagation for Monoclinic Materials (Orthotropic Materials)

B.1 Wave Propagation of an Incident Beam in Fabric Direction Plane for Orthotropic Materials

Wave Propagation in a Single Layer Material

For orthotropic materials, the formal general solutions are written as:

$$(u_1, u_3) = (U_1, U_3)e^{i\zeta(x_1 \sin\theta + \alpha x_3 - vt)} \tag{B.1}$$

Substituting equation (B.1) into motion and constitutive equations, the two coupled eigen-equation are expressed as:

$$K_{mn}(\alpha)U_n = 0\text{, for m, n=1, 3} \tag{B.2}$$

where $[K]$ is a symmetric matrix shown in Appendix C. Substituting the elements of matrix K, the eigen equation is derived as:

$$A_1\alpha^4 + A_2\alpha^2 + A_3 = 0 \tag{B.3}$$

where A_1, A_2, A_3 are $C_{11}, C_{22}, C_{33}, \cdots C_{66}$'s functions shown in Appendix C. Eigen-values α_1, α_2, α_3, α_4 and eigenvectors U_{nq} ($q = 1 \cdots 4$) are obtained by solving the eigen-equation. The eigen-values have the following symmetric properties:

$$\alpha_2 = -\alpha_1,\ \alpha_4 = -\alpha_3 \tag{B.4}$$

The displacements and stresses are expressed as:

$$(u_1, u_3) = \sum_{q=1}^{4} (1, W_q) U_{1q} e^{i\zeta(x_1 \sin\theta + \alpha x_3 - vt)} \tag{B.5}$$

$$(\sigma_1^*, \sigma_3^*) = \sum_{q=1}^{4} (D_{1q}, D_{3q}) U_{1q} e^{i\zeta(x_1 \sin\theta + \alpha x_3 - vt)} \tag{B.6}$$

where W_q, D_{1q}, D_{2q} and D_{3q} are expressed as:

$$W_q = \frac{\rho v^2 - C_{11}\sin^2\theta - C_{55}\alpha_q^{\ 2}}{(C_{13}+C_{55})\alpha_q \sin\theta}$$

$$D_{1q} = C_{13}\sin\theta + C_{33}\alpha_q W_q$$

$$D_{2q} = C_{55}(\alpha_q + W_q \sin\theta)$$

$$\sigma_{ij}^{\ *} = \sigma_{ij} / i\zeta$$

The corresponding matrix form is expressed as:

$$\begin{bmatrix} u_1 \\ u_3 \\ \sigma_{33}^{\ *} \\ \sigma_{13}^{\ *} \end{bmatrix} = \begin{bmatrix} 1 & 1 & 1 & 1 \\ W_1 & -W_1 & W_3 & -W_3 \\ D_{11} & D_{11} & D_{13} & D_{13} \\ D_{21} & -D_{21} & D_{23} & -D_{23} \end{bmatrix} \begin{bmatrix} E_1 & 0 & 0 & 0 \\ 0 & E_2 & 0 & 0 \\ 0 & 0 & E_3 & 0 \\ 0 & 0 & 0 & E_4 \end{bmatrix} \begin{bmatrix} U_{11} \\ U_{12} \\ U_{13} \\ U_{14} \end{bmatrix} \tag{B.7}$$

P is defined as the displacement-stress vector, U is defined as the eigenvector of displacement amplitude and E is defined as a diagonal matrix whose entries are $E_q = e^{i\varsigma\alpha_q x_3}$. Equation (B.7) is rewritten as:

$$P = XEU \tag{B.8}$$

For a single layer, the top P^+, the bottom P^-, the amplitude U is considered as the same inside a layer. So, the top displacement-stress vector is related to the bottom displacement vector:

$$P^+ = AP^-$$

where

$$A = XDX^{-1} \tag{B.9}$$

$$D = [E]_{x=d}$$

Boundary Condition of Solid Continuity

In the interface between layers, boundary conditions are assumed to be continuous, i.e. stresses are continuous, and displacements are continuous. For k layer, the displacement-stress vector across the interface is continuous:

$$P_{k-1}^{\ +} = P_k^{\ -}$$

for multi-layer materials, displacement-vector from the layer 1 to layer 4 is derived as:

$$P^{+} = AP^{-} \tag{B.10}$$

where

$$A = A_4 A_3 A_2 A_1$$

Boundary Condition Between a Solid and Fluid Water

The normal stress and displacement are continuous between the solid layer and the fluid water, but the shear displacement is discontinuous and the shear stress vanishes. The stress and displacement between the layer 4 and fluid water shown are expressed as:

$$\begin{bmatrix} u_1 \\ u_3 \\ \sigma_{33}^{\ *} \end{bmatrix}_4^+ = \begin{bmatrix} 1 & 1 \\ -\alpha_w & \alpha_w \\ \rho_w v^2 \sin\theta & \rho_w v^2 \sin\theta \end{bmatrix} \begin{bmatrix} e^{-i\zeta\alpha_w(x-d)} \\ \mathrm{R}e^{i\zeta\alpha_w(x-d)} \end{bmatrix} \tag{B.11}$$

where $x_3 = d$ is the total thickness of the layers. The stress and displacement between the layer 1 and fluid water are expressed as:

$$\begin{bmatrix} u_1 \\ u_3 \\ \sigma_{33}^{\ *} \end{bmatrix}_1^- = \begin{bmatrix} 1 \\ -\alpha_w \\ \rho_w v^2 \sin\theta \end{bmatrix} T e^{-i\zeta\alpha_w x_3} \tag{B.12}$$

Transmission Coefficients

The continuous boundary condition from layer 1 to layer 4 shown in Figure 2.1 results in equation (B.10) for orthotropic materials, the boundary condition between a solid and fluid water results in equation (B.11) and (B.12). When the elastic wave propagates from coupled water to multilayered materials, the matrix equation is rewritten as:

$$\begin{bmatrix} u_3 \\ \sigma_{33}^{\ *} \end{bmatrix}_4^+ = \begin{bmatrix} M_{11} & M_{12} \\ M_{21} & M_{22} \end{bmatrix} \begin{bmatrix} u_3 \\ \sigma_{33}^{\ *} \end{bmatrix}_1^- \tag{B.13}$$

where:

$$M_{11} = -A_{41}^{\ -1} \begin{vmatrix} A_{21} & A_{22} \\ A_{41} & A_{42} \end{vmatrix}, \quad M_{12} = -A_{41}^{\ -1} \begin{vmatrix} A_{21} & A_{23} \\ A_{41} & A_{43} \end{vmatrix}$$

$$M_{21} = -A_{41}^{-1}\begin{vmatrix} A_{31} & A_{32} \\ A_{41} & A_{42} \end{vmatrix},\; M_{22} = -A_{41}^{-1}\begin{vmatrix} A_{31} & A_{33} \\ A_{41} & A_{43} \end{vmatrix}$$

substituting the boundary conditions (B.12) and (B.13), the expressions of the transmission coefficients and reflection coefficients are derived as:

$$T = \frac{2\rho_w v^2 \alpha_w}{(M_{11} + M_{22})\rho_w v^2 \alpha_w - (M_{21}\alpha_w^{\;2} + M_{12}(\rho_w v^2)^2)} \tag{B.14a}$$

$$R = \frac{M_{12}(\rho_w v^2)^2 + \rho_w v^2 \alpha_w M_{22} - \alpha_w^{\;2} M_{21} - \rho_w v^2 \alpha_w M_{11}}{(M_{11} + M_{22})\rho_w v^2 \alpha_w - (M_{21}\alpha_w^{\;2} + M_{12}(\rho_w v^2)^2)} \tag{B.14b}$$

B.2 Wave Propagation of Incident Beam in Non-Fabric Direction Plane for Orthotropic Materials

Wave propagation in a single layer

For monoclinic material, a general solution for the displacement u_i is supposed:

$$(u_1, u_2, u_3) = (U_1, U_2, U_3)e^{i\zeta(x_1 \sin\theta + \alpha x_3 - vt)} \tag{B.15}$$

U_1, U_2 *and* U_3 are the amplitudes of the displacements, v is the wave phase velocity, ζ is the wave-number, θ is the incident beam angle, α is an unknown variable related to the velocity, wave-number and incident beam angle.

Substituting equation (B.15) into motion and constitutive equations, the three coupled eigen-equations are expressed as:

$$K_{mn}(\alpha)U_n = 0, \text{ for m, n=1, 2, 3} \tag{B.16}$$

where $[K]$ is symmetric matrix shown in Appendix C, by substituting the elements of matrix K, the eigen equation is derived as:

$$\alpha^6 + A_1\alpha^4 + A_2\alpha^2 + A_3 = 0 \tag{B.17}$$

where A_1, A_2, A_3 are $C_{11}, C_{22}, C_{33}, \cdots C_{66}$'s functions shown in Appendix C. Eigen-values α_1, α_2, α_3, α_4, α_5, α_6 are from the equation (B.17) and eigen-values U_{nq} are from equation (B.16). From the symmetric property of monoclinic materials, the solutions of the eigen-equation have the following property:

$$\alpha_2 = -\alpha_1,\; \alpha_3 = -\alpha_4,\; \alpha_5 = -\alpha_6 \tag{B.18}$$

where α_1, α_3 and α_5 correspond to the reflection waves of three coupled, and α_2, α_4, and α_6 correspond to the incident waves for the layered structure shown in figure 2.1. The displacement and stress can be expressed as:

$$\begin{bmatrix} u_1 \\ u_2 \\ u_3 \\ \sigma_{33}^* \\ \sigma_{13}^* \\ \sigma_{23}^* \end{bmatrix} = \begin{bmatrix} 1 & 1 & 1 & 1 & 1 & 1 \\ V_1 & V_1 & V_3 & V_3 & V_5 & V_5 \\ W_1 & -W_1 & W_3 & -W_3 & W_5 & -W_5 \\ D_{11} & D_{11} & D_{13} & D_{13} & D_{15} & D_{15} \\ D_{21} & -D_{21} & D_{23} & -D_{23} & D_{25} & -D_{25} \\ D_{31} & -D_{31} & D_{33} & -D_{33} & D_{35} & -D_{35} \end{bmatrix} \begin{bmatrix} E_1 & 0 & 0 & 0 & 0 & 0 \\ 0 & E_2 & 0 & 0 & 0 & 0 \\ 0 & 0 & E_3 & 0 & 0 & 0 \\ 0 & 0 & 0 & E_4 & 0 & 0 \\ 0 & 0 & 0 & 0 & E_5 & 0 \\ 0 & 0 & 0 & 0 & 0 & E_6 \end{bmatrix} \begin{bmatrix} U_{11} \\ U_{12} \\ U_{13} \\ U_{14} \\ U_{15} \\ U_{16} \end{bmatrix}$$

(B.19)

where

$$\sigma_{ij}^* = \sigma_{ij} / i\zeta$$

$$E_q = e^{i\zeta\alpha_q x_3}$$

$$D_{1q} = C_{13}\sin\theta + C_{36}V_q\sin\theta + C_{33}\alpha_q W_q$$

$$D_{2q} = C_{55}(\alpha_q + W_q\sin\theta) + C_{45}\alpha_q V_q$$

$$D_{3q} = C_{45}(\alpha_q + W_q\sin\theta) + C_{44}\alpha_q V_q$$

$$V_q = \frac{K_{11}(\alpha_q)K_{23}(\alpha_q) - K_{13}(\alpha_q)K_{12}(\alpha_q)}{K_{13}(\alpha_q)K_{22}(\alpha_q) - K_{12}(\alpha_q)K_{23}(\alpha_q)}$$

$$W_q = \frac{K_{11}(\alpha_q)K_{23}(\alpha_q) - K_{12}(\alpha_q)K_{13}(\alpha_q)}{K_{13}(\alpha_q)K_{33}(\alpha_q) - K_{23}(\alpha_q)K_{13}(\alpha_q)}$$

$$q = 1, 2, 3, ..., 6$$

Similarly, P is defined as the displacement-stress vector, U is defined as the eigen-vector of displacement amplitude, and E is defined as diagonal matrix whose entries are E_q. Equation (B.19) is rewritten as:

$$P = XEU \qquad \text{(B.20)}$$

and

$$P^+ = AP^-$$

Boundary conditions

In the interface between solid layers, boundary conditions are assumed to be continuous, i.e. stresses are continuous, and displacements are continuous. For the k layer, the displacement-stress vector across the interface is continuous:

$$P_{k-1}{}^{+} = P_k{}^{-}$$

and

$$P^+ = AP^- \tag{B.21}$$

The boundary condition between solid and fluid water is the same as in the orthotropic case. The continuous boundary condition from layer 1 to layer 4 shown in figure 2.1 results in equation (B.21) for monoclinic materials. The displacement and stress are derived as:

$$\begin{bmatrix} u_3{}^{(5)} \\ \sigma_{33}{}^{*(5)} \end{bmatrix} = \begin{bmatrix} M_{11} & M_{12} \\ M_{21} & M_{22} \end{bmatrix} \begin{bmatrix} u_3{}^{(1)} \\ \sigma_{33}{}^{*(1)} \end{bmatrix} \tag{B.22}$$

where:

$$M_{11} = |A|^{-1} \begin{vmatrix} A_{31} & A_{32} & A_{33} \\ A_{51} & A_{52} & A_{53} \\ A_{61} & A_{62} & A_{63} \end{vmatrix}, \; M_{12} = |A|^{-1} \begin{vmatrix} A_{31} & A_{32} & A_{34} \\ A_{51} & A_{52} & A_{54} \\ A_{61} & A_{62} & A_{64} \end{vmatrix} \tag{B.23}$$

$$M_{21} = |A|^{-1} \begin{vmatrix} A_{41} & A_{42} & A_{43} \\ A_{51} & A_{52} & A_{53} \\ A_{61} & A_{62} & A_{63} \end{vmatrix}, \; M_{22} = |A|^{-1} \begin{vmatrix} A_{41} & A_{42} & A_{44} \\ A_{51} & A_{52} & A_{54} \\ A_{61} & A_{62} & A_{64} \end{vmatrix} \tag{B.24}$$

$$|A| = \begin{vmatrix} A_{51} & A_{52} \\ A_{61} & A_{62} \end{vmatrix}$$

The boundary conditions are substituted, and the expressions of the transmission coefficients and reflection coefficients are the same as equation (B.14a), (B.14b).

Appendix C Coefficients of Eigen-matrix K

C.1 Coefficients of Eigen-matrix K for Orthotropic Materials

The coefficients of eigen-matrix K are expressed as:

$$K_{11} = C_{11}\sin^2\theta - \rho v^2 + C_{55}\alpha^2$$

$$K_{13} = (C_{13} + C_{55})\alpha\sin\theta \tag{C.1}$$

$$K_{33} = C_{55}\sin^2\theta - \rho v^2 + C_{33}\alpha^2$$

The determinant of eigen matrix K is a 4th order function of α. The coefficients of the eigen equation are the functions of material constants.

$$A_1 = C_{33}C_{55}$$

$$A_2 = C_{55}\left(C_{55}\sin^2\theta - \rho v^2\right) + C_{33}\left(C_{11}\sin^2\theta - \rho v^2\right) - \left(C_{13} + C_{55}\right)^2\sin^2\theta$$

$$A_3 = \left(C_{55}\sin^2\theta - \rho v^2\right)\left(C_{11}\sin^2\theta - \rho v^2\right)$$

C.2 Coefficients of Eigen-matrix K for Monoclinic Materials

The coefficients of eigen-matrix K for monoclinic materials are expressed as:

$$K_{11} = C_{11}\sin^2\theta - \rho v^2 + C_{55}\alpha^2$$

$$K_{12} = C_{16}\sin^2\theta + C_{45}\alpha^2$$

$$K_{13} = (C_{13} + C_{55})\alpha\sin\theta$$

$$K_{22} = C_{66}\sin^2\theta - \rho v^2 + C_{44}\alpha^2 \tag{C.2}$$

$$K_{23} = (C_{36} + C_{45})\alpha\sin\theta$$

$$K_{33} = C_{55}\sin^2\theta - \rho v^2 + C_{33}\alpha^2$$

The determinant of eigen matrix K is a 6th order function of α, and the coefficients of the eigen equation are the functions of material constants. The eigen equation is expressed as:

$$\alpha^6 + A_1\alpha^4 + A_2\alpha^2 + A_3 = 0$$

the expressions of coefficients for monoclinic materials follow:

$$\Delta = C_{33}C_{44}C_{55} - C_{45}{}^2C_{33}$$

$$A_1 = [(C_{11}C_{33}C_{44} + C_{33}C_{55}C_{66} - C_{55}C_{36}{}^2 - C_{13}{}^2C_{44} + 2C_{13}C_{36}C_{45} - 2C_{16}C_{33}C_{45} + 2C_{13}C_{45}{}^2 - 2C_{13}C_{44}C_{55})\sin^2\theta - (C_{33}C_{44} + C_{33}C_{55} + C_{44}C_{55} - C_{45}{}^2)\rho v^2]/\Delta$$

$$A_2 = [(C_{55} + C_{44} + C_{33})(\rho v^2)^2 + (C_{13}{}^2 + C_{45}{}^2 + C_{36}{}^2 - C_{11}C_{33} - C_{11}C_{44} - C_{33}C_{66} - C_{44}C_{55} - C_{55}C_{66} + 2C_{13}C_{55} + 2C_{36}C_{45} + 2C_{45}C_{16})\sin^2\theta\,\rho v^2 - (C_{11}C_{45}{}^2 + C_{11}C_{36}{}^2 + C_{33}C_{16}{}^2 + C_{66}C_{13}{}^2 - C_{11}C_{33}C_{66} - C_{11}C_{44}C_{55} - 2C_{55}C_{16}C_{36} - 2C_{13}C_{16}C_{36} - 2C_{13}C_{16}C_{45} + 2C_{13}C_{55}C_{66} + 2C_{11}C_{36}C_{45})\sin^4\theta]/\Delta$$

$$A_3 = [(C_{11}C_{55}C_{66} - C_{16}{}^2C_{55})\sin^6\theta - (C_{11}C_{55} + C_{11}C_{66} + C_{55}C_{66} - C_{16}{}^2)\sin^4\theta\,\rho v^2 + (C_{11} + C_{55} + C_{66})\sin^2\theta\,(\rho v^2)^2 - (\rho v^2)^3]/\Delta$$

Appendix D Experimental Procedures of Material Properties for Orthotropic Material

Part A Procedures for E_1, G_{13}, G_{23} Measurement

Procedure for G_{13} measurement

I. System setup

The experimental system is shown in figure 2.7

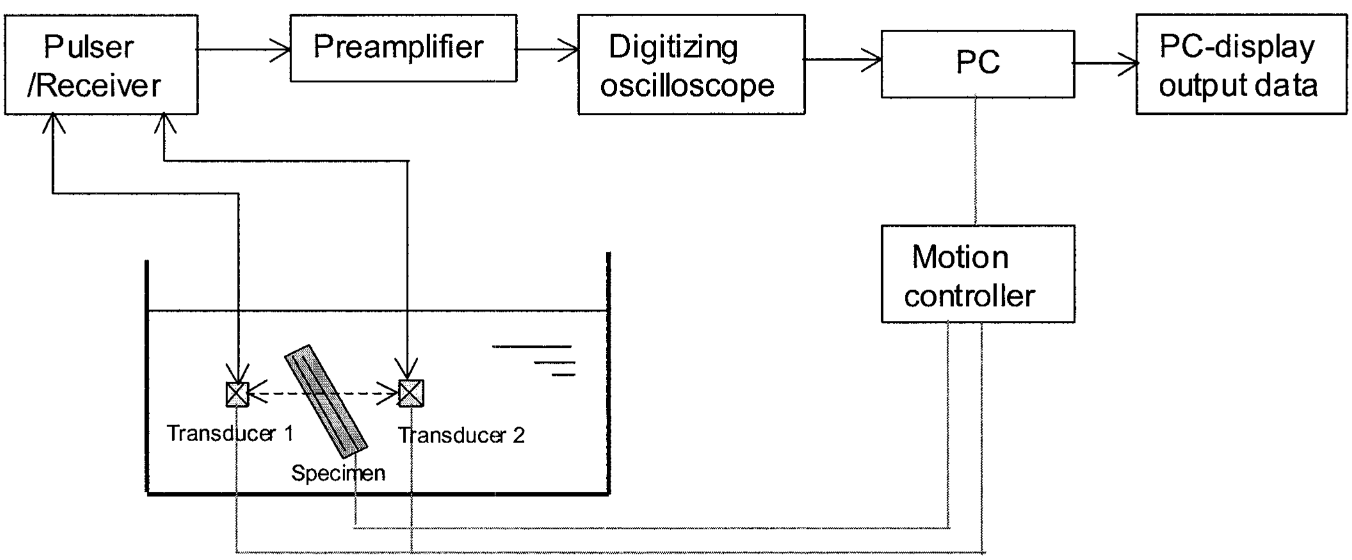

Figure D.1 Experimental apparatus system

1) Pulser/receiver

2) Transducer

3) Preamplifier

4) Digitizing oscilloscope

5) Water tank

6) Personal computer and monitor

II. Operation

1) Turn on power

2) Turn on motion controller

3) Turn on pulser/receiver

4) Turn on preamplifier

5) Turn on digitizing oscilloscope

6) Turn on personal computer and monitor

III. Adjust:

1) Pulser/receiver, delay attenuate to suitable signal

2) Adjust specimen, transducers to suitable place by the motion controller

3) Adjust preamplifier, suitable signal is shown in the oscilloscope screen

4) PC record the signals

IV. Specimen measurement

1. Adjust motion controller:

Purpose: To acquire a transverse wave while transducer 2 is moved along vertical direction. Incident angle is related to refracted angle by Snell's law:

$$\frac{\sin\theta_i}{c_i} = \frac{\sin\theta_{rl}}{c_l} = \frac{\sin\theta_{rt}}{c_t}$$

1) Specimen oblique about 50^0 or more at transducer direction in order to obtain transverse wave of specimen for epoxy material.

2) Fiber direction parallel to paper plane shown in figure

3) Move the transducer 2 acquire the maximum signal

4) Record the signal from PC

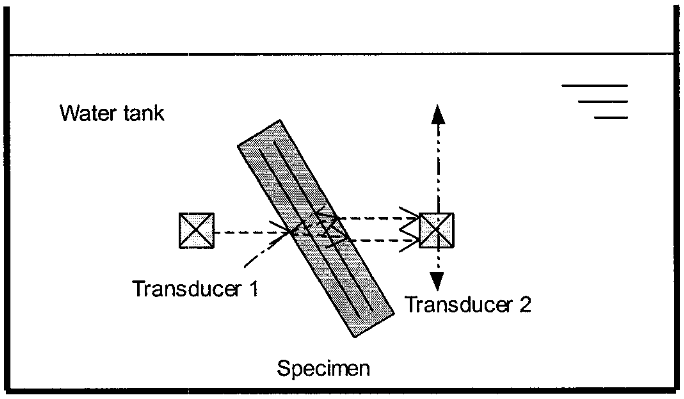

Figure D.2 Water tank for measurement of material constants

2. Signal without specimen

Transducer 1 and transducer 2 align, and acquire the signal by the computer

3. Specimen thickness

Measured by micrometer

V. Computer operation

1) Time delay =0

2) Record point =2500 points

3) Channel choice for input and output

4) Record into a disk

V. Data sheet for G_{13} measurement

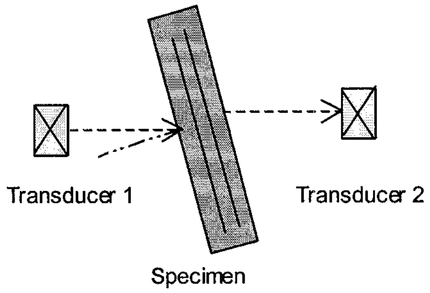

Figure D.3 Specimen and transducers

Specimen No:__________________________

1. Incident angle θ:____________________ ^{0} Fiber direction: Shown as figure D.3

2. Through-transmission signal with specimen is saved on a disk.

   Disk No: _______________ File name:__________________

3. Through-transmission signal without specimen is saved on a disk (Transverse wave signal)

   Disk No: _______________ File name:__________________

4. Specimen thickness: _______________________ mm

Procedure for G_{23} measurement

I. System setup

The same as G_{13} measurement

II. Operation

The same as G_{13} measurement

III. Specimen measurement

1. Adjust motion controller:

   1) Specimen oblique about 50^0 or more at transducer direction in order to obtain transverse wave of specimen for epoxy material

   2) Fiber direction perpendicular to paper plane shown in figure

   3) Move the transducer 2 acquire the maximum signal

   4) Record the signal from PC

2. Signal without specimen

   Transducer 1 and transducer 2 are aligned, and acquire the signal by computer

3. Specimen thickness

   Measured by micrometer

IV. Computer operation

   1) Time delay =0

   2) Record point =2500 points

   3) Channel choice for input and output

   4) Record into disk

V. Data sheet for G_{23} measurement

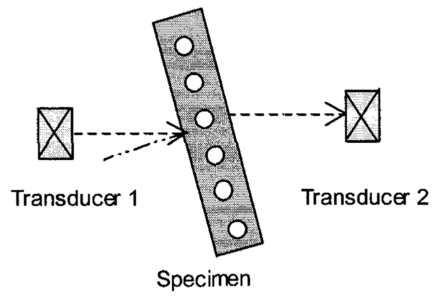

Figure D.4 Transducers and specimen at perpendicular fiber direction

Specimen No:____________________

1. Incident angle θ:_______________ ^{0} Fiber direction: perpendicular to paper

2. Through-transmission signal with specimen is saved on disk.

   Disk No: ______________ File name:________________

3. Through-transmission signal without specimen is saved on disk (Transverse wave signal)

   Disk No: ______________ File name:________________

4. Specimen thickness: ____________________ mm

VI. Data sheet for E_3 measurement

Procedure is the same as procedure for G_{13}, G_{23} measurement. But incident angle equal to 0^0

Specimen No:__________________________

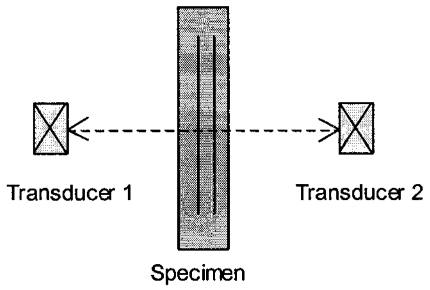

Figure D.5 Specimen and transducers at parallel fiber direction.

1. Incident angle θ: 0 _______________ ^{0} Fiber direction: parallel to paper
2. Through-transmission signal with specimen is saved on disk.

   Disk No: _______________ File name:__________________

3. Through-transmission signal without specimen is saved on disk

   Disk No: _______________ File name:__________________

4. Specimen thickness: _______________________ mm

Part B Procedures for E_1, E_2 measurement

E_1 and E_2 measurement by plate wave method

1. Plate wave is excited in specimen at low frequency in order to measure elastic modulus E_1 and E_2. The so called low frequency is the frequency of an incident wave while the incident wavelength is large greater than fiber diameter, i.e $\lambda_i >> \lambda_f$, approximately let $\lambda_i \approx 10\lambda_f$, generally, $\lambda_i \approx 50$ KHz

2. System setup

   The ultrasonic system is the same as the system of E_3 measurement, but setup of the transducers and specimen are like figure D.1

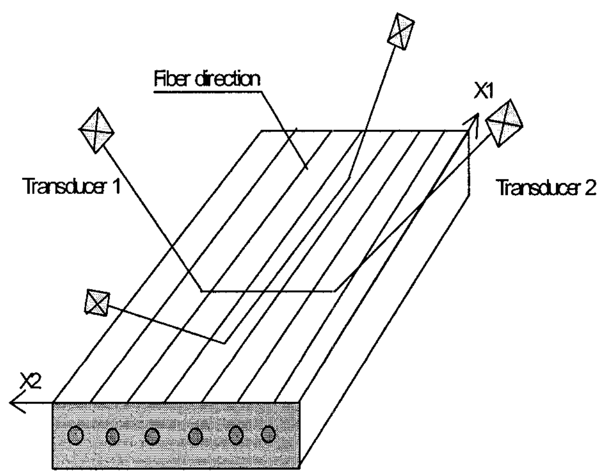

Figure D.6. Transducers and specimen for plate wave

3. E_2 measurement by propagation of ultrasonic wave cross fiber direction along x_2 direction

   1) Specimen is immersed in water, is set down horizontally.

   2) Transducer 1 acts as transmitter that transmits ultrasonic signal. Transducer 2 acts as receiver that receives ultrasonic signal.

   3) Orientation of transducers

      a) Incident angle θ lies in $x_2 - x_3$ plane.

b) Orientation angle $-\theta$ of received signal lies at incident beam plane in $x_2 - x_3$ plane

4) Keep transducer 1 and transducer 2 the same height, keep the distance between transducer 1 and transducer 2 in order to measure plate wave along plate direction $-x_2$.

5) Record the received ultrasonic signal

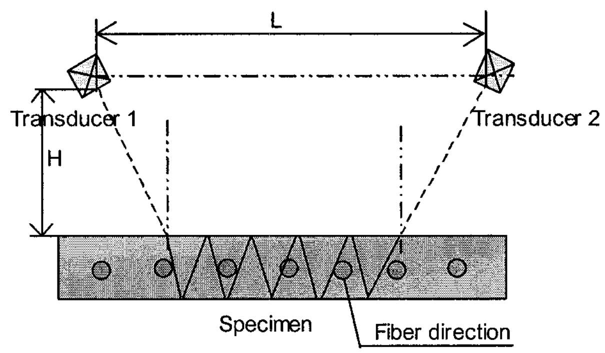

Figure D.7 Wave propagation cross fiber direction

4. E_1 measurement by propagation of ultrasonic wave along fiber direction, i.e. along x_1 direction

1) Specimen is immersed in water, is set down horizontally.

2) Transducer 1 acts as a transmitter that transmits ultrasonic signal. Transducer 2 acts as a receiver that receives ultrasonic signal.

3) Orientation of transducers

a) Incident angle θ lies in $x_1 - x_3$ plane.

b) Orientation angle $-\theta$ of received signal lies at incident beam plane in $x_1 - x_3$ plane

4) Keep transducer 1 and transducer 2 the same height, keep the distance between transducer 1 and transducer 2 in order to measure plate wave along plate direction $-x_1$.

5) Record the received ultrasonic signal

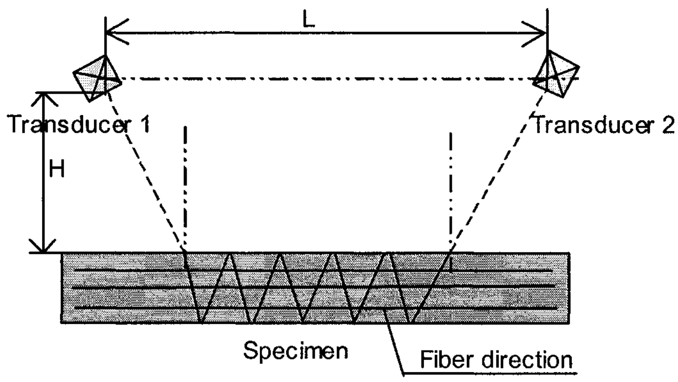

Figure D.8 Wave propagation along fiber direction

DATA SHEET

1. Specimen No.________________

   Fiber direction: Perpendicular to paper direction shown in figure 2

2. Incident angle of transducer 1: ____________________ ^{0}

   Adjust transducer 2 to keep opposite incident angle.

3. Incident frequency: ________________ KHz

4. Distance between transducer 1 and transducer 2: __________________ mm

5. Height between the center of excitation surface of transducers and the top surface of specimen: __________________ mm

6. Record the received signal of transducer 2 on disk

   Disk No.: ______________

   File name of received signal: __________________

DATA SHEET

1. Specimen No.___________________

   Fiber direction: Parallel to paper direction shown in figure 3

2. Incident angle of transducer 1: _____________________ ^{0}

   Adjust transducer 2 to keep opposite incident angle.

3. Incident frequency: _________________ KHz

4. Distance between transducer 1 and transducer 2: ___________________ mm

5. Height between the center of excitation surface of transducers and the top surface of specimen:___________________ mm

6. Record the received signal of transducer 2 on disk

   Disk No.:______________

   File name of received signal: __________________

Part C Procedures for Attenuation Measurement

Longitudinal wave attenuation – immersion method

Measurement of attenuation for visco-elastic properties

1. Attenuation of longitude wave with specimen by immersed in water. Specimen is immersed in water. Method: measurement of transmission with specimen, without specimen and reflection with specimen and with smooth, large impedance hard surface.

1) Measurement with specimen.

   a) Transducer 1 acts as a transmitter, transducer 2 acts as a receiver, record the signal of transmitted $y_{12}(t)$.

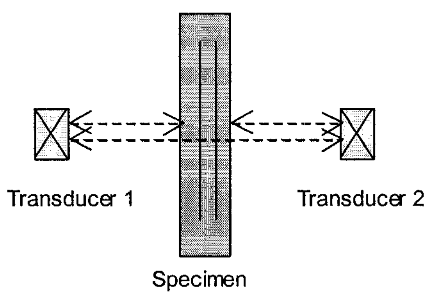

Figure D.9 Transducer and Specimen

   b) Transducer 2 acts as a transmitter, transducer 1 acts as a receiver, record the signal of transmitted $y_{21}(t)$

   c) Transducer 1 acts as both transmitter and receiver, record the reflected signal $r_{11}(t)$

   d) Transducer 2 acts as both a transmitter and a receiver, record the reflected signal $r_{22}(t)$

2) Measurement without specimen

a) Transducer 1 acts as transmitter, transducer 2 acts as receiver, record the transmitted signal $y_{w12}(t)$

b) Transducer 2 acts as a transmitter, transducer 1 acts as a receiver, record the transmitted signal $y_{w21}(t)$

3) Measurement with smooth, large impedance hard surface comparison with water such as steel, copper... and so on, reflection coefficient approximately equal to 1

a) Transducer 1 acts as both a transmitter and a receiver, record the reflected signal $r_{m11}(t)$

b) Transducer 2 acts as both a transmitter and a receiver, record the reflected signal $r_{m22}(t)$

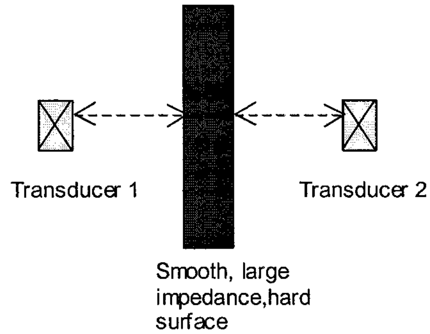

Figure D.10 Reflected measurement for large impedance, smooth hard surface

DATA SHEET FOR ATTENUATION OF LONGITUDE WAVE

1. Record transmitted signal from transducer 1 to transducer 2

   File name: ____________________ Disk #: ____________________

2. Record transmitting signal from transducer 2 to transducer 1

   File name: ____________________ Disk #: ____________________

3. Record reflected signal from transducer 1 to specimen

   File name: ____________________ Disk #: ____________________

4. Record reflected signal from transducer 2 to specimen

   File name: ____________________ Disk #: ____________________

5. Transmitted signal from transducer 1 to transducer 2 without specimen

   File name: ____________________ Disk #: ____________________

6. Transmitted signal from transducer 2 to transducer 1 without specimen

   File name: ____________________ Disk #: ____________________

7. Record reflected signal from transducer 1 to smooth, large impedance hard surface

   File name: ____________________ Disk #: ____________________

8. Record reflected signal from transducer 2 to smooth, large impedance hard surface

   File name: ____________________ Disk #: ____________________

Shear wave attenuation – contact method

Attenuation of transverse wave with specimen is measured by contact method. Specimen is directly contacted with perpex as buffer. Shear transducer is directly contacted with perpex. Method: measurement of transmission with specimen, without specimen and reflection with specimen and with smooth, large impedance hard surface.

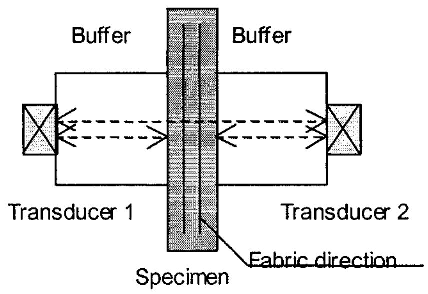

Figure D.11 Contact transducer and specimen

1) Measurement with specimen, fabric direction parallel to paper

   a) Transducer 1 acts as a transmitter, transducer 2 acts as a receiver, record the signal of transmitted $y_{12}(t)$

   b) Transducer 2 acts as a transmitter, transducer 1 acts as a receiver, record the signal of transmitted $y_{21}(t)$

   c) Transducer 1 acts as both transmitter and receiver, record the reflected signal $r_{11}(t)$

   d) Transducer 2 acts as both a transmitter and a receiver, record the reflected signal $r_{22}(t)$

2) Measurement without specimen

   a) Transducer 1 acts as transmitter, transducer 2 acts as receiver, record the transmitted signal $y_{p12}(t)$

   b) Transducer 2 acts as a transmitter, transducer 1 acts as a receiver, record the transmitted signal $y_{p21}(t)$

3) Measurement with smooth, large impedance hard surface comparison with water such as steel, copper… and so on, reflection coefficient approximately equal to 1

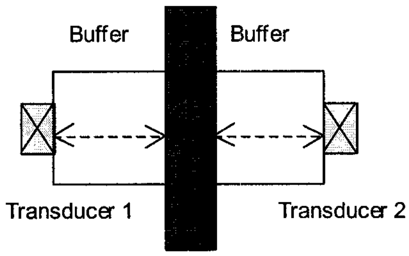

Figure D.12. Reflected measurement for large impedance, smooth hard surface

a) Transducer 1 acts as both a transmitter and a receiver, record the reflected signal $r_{m11}(t)$

b) Transducer 2 acts as both a transmitter and a receiver, record the reflected signal $r_{m22}(t)$

DATA SHEET FOR ATTENUATION OF TRANSVERSE WAVE
(FABRIC DIRECTION PARALLELS TO PAPER)

1. Record transmitted signal from transducer 1 to transducer 2

   File name: ____________________ Disk #: ____________________

2. Record transmitting signal from transducer 2 to transducer 1

   File name: ____________________ Disk #: ____________________

3. Record reflected signal from transducer 1 to specimen

   File name: ____________________ Disk #: ____________________

4. Record reflected signal from transducer 2 to specimen

   File name: ____________________ Disk #: ____________________

5. Transmitted signal from transducer 1 to transducer 2 without specimen

   File name: ____________________ Disk #: ____________________

6. Transmitted signal from transducer 2 to transducer 1 without specimen

   File name: ____________________ Disk #: ____________________

7. Record reflected signal from transducer 1 to smooth, large impedance hard surface

   File name: ____________________ Disk #: ____________________

8. Record reflected signal from transducer 2 to smooth, large impedance hard surface

   File name: ____________________ Disk #: ____________________

DATA SHEET FOR ATTENUATION OF TRANSVERSE WAVE
(FABRIC DIRECTION PERPENDICULAR TO PAPER)

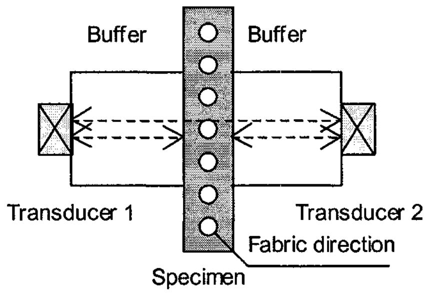

Figure D.13. Attenuation measurement for different fabric directions

1. Record transmitted signal from transducer 1 to transducer 2

   File name: ____________________ Disk #: ____________________

2. Record transmitting signal from transducer 2 to transducer 1

   File name: ____________________ Disk #: ____________________

3. Record reflected signal from transducer 1 to specimen

   File name: ____________________ Disk #: ____________________

4. Record reflected signal from transducer 2 to specimen

   File name: ____________________ Disk #: ____________________

5. Transmitted signal from transducer 1 to transducer 2 without specimen

   File name: ____________________ Disk #: ____________________

6. Transmitted signal from transducer 2 to transducer 1 without specimen

   File name: ____________________ Disk #: ____________________

7. Record reflected signal from transducer 1 to smooth, large impedance hard surface

   File name: ____________________ Disk #: ____________________

8. Record reflected signal from transducer 2 to smooth, large impedance hard surface

   File name: ____________________ Disk #: ____________________

Appendix E Relations Between Engineering Constants and Stiffness Elastic Coefficients

$$C_{11} = \frac{E_1(1-\upsilon_{23}\upsilon_{32})}{\Delta}$$
$$C_{12} = \frac{E_1(\upsilon_{21}+\upsilon_{23}\upsilon_{31})}{\Delta}$$
$$C_{13} = \frac{E_1(\upsilon_{31}+\upsilon_{21}\upsilon_{32})}{\Delta}$$
$$C_{21} = \frac{E_2(\upsilon_{12}+\upsilon_{13}\upsilon_{32})}{\Delta}$$
$$C_{22} = \frac{E_2(1-\upsilon_{13}\upsilon_{31})}{\Delta}$$
$$C_{23} = \frac{E_2(\upsilon_{12}\upsilon_{31}+\upsilon_{32})}{\Delta}$$
$$C_{31} = \frac{E_3(\upsilon_{13}+\upsilon_{12}\upsilon_{23})}{\Delta}$$
$$C_{23} = \frac{E_3(\upsilon_{13}\upsilon_{21}+\upsilon_{23})}{\Delta}$$
$$C_{33} = \frac{E_3(1-\upsilon_{12}\upsilon_{21})}{\Delta}$$
$$\Delta = 1-\upsilon_{12}\upsilon_{21}-\upsilon_{13}\upsilon_{31}-\upsilon_{12}\upsilon_{23}\upsilon_{31}-\upsilon_{13}\upsilon_{21}\upsilon_{32}-\upsilon_{23}\upsilon_{32}$$

and,

$$C_{44} = G_{23},\ \ C_{55} = G_{13}, C_{66} = G_{12}$$

also,

$$\frac{\upsilon_{21}}{E_2} = \frac{\upsilon_{12}}{E_1},\ \frac{\upsilon_{31}}{E_3} = \frac{\upsilon_{13}}{E_1},\ \ \frac{\upsilon_{23}}{E_2} = \frac{\upsilon_{32}}{E_3}$$

E is a Young's modulus, G is a shear modulus, ν is a Poisson ratio.

Appendix F Comparisons of Figures and Results for Calculated and Previous Works

Instruction

The calculations of transmission coefficients and reflection coefficients are completed by C++ program, which is programmed following the flow chart shown in Figure 2.2. The figures in the following sections are for comparisons the calculated results by the C++ program with the papers [Kriz, 1979, Chimenti, 1990], and for verifications of the availability of the programs for the wave propagation in multi-layered materials.

Figures and Comparison for Composite Materials

Input data is from reference [Chimenti, 1990] for composite structure $[0_2\ 90_2]_S$ and $[0\ 90]_S$ lay up

$$C = \begin{bmatrix} 161 & 6.5 & 6.5 & 0 & 0 & 0 \\ 6.5 & 14.5 & 7.24 & 0 & 0 & 0 \\ 6.5 & 7.24 & 14.5 & 0 & 0 & 0 \\ 0 & 0 & 0 & 3.63 & 0 & 0 \\ 0 & 0 & 0 & 0 & 7.1 & 0 \\ 0 & 0 & 0 & 0 & 0 & 7.1 \end{bmatrix} GPa$$

$$\rho = 1610.kg/m^3$$

and

$$d = 1.0\ mm$$

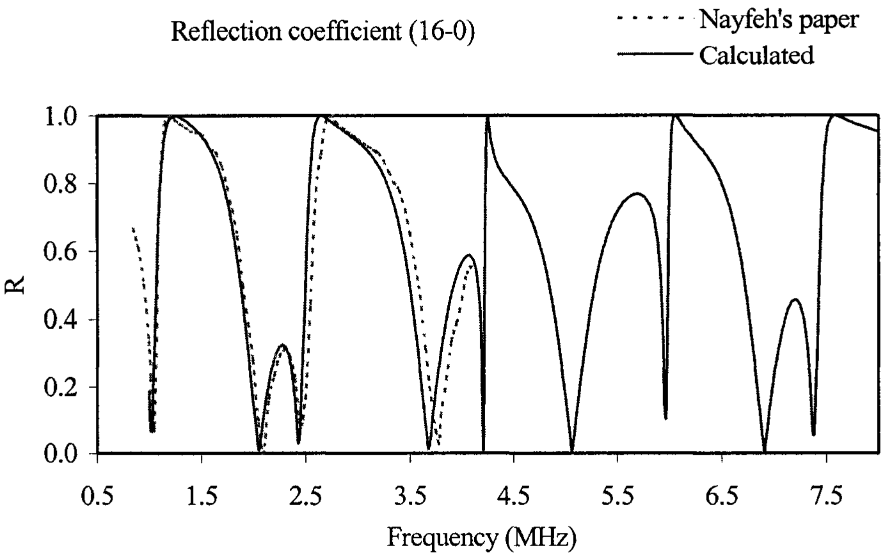

Figure F.1 Reflection spectrum for fluid coupled composite laminate with $\theta = 16^0$ and the fiber direction in the uppermost ply contained in the incident plane $\phi = 0^0$ for the $[0_2\ 90_2]_s$ (Nayfeh's scale is 9.0). Black curve is drawn in terms of data picked up from Chimenti and Nayfeh's paper. Red cure is drawn in terms of calculated data from the C++ program.

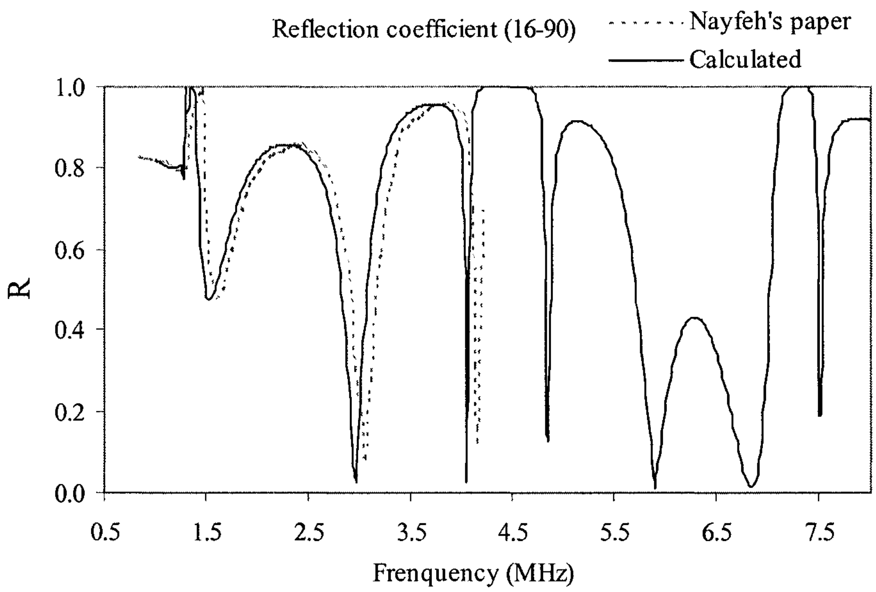

Figure F.2 Reflection spectrum for fluid coupled composite laminate with $\theta = 16^0$ and the fiber direction in the uppermost ply perpendicular to the incident plane $\phi = 90^0$ for the $[0_2\ 90_2]_s$ (Nayfeh's scale is 1.0 [2])

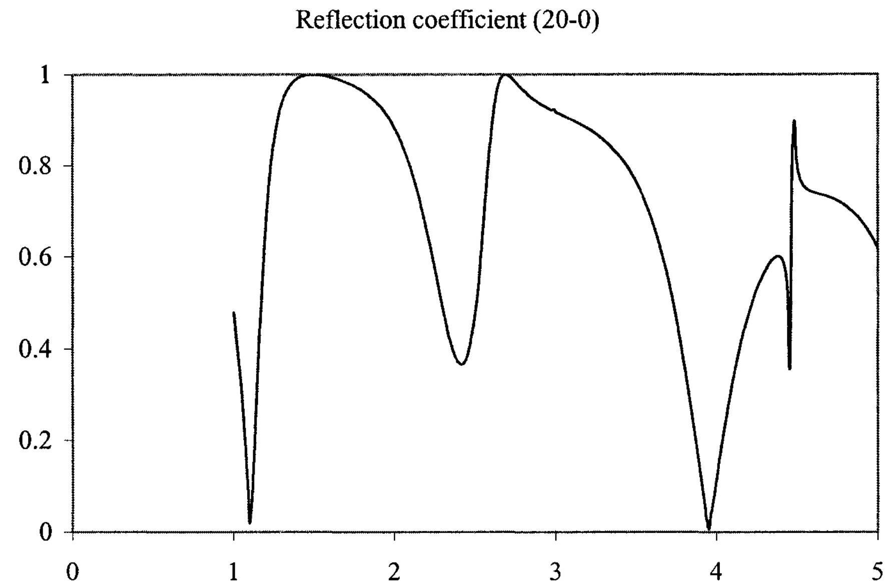

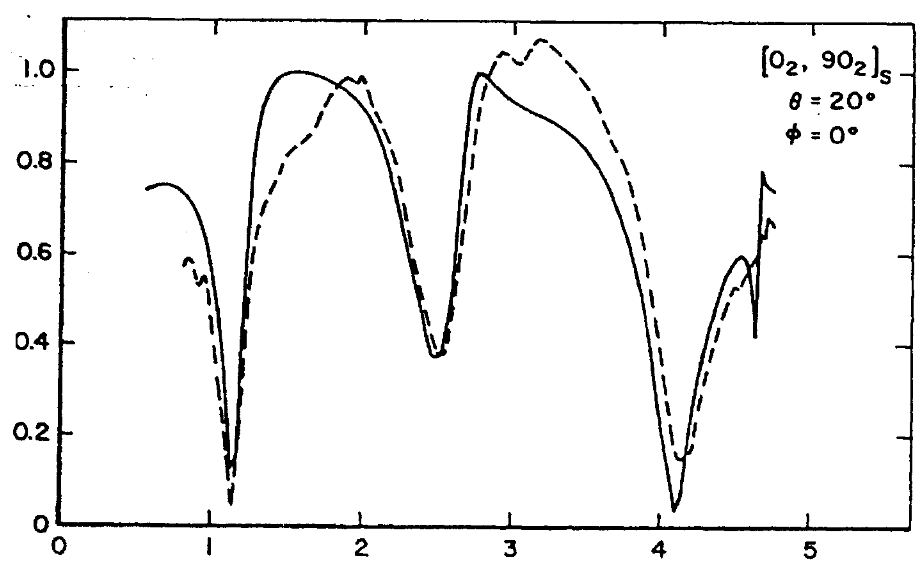

Figure F.3 With $\theta = 20^0$, $\phi = 0^0$ for the $\left[0_2\ 90_2\right]_s$, the top figure is calculated from the program, the bottom figure from Nayfeh's paper. Solid curve is theoretical, dashed curve on the bottom from Nayfeh's paper is experimental [2].

Reflection coefficient 20-90

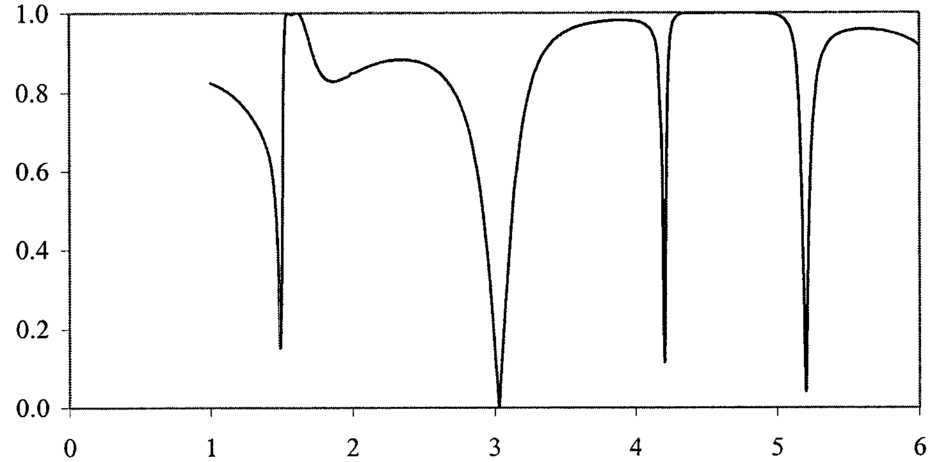

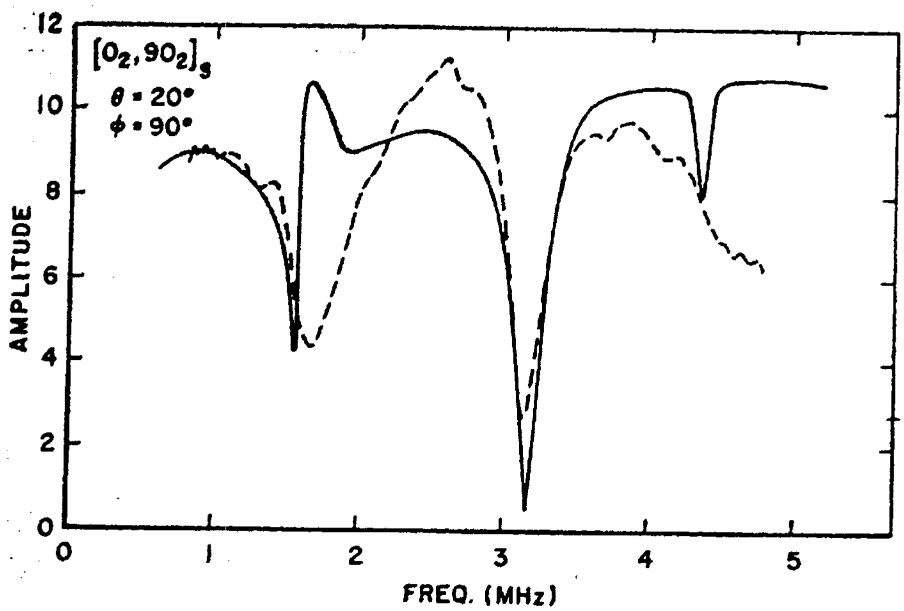

Figure F.4 With $\theta = 20^0$, $\phi = 90^0$ for the $\left[0_2\ 90_2\right]_s$, the top figure is calculated from the program, the bottom figure from Nayfeh's paper. Solid curve is theoretical, dashed curve on the bottom from Nayfeh's paper is experimental [2].

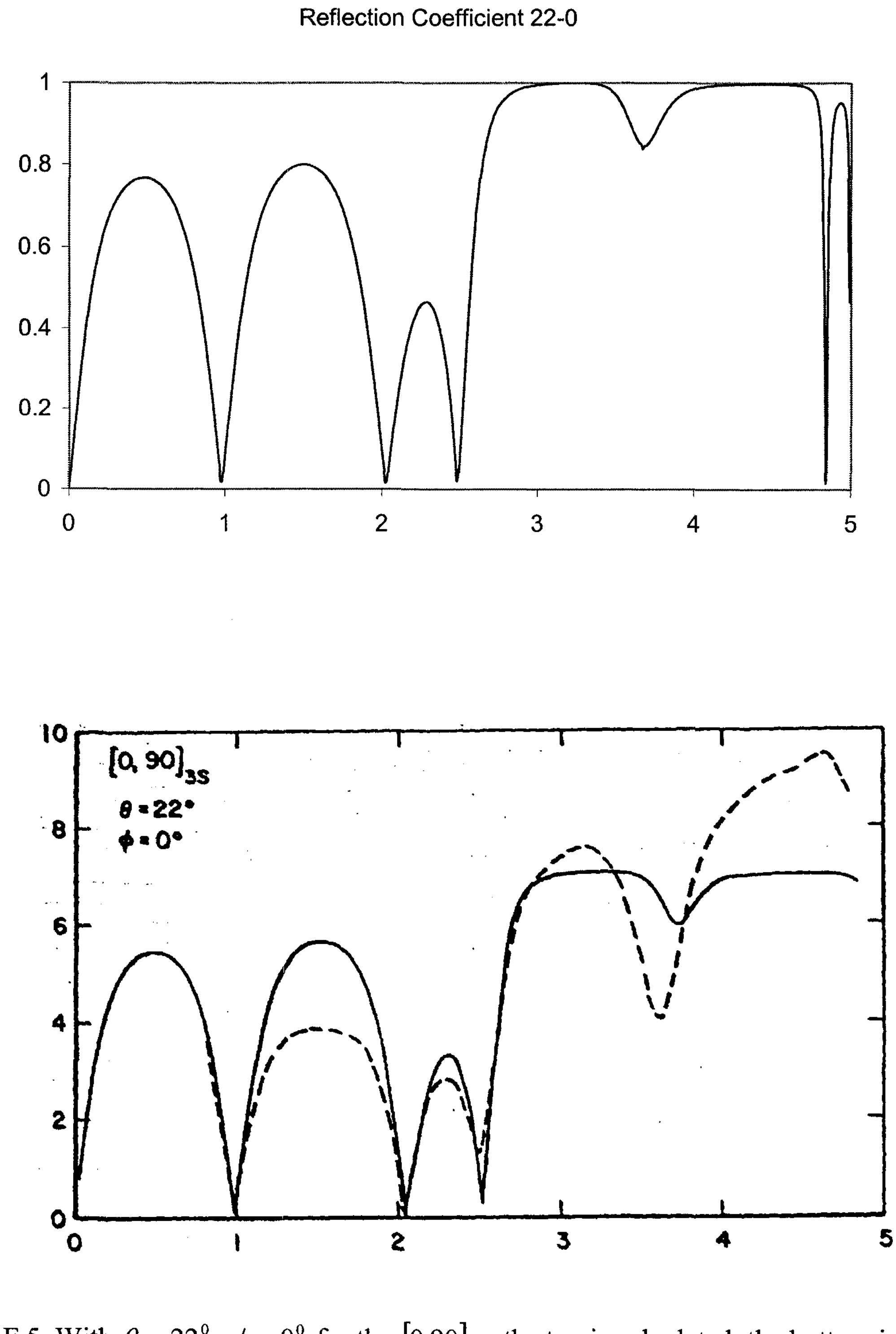

Figure F.5 With $\theta = 22^{0}$, $\phi = 0^{0}$ for the $[0\ 90]_{3s}$, the top is calculated, the bottom is from Nafeh's paper (black solid is theoretical, dashed curve is experimental [2]).

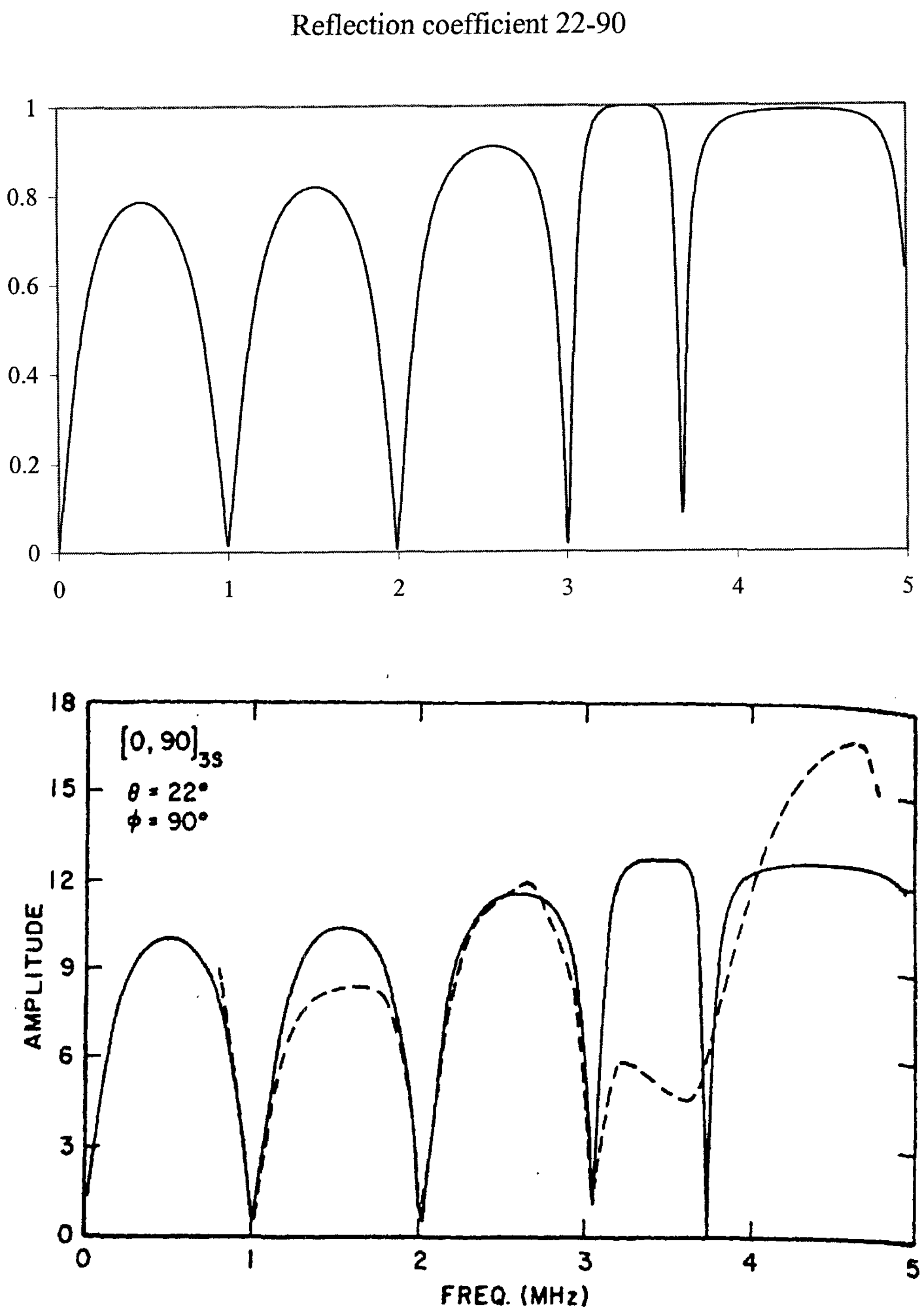

Figure F.6 With $\theta = 22^0$, $\phi = 0^0$ for the $[0\ 90]_{3s}$, the top is calculated, the bottom is from Nayfeh's paper (black solid is theoretical, dashed curve is experimental [2]).

Figures and Comparison for Rubber Materials

The transmission coefficients of a 5-layer rubber structure immersed in water are calculated in isotropic model in chapter 1 by Fortran program and in corresponding anisotropic model in chapter 2 by C++ program. Both results drawn in Figure G.4 almost are the same, which explain that the anisotropic material model may be used as isotropic material model, isotropic model is a special case of anisotropic model. Meantime, the comparisons have proven the availability from different models.

Layer 1: Input data for materials constants and density

$$C = \begin{bmatrix} 1.97e09 & 1.07e09 & 1.07e09 & 0 & 0 & 0 \\ 1.07e09 & 1.97e09 & 1.07e09 & 0 & 0 & 0 \\ 1.07e09 & 1.07e09 & 1.97e09 & 0 & 0 & 0 \\ 0 & 0 & 0 & 0.45e09 & 0 & 0 \\ 0 & 0 & 0 & 0 & 0.45e09 & 0 \\ 0 & 0 & 0 & 0 & 0 & 0.45e09 \end{bmatrix}$$

$\rho = 900\ kg/m^3$

Layer 2: Input data for materials constants and density

$$C = \begin{bmatrix} 4.04e09 & 2.2e09 & 2.2e09 & 0 & 0 & 0 \\ 2.2e09 & 4.04e09 & 2.2e09 & 0 & 0 & 0 \\ 2.2e09 & 2.2e09 & 4.04e09 & 0 & 0 & 0 \\ 0 & 0 & 0 & 0.92e09 & 0 & 0 \\ 0 & 0 & 0 & 0 & 0.92e09 & 0 \\ 0 & 0 & 0 & 0 & 0 & 0.92e09 \end{bmatrix}$$

$\rho = 1500\ kg/m^3$

Layer 3: Input data for materials constants and density

$$C = \begin{bmatrix} 9.29e09 & 5.07e09 & 5.07e09 & 0 & 0 & 0 \\ 5.07e09 & 9.29e09 & 5.07e09 & 0 & 0 & 0 \\ 5.07e09 & 5.07e09 & 9.29e09 & 0 & 0 & 0 \\ 0 & 0 & 0 & 2.11e09 & 0 & 0 \\ 0 & 0 & 0 & 0 & 2.11e09 & 0 \\ 0 & 0 & 0 & 0 & 0 & 2.11e09 \end{bmatrix}$$

$\rho = 1600\ kg/m^3$

Layer 4: Input data for materials constants and density

$$C = \begin{bmatrix} 12.37e09 & 6.75e09 & 6.75e09 & 0 & 0 & 0 \\ 6.75e09 & 12.37e09 & 6.75e09 & 0 & 0 & 0 \\ 6.75e09 & 6.75e09 & 12.37e09 & 0 & 0 & 0 \\ 0 & 0 & 0 & 2.81e09 & 0 & 0 \\ 0 & 0 & 0 & 0 & 2.81e09 & 0 \\ 0 & 0 & 0 & 0 & 0 & 2.81e09 \end{bmatrix}$$

$\rho = 1600\ kg/m^3$

Layer 5: Input data for materials constants and density

$$C = \begin{bmatrix} 7.0e09 & 3.82e09 & 3.82e09 & 0 & 0 & 0 \\ 3.82e09 & 7.0e09 & 3.82e09 & 0 & 0 & 0 \\ 3.82e09 & 3.82e09 & 7.0e09 & 0 & 0 & 0 \\ 0 & 0 & 0 & 1.59e09 & 0 & 0 \\ 0 & 0 & 0 & 0 & 1.59e09 & 0 \\ 0 & 0 & 0 & 0 & 0 & 1.59e09 \end{bmatrix}$$

$\rho = 1500\ kg/m^3$

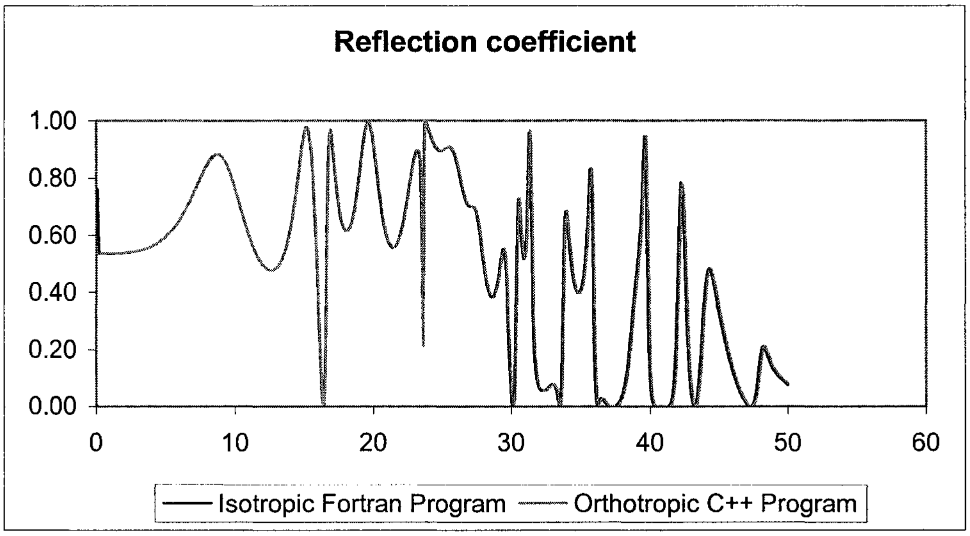

Figure G.7. Calculated Results of a 5-layered rubber material in an isotropic material model of chapter1 and in an anisotropic material model of Chapter 2, the isotropic model is performed by Fortran program, the anisotropic model is performed by C++ program.

References:

1. Kriz, R.D and Stinchcomb, W. W, 1979, 'Elastic Moduli of Transversly Isotropic Graphite Fibers and Their Composites', Experimental Mechanics, 19, 41-49.

2. Chimenti, D.E. and Nayfeh, Adnan H., 1990, 'Ultrasonic Reflection And Guided Wave Propagation In Biaxially Laminated Composite Plates', J. Acoust. Soc. Am. 87(4), 1409-1415.

Appendix G Analysis Method of Material Attenuation in Water for an Orthotropic Material

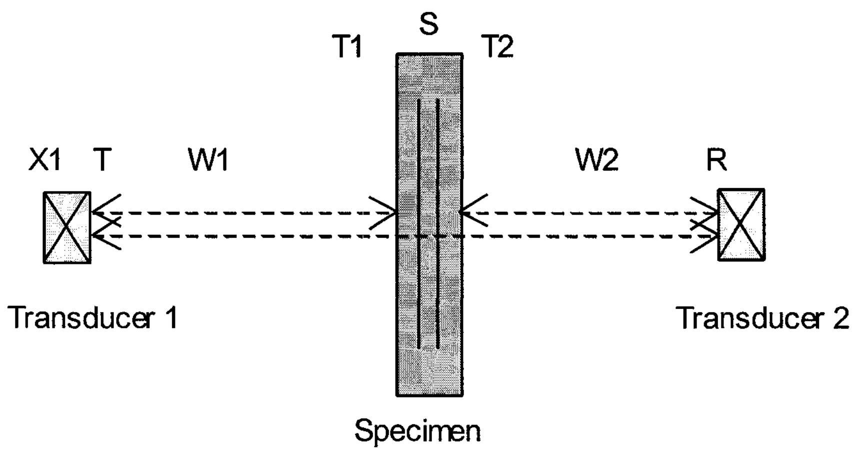

1) Through transmission coefficient from transducer 1 to transducer 2 is expressed as:

$$Y_{12}(\omega) = X_1(\omega)\cdot T(\omega)\cdot W_1(\omega)\cdot T_1(\omega)\cdot S(\omega)\cdot T_2(\omega)\cdot W_2(\omega)\cdot R(\omega)$$

2) Through transmission coefficient from transducer 2 to transducer 1 is expressed as (superscript expresses from transducer 2 to transducer1):

$$Y_{21}(\omega) = X_2(\omega)\cdot R(\omega)\cdot W_2(\omega)\cdot T_2'(\omega)\cdot S(\omega)\cdot T'_1(\omega)\cdot W_1(\omega)\cdot T(\omega)$$

3) Through transmission coefficient without specimen is expressed as:

$$Y_{w21}(\omega) = X_2(\omega)\cdot R(\omega)\cdot W_2(\omega)\cdot W_s(\omega)\cdot W_1(\omega)\cdot T(\omega)$$

4) Through transmission coefficient without specimen is expressed as:

$$Y_{w12}(\omega) = X_1(\omega)\cdot T(\omega)\cdot W_1(\omega)\cdot W_S(\omega)\cdot W_2(\omega)\cdot R(\omega)$$

$$\Rightarrow \quad \frac{Y_{12}(\omega)}{Y_{W12}(\omega)} = \frac{T_1(\omega)\cdot T_2(\omega)\cdot S(\omega)}{W_S(\omega)}$$

If let $W_S(\omega) = 1$.

$$\Rightarrow \quad \frac{Y_{12}(\omega)}{Y_{w12}(\omega)} = T_1(\omega)\cdot T_2(\omega)\cdot S(\omega)$$

$$\text{and,} \quad \frac{Y_{21}(\omega)}{Y_{w21}(\omega)} = T_1{}'(\omega)\cdot T_2{}'(\omega)\cdot S(\omega)$$

5) reflection transducer 1 to specimen

$$Y_{R1}(\omega) = X_1(\omega)\cdot T(\omega)\cdot W_1(\omega)\cdot R_1(\omega)\cdot W_1(\omega)\cdot T(\omega)$$

6) Reflection from transducer 1 to smooth, large impedance hard surface

$$Y_{M1}(\omega) = X_1(\omega)\cdot T(\omega)\cdot W_1(\omega)\cdot R_m(\omega)\cdot W_1(\omega)\cdot T(\omega)$$

$\Rightarrow$

$$\frac{Y_{R1}(\omega)}{Y_{M1}(\omega)} = \frac{R_1(\omega)}{R_M(\omega)} \approx R_1(\omega)$$

7) Reflection from transducer 2 to specimen

$$Y_{R2}(\omega) = X(\omega)\cdot R(\omega)\cdot W_2(\omega)\cdot R_2{}'(\omega)\cdot W_2(\omega)\cdot R(\omega)$$

8) Reflection from transducer 2 to smooth, large impedance hard surface

$$Y_{M2}(\omega) = X(\omega)\cdot R(\omega)\cdot W_2(\omega)\cdot R_m(\omega)\cdot W_2(\omega)\cdot R(\omega)$$

$$\Rightarrow \quad \frac{Y_{R2}(\omega)}{Y_{M2}(\omega)} = \frac{R_2{}'(\omega)}{R_m(\omega)} \approx R_2{}'(\omega)$$

Also, $T_2{}'(\omega) = 1 + R_2{}'(\omega)$ and $T_2(\omega) + R_2{}'(\omega) = 1$

$$T_2(\omega) = 1 - R_2{}'(\omega)$$

Similar, $T_1(\omega) = 1 + R_1(\omega)$

From above 3), we have:

$$S(\omega) = \frac{Y_{12}}{Y_{W12}\cdot T_1(\omega)\cdot T_2(\omega)} = \frac{Y_{12}}{Y_{W12}} \frac{1}{\left(1+\frac{Y_{R1}}{Y_{M1}}\right)} \frac{1}{\left(1-\frac{Y_{R2}}{Y_{M2}}\right)}$$

Where $\alpha = S(\omega)$

Appendix H Measurement Methods of Young's Modulus and Shear Modulus for an Isotropic Material

Young's modulus E and shear modulus G - through-transmission method

Through-transmission method is used for the measurement of Young's modulus, experimental equipment is shown in figure 2. An experiment is conducted by experimental procedures in Appendix B. Phase velocity is acquired from experiment data by spectral analysis. If material is non-dispersive, phase velocity is directly acquired from time delay and plate thickness. If material is dispersive, spectral analysis must be used to acquire time delay. When incident wave is along x_3 direction, the fiber direction is parallel to paper, further perpendicular to paper direction, the longitudinal wave and shear wave are measured. Generally, Young's modulus E and shear modulus G are obtained by relations between phase velocity and elastic modulus. The expressions are the following:

$$c_L^{\,2} = \frac{E(1-\upsilon)}{\rho\,(1+\upsilon)(1-2\upsilon)}$$

$$E = \frac{c_L^{\,2}\rho(1+\upsilon)(1-2\upsilon)}{(1-\upsilon)}$$

for shear wave velocity, elastic modulus are derived as:

$$c_s^{\,2} = \frac{G}{\rho}, \quad \Rightarrow \; G = c_s^{\,2}\rho$$

$$G = \frac{E}{2\,(1+\upsilon)} \text{ and } \frac{1-2\upsilon}{1-\upsilon} = 2\left(\frac{c_s}{c_l}\right)^2$$

Young's modulation E - plate wave method

Plate wave method is used to the measurement of Young's modulation. When an incident wave impacts a surface of material at some angle, the refraction wave is reflected at zagzig in plate cross section. A superposition of reflected waves forms plate wave along the plate direction. Plate is categorized into extensional mode wave and flexural mode wave. The nondispersive extensional mode wave propagates is the faster than dispersive flexural mode wave. The extensional wave is used in the measurement of elastic modulus. From reference, the relationship between phase and modulus is expressed as the following:

$$c_o = \left[\frac{E}{\rho\left(1-\upsilon^2\right)}\right]^{\frac{1}{2}} \Rightarrow E = c_0^{\ 2}\rho\left(1-\upsilon^2\right)$$

where c_o plate wave velocity along plate cross section

Appendix I Analysis Method of Material Attenuation in Water for an Isotropic Material

Longitudinal wave attenuation analysis

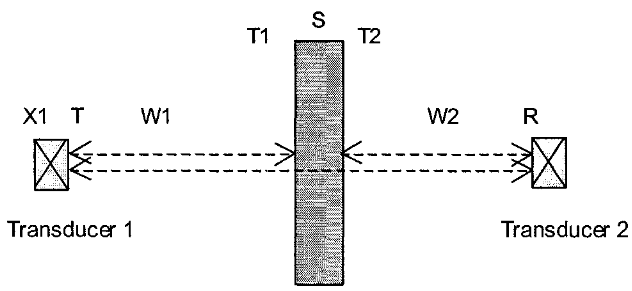

Figure I.1. Transducers, specimen and paths of wave propagation in an immersion through transmission method

1) Through transmission coefficient from transducer 1 to transducer 2 is expressed as:

$$Y_{12}(\omega) = X_1(\omega)\cdot T(\omega)\cdot W_1(\omega)\cdot T_1(\omega)\cdot S(\omega)\cdot T_2(\omega)\cdot W_2(\omega)\cdot R(\omega)$$

2) Through transmission coefficient from transducer 2 to transducer 1 is expressed as:

$$Y_{21}(\omega) = X_2(\omega)\cdot R(\omega)\cdot W_2(\omega)\cdot T_2'(\omega)\cdot S(\omega)\cdot T'_1(\omega)\cdot W_1(\omega)\cdot T(\omega)$$

3) Through transmission coefficient without specimen is expressed as:

$$Y_{w21}(\omega) = X_2(\omega)\cdot R(\omega)\cdot W_2(\omega)\cdot W_s(\omega)\cdot W_1(\omega)\cdot T(\omega)$$

4) Through transmission coefficient without specimen is expressed as:

$$Y_{w12}(\omega) = X_1(\omega)\cdot T(\omega)\cdot W_1(\omega)\cdot W_S(\omega)\cdot W_2(\omega)\cdot R(\omega)$$

$$\Rightarrow \frac{Y_{12}(\omega)}{Y_{W12}(\omega)} = \frac{T_1(\omega)\cdot T_2(\omega)\cdot S(\omega)}{W_S(\omega)}$$

If let $W_S(\omega) = 1$.

$$\Rightarrow \quad \frac{Y_{12}(\omega)}{Y_{w12}(\omega)} = T_1(\omega)\cdot T_2(\omega)\cdot S(\omega)$$

and,

$$\frac{Y_{21}(\omega)}{Y_{w21}(\omega)} = T_1^{'}(\omega)\cdot T_2^{'}(\omega)\cdot S(\omega)$$

5) Reflection transducer 1 to specimen

$$Y_{R1}(\omega) = X_1(\omega)\cdot T(\omega)\cdot W_1(\omega)\cdot R_1(\omega)\cdot W_1(\omega)\cdot T(\omega)$$

6) Reflection from transducer 1 to smooth, large impedance hard surface

$$Y_{M1}(\omega) = X_1(\omega)\cdot T(\omega)\cdot W_1(\omega)\cdot R_m(\omega)\cdot W_1(\omega)\cdot T(\omega)$$

$\Rightarrow$

$$\frac{Y_{R1}(\omega)}{Y_{M1}(\omega)} = \frac{R_1(\omega)}{R_M(\omega)} \approx R_1(\omega)$$

7) Reflection from transducer 2 to specimen

$$Y_{R2}(\omega) = X(\omega)\cdot R(\omega)\cdot W_2(\omega)\cdot R_2^{'}(\omega)\cdot W_2(\omega)\cdot R(\omega)$$

8) Reflection from transducer 2 to smooth, large impedance hard surface

$$Y_{M2}(\omega) = X(\omega)\cdot R(\omega)\cdot W_2(\omega)\cdot R_m(\omega)\cdot W_2(\omega)\cdot R(\omega)$$

$$\Rightarrow \quad \frac{Y_{R2}(\omega)}{Y_{M2}(\omega)} = \frac{R_2^{'}(\omega)}{R_m(\omega)} \approx R_2^{'}(\omega)$$

Also, $T_2^{'}(\omega) = 1 + R_2^{'}(\omega)$ and $T_2(\omega) + R_2^{'}(\omega) = 1$

$$T_2(\omega) = 1 - R_2^{'}(\omega)$$

Similar, $T_1(\omega) = 1 + R_1(\omega)$

From above 3), we have:

$$S(\omega) = \frac{Y_{12}}{Y_{W12}\cdot T_1(\omega)\cdot T_2(\omega)} = \frac{Y_{12}}{Y_{W12}} \frac{1}{\left(1+\frac{Y_{R1}}{Y_{M1}}\right)} \frac{1}{\left(1-\frac{Y_{R2}}{Y_{M2}}\right)}$$

Shear wave attenuation analysis

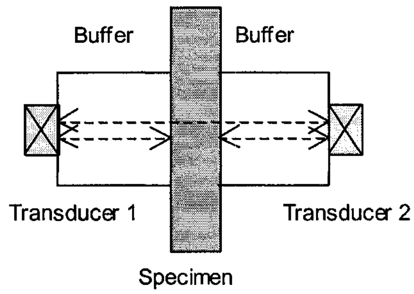

Figure I.2 Transducers, specimen and paths of wave propagation in contact method for measurement of shear wave attenuation

It is very similar to longitudinal wave attenuation analysis

$$S(\omega)=\frac{Y_{12}}{Y_{W12}\cdot T_1(\omega)\cdot T_2(\omega)}=\frac{Y_{12}}{Y_{W12}}\frac{1}{\left(1+\dfrac{Y_{R1}}{Y_{M1}}\right)}\frac{1}{\left(1-\dfrac{Y_{R2}}{Y_{M2}}\right)}$$

Appendix J

Automatic Gain Correction Exploration for Detection of Delamination in a Layered Composite Plate

J.1 Introduction

The appendix presents a delamination investigation for a visco-elastic composite plate as an addendum, the study explores a defective visco-elastic composite plate, and extends the previous isotropic slip in Chapter 1 to the orthotropic slip, and extends the continuous boundary condition of the carbon fiber/epoxy composite plate in Chapter 3 to a delaminated boundary condition. The objective is to insight the wave propagation sensitivity in a delaminated composite plate at arbitrary incident angles for auto-gain correction of ultrasonic reduced axis inspection, to analyze the impact of delamination, and to recommend a technology for the inspection of the delaminated composite plate.

In the appendix, the research approach is the combination of the isotropic slip model and the visco-elastic composite plate model. The following sections present the theoretical derivation of the transmission coefficient in a delaminated composite plate, the arithmetic method of computer calculation and the comparisons of the defective boundary condition and continuous boundary condition at the different frequencies and incident angles. The calculated samples are $[0, 90]_S$, $[90, 0]_S$ and $[0]_{4T}$ lay up carbon fiber/epoxy composite plates, the same as in Chapter 3.

J.2 Transmission coefficients

Calculation of the transmission coefficients is the key for delamination detection in multi-layered orthotropic plates in the configuration discussed previously. Results for these calculations are shown in the following sections.

J.2.1 Boundary conditions

In a layered structure with a delamination immersed in fluid, the boundary conditions are classified based on the type of delamination. The absence of a defect provides a continuity of stresses and displacement at the boundary between the solid layers. At the boundary with the fluid, the normal stress is continuous as are displacements between the solid layer and fluid. The slip boundary condition exists when a delamination exists between solid layers. In this case normal compressive stresses are transmitted, and tensile stresses are not. Shear stresses are not transmitted.

J.2.1.1 Boundary condition of solid continuity

A multi-layered structure immersed in invicid fluid water is shown in Figure J.1, typically the case of a 4-layer structure is assumed. If the multi-layered structure is a fiber reinforced, epoxy matrix composite material, the fiber direction is in $X_1 - X_2$ plane. A slip defect boundary is assumed to exist between layer 2 and layer 3. When the incident elastic wave insonifies the upper surface of layer 4, it passes through the multi-layered structure to the lower surface of layer 1. Except for the assumed defective boundary condition, all other boundaries are assumed to be continuous. In the interface between layers, if boundary conditions are assumed to be continuous, then stresses are continuous, and displacements are continuous. Further, the displacement-stress vector, which consists of ordered displacements and stresses, is continuous. More generally, for layer k of a N-layer structure, the continuous displacement-stress vector across the interface is expressed as:

$$P_{k-1}^{\ +} = P_k^{\ -} \tag{J.1}$$

Except for the delaminated defective boundary between layer 2 and layer 3, for all of the continuous boundary conditions from the layer 1 to layer 2 and from layer 3 to layer 4, the displacement-vectors are derived using the transfer matrix method [Appendix B]:

$$P_4^+ = [A]_1 P_3^- \tag{J.2}$$

$$P_2^+ = [A]_2 P_1^- \tag{J.3}$$

where

$$[A]_1 = A_4 A_3$$

using the derivative and symbol notation shown in Appendix B

J.2.1.2 Boundary condition of solid slip

The slip defect boundary condition is assumed to be between the layer 2 and layer 3. The result is that the normal stress is continuous when stress is positive, and the shear stresses vanish, the normal displacement is continuous when the displacement is positive displacement, and the shear displacement is discontinuous. Then, if an elastic wave impinges a solid structure with a slip defect, its positive half period couples to pass through the interface and its negative half period disappears for normal stress and displacement. The expressions of the slip defective boundary condition are following:

$$[A]_2 = A_2 A_1$$

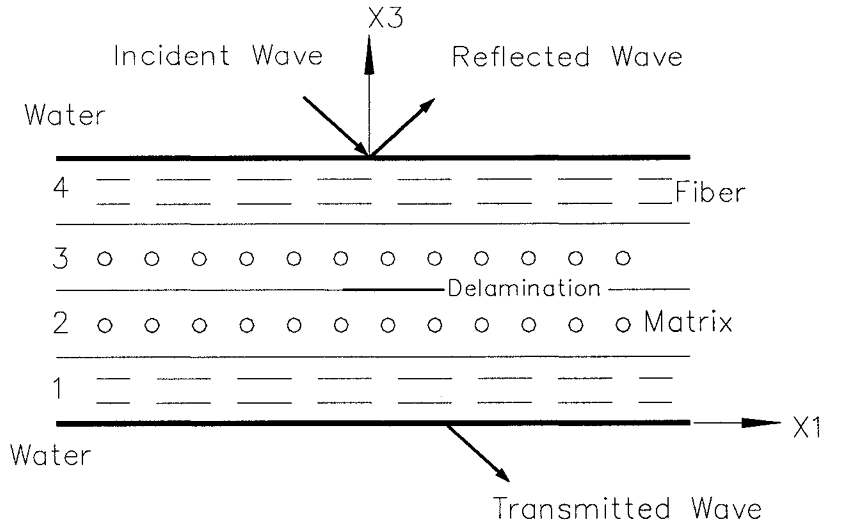

Figure J.1 A laminated composite plate with a delamination defect immersed in water

When

$$\sigma_{33}^{(3+)} < 0$$

then

$$[u_3]_2^+ = [u_3]_3^- \text{ and } [\sigma_{33}]_2^+ = [\sigma_{33}]_3^- \tag{J.4}$$

when

$$\sigma_{33}^{(3+)} > 0$$

$$\sigma_{33}^{(3-)} = 0,\ \sigma_{33}^{(2+)} = 0$$

and

$$[\sigma_{31}]_2^+ = [\sigma_{32}]_2^+ = 0,\ [\sigma_{31}]_3^- = [\sigma_{32}]_3^- = 0 \tag{J.5}$$

The above boundary condition is suitable for the so called light kissing contact disbond or boundary condition. This is a reasonable model for defects in many composite materials, where the model is used to describe a delamination between layers.

J.2.1.3 Boundary condition between a solid and fluid water

The sample or specimen is immersed in fluid, generally water, which is used as a coupling media for elastic wave passing through the solid object. The couplant is used in order to improve the elastic wave transmission efficiency at the solid surface interface. The boundary condition of interface between the fluid and solid is important to understand the coupling of the elastic wave into the object. The boundary condition is assumed in the analysis to be a continuous normal stress and displacement between the solid layer and the fluid. A discontinuous shear displacement and vanishing shear stress is also assumed at the solid-liquid interface. Only longitudinal wave propagates in the fluid if the properties of the water are assumed to have finite viscosity. However, the longitudinal wave and the shear wave both propagate in the solid. Further, for an orthotropic structure, the shear wave and longitudinal wave are coupled, thus making understanding of wave propagation more complicated. For the special case shown in figure J.1, the elastic wave insonifies the upper surface of layer 4 of a multi-layered composite plate. The stress and displacement of the interface of the layer 4 and the fluid are expressed as:

$$\begin{bmatrix} u_1 \\ u_3 \\ \sigma_{33}^{*} \end{bmatrix}_4^{+} = \begin{bmatrix} 1 & 1 \\ -\alpha_w & \alpha_w \\ \rho_w c^2 \sin\theta & \rho_w c^2 \sin\theta \end{bmatrix} \begin{bmatrix} e^{-i\xi\alpha_w(x-d)} \\ \mathrm{R}e^{i\xi\alpha_w(x-d)} \end{bmatrix} \tag{J.6}$$

where $x_3 = d$ is the total thickness of the layers, ρ_w is the fluid density, v is the phase velocity of wave and R is the reflection coefficient. Similarly, the stress and displacement between layer 1 and the fluid are expressed as:

$$\begin{bmatrix} u_1 \\ u_3 \\ \sigma_{33}^{*} \end{bmatrix}_1^{-} = \begin{bmatrix} 1 \\ -\alpha_w \\ \rho_w c^2 \sin\theta \end{bmatrix} Te^{-i\xi\alpha_w x_3} \tag{J.7}$$

where T is the transmission coefficient of a multi-layered composite material.

J.2.2 Transmission coefficients

Considering the slip defect boundary condition between layer 2 and layer 3, the corresponding displacement-stress matrix from equation (J.2) and (J.3) can be rewritten as:

$$\begin{bmatrix} u_1 \\ u_2 \\ u_3 \\ \sigma_{33}^{*} \\ 0 \\ 0 \end{bmatrix}_2^{+} = \begin{bmatrix} A_{11} & A_{12} & A_{13} & A_{14} \\ A_{21} & A_{22} & A_{23} & A_{24} \\ A_{31} & A_{32} & A_{33} & A_{34} \\ A_{41} & A_{42} & A_{43} & A_{44} \\ A_{51} & A_{52} & A_{53} & A_{54} \\ A_{61} & A_{62} & A_{63} & A_{64} \end{bmatrix} \begin{bmatrix} u_1 \\ u_2 \\ u_3 \\ \sigma_{33}^{*} \end{bmatrix}_1^{-} \tag{J.8}$$

$$\begin{bmatrix} u_3 \\ \sigma_{33}^{*} \end{bmatrix}_2^{+} = \begin{bmatrix} M_{11} & M_{12} \\ M_{21} & M_{22} \end{bmatrix}_1 \begin{bmatrix} u_3 \\ \sigma_{33}^{*} \end{bmatrix}_1^{-} \tag{J.9}$$

$$\begin{bmatrix} u_3 \\ \sigma_{33}^{*} \end{bmatrix}_4^{+} = \begin{bmatrix} M_{11} & M_{12} \\ M_{21} & M_{22} \end{bmatrix}_2 \begin{bmatrix} u_3 \\ \sigma_{33}^{*} \end{bmatrix}_3^{-} \tag{J.10}$$

where matrix $[M]$ for an incident wave along the fiber direction of orthotropic material is

$$M_{11} = -A_{41}^{-1}\begin{vmatrix} A_{21} & A_{22} \\ A_{41} & A_{42} \end{vmatrix},\ M_{12} = -A_{41}^{-1}\begin{vmatrix} A_{21} & A_{23} \\ A_{41} & A_{43} \end{vmatrix} \tag{J.11}$$

$$M_{21} = -A_{41}^{-1}\begin{vmatrix} A_{31} & A_{32} \\ A_{41} & A_{42} \end{vmatrix},\ M_{22} = -A_{41}^{-1}\begin{vmatrix} A_{31} & A_{33} \\ A_{41} & A_{43} \end{vmatrix} \tag{J.12}$$

where $[A]$ is the global transfer matrix for the 4 layers. However, when the propagation vector of the incident beam deviates from the fiber direction plane at an angle, the axis of symmetry is changed. The propagation of the wave is more complicated and the orthotropic material symmetry becomes effectively a monoclinic material. The horizontally polarized quasi-shear wave (SH), the vertically polarized quasi-shear wave (SV) and the quasi-longitudinal wave (L) are all coupled. Then, a 6th order matrix expression is used in the calculation of the transmission coefficient. M_{11}, M_{12}, M_{21} and M_{22} becomes 3rd order determinant with a complex dependence on the material properties in the general orientation of the sample. Terms M_{11}, M_{12}, M_{21}, M_{22} may be derived, [Brekhovskikh and Godin, 1990, Nayfeh, 1995, Nayfeh and Chimenti, 1989], described in Appendix B.

$$M_{11} = |A|^{-1}\begin{vmatrix} A_{31} & A_{32} & A_{33} \\ A_{51} & A_{52} & A_{53} \\ A_{61} & A_{62} & A_{63} \end{vmatrix},\ M_{12} = |A|^{-1}\begin{vmatrix} A_{31} & A_{32} & A_{34} \\ A_{51} & A_{52} & A_{54} \\ A_{61} & A_{62} & A_{64} \end{vmatrix} \tag{J.13}$$

$$M_{21} = |A|^{-1}\begin{vmatrix} A_{41} & A_{42} & A_{43} \\ A_{51} & A_{52} & A_{53} \\ A_{61} & A_{62} & A_{63} \end{vmatrix},\ M_{22} = |A|^{-1}\begin{vmatrix} A_{41} & A_{42} & A_{44} \\ A_{51} & A_{52} & A_{54} \\ A_{61} & A_{62} & A_{64} \end{vmatrix} \tag{J.14}$$

$$|A| = \begin{vmatrix} A_{51} & A_{52} \\ A_{61} & A_{62} \end{vmatrix}$$

When the delaminated boundary condition and the boundary condition between the solid and fluid water are introduced, equation (J.9) is substituted into equation (J.10) because of continuous normal stress and displacement. The expression for the positive half period is derived as:

$$\begin{bmatrix} -\alpha_w(1-R) \\ \rho_w c^2(1+R) \end{bmatrix}_4^+ = \begin{bmatrix} M_{11} & M_{12} \\ M_{21} & M_{22} \end{bmatrix}\begin{bmatrix} -\alpha_w T \\ \rho_w c^2 T \end{bmatrix}_1^- \tag{J.15}$$

where

$$\begin{bmatrix} M_{11} & M_{12} \\ M_{21} & M_{22} \end{bmatrix} = \begin{bmatrix} M_{11} & M_{12} \\ M_{21} & M_{22} \end{bmatrix}_2 \begin{bmatrix} M_{11} & M_{12} \\ M_{21} & M_{22} \end{bmatrix}_1 \tag{J.16}$$

Thus, the transmission coefficients and reflection coefficients can be solved from the above equations. The transmission coefficient in both orthotropic and monoclinic cases is exactly expressed as the following:

$$T = \frac{2\rho_w v^2 \alpha_w}{(M_{11} + M_{22})\rho_w v^2 \alpha_w - (M_{21}\alpha_w{}^2 + M_{12}(\rho_w v^2)^2)} \tag{J.17}$$

J.3 Calculation results for delamination of composite materials

The calculations of transmission coefficients with the delaminated boundary condition are completed using a program written in C++, a flow chart for the calculation is shown in Figure J.2. The transmission coefficient for the carbon fiber reinforced, epoxy matrix composite plate is calculated. The results are then compared with the results for the same materials with a defect free continuous boundary condition.

J.3.1 Carbon fiber/epoxy composite plate $[0, 90]_S$, $[90, 0]_S$ and $[0]_{4T}$ lay up

Visco-elastic material constants of the composite plate of carbon fiber reinforced epoxy matrix for each layer are shown in Table 3.1. The samples consist of 4 layers using a $[0, 90]_S$, $[90, 0]_S$ and $[0]_{4T}$ lay up. The sample thicknesses are 0.635mm, 0.584mm and 0.508mm, respectively, the same as in Chapter 3. For the calculated cases, the delaminated defect exists in the plane between layer 2 and layer 3.

J.3.2 Calculated curves and results – continuous boundary condition and delaminated defective boundary condition for carbon fiber/epoxy composite plate

Results are shown in Figure J.3 for the carbon fiber reinforced epoxy matrix composite plate with a $[0, 90]_S$ lay-up. Figure J.4 shows the carbon fiber reinforced epoxy matrix composite plate with a $[90, 0]_S$ lay-up and Figure J.5 shows the carbon fiber reinforced epoxy matrix composite plate with a $[0]_{4T}$ lay up. The delaminated defect boundary does not significantly impact the transmission coefficient for small incident angles at lower frequencies. Lower frequencies are associated with the longer wavelengths, which appear to be less sensitive to the defect. In the region of small incident angles, below 20 degrees, the delaminated defect cannot be detected by a comparison of transmission coefficients. When the incident angle is increased, the transmission coefficients are different for the defect and defect free conditions. Lower frequencies may be used to detect the defect if a large incident angle is used. With an increase in the incident wave frequency, the transmission coefficients quickly shift in some areas, and the distinction between boundary conditions is obvious. When a sample is tested, an area of steep change of transmission coefficients should be chosen.

Figure J.2 Flow chart for the calculation of transmission coefficients through a delaminated solid layer

However, in a practical sensor, the measurement and inspection is difficult in the critical area. Very small incident angle changes can produce a large change of transmission coefficient. In general, however, when the incident wave is a near normal incident angle, defects cannot be easily detected by the comparison of the transmission coefficient. This is consistent with observations and the results of Chapter 1 [P. Zhang and M. Peterson, 1998]. For the different lamina lay up, the fiber directions also produce a large change in the transmission coefficient. In a carbon fiber composite with a $[90, 0]_S$ lay-up, the differences between the defective and defective free boundary conditions are very small. In that case, the defect is difficult to inspect in the fiber directions and at many incident angles. Thus a change in the plane of the incident wave is required and a range of incident plane from 0 into 90 degree is recommended. When a 90 incident plane is used, the carbon fiber lay up of $[90, 0]_S$ lay up effectively replicates the carbon fiber transmission coefficient for 0 degree with a lay up of $[0, 90]_S$ lay up.

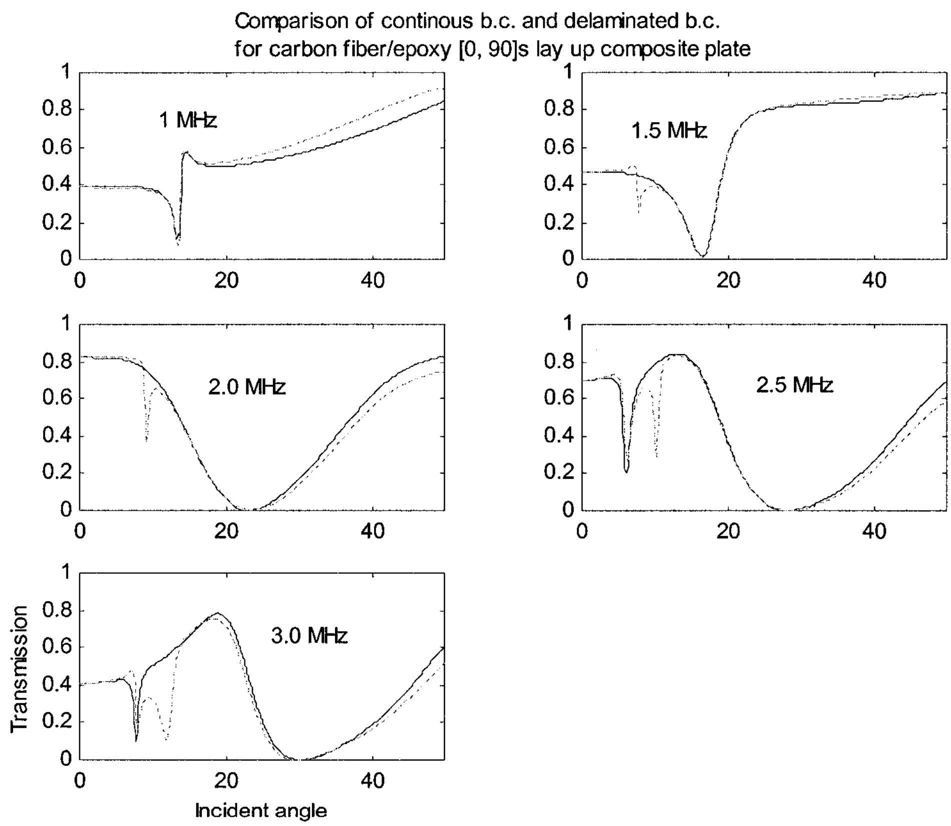

Figure J.3. Calculated curves for the comparison of continuous boundary condition and delaminated boundary condition for carbon fiber/epoxy composite plate $[0, 90]_S$ lay up

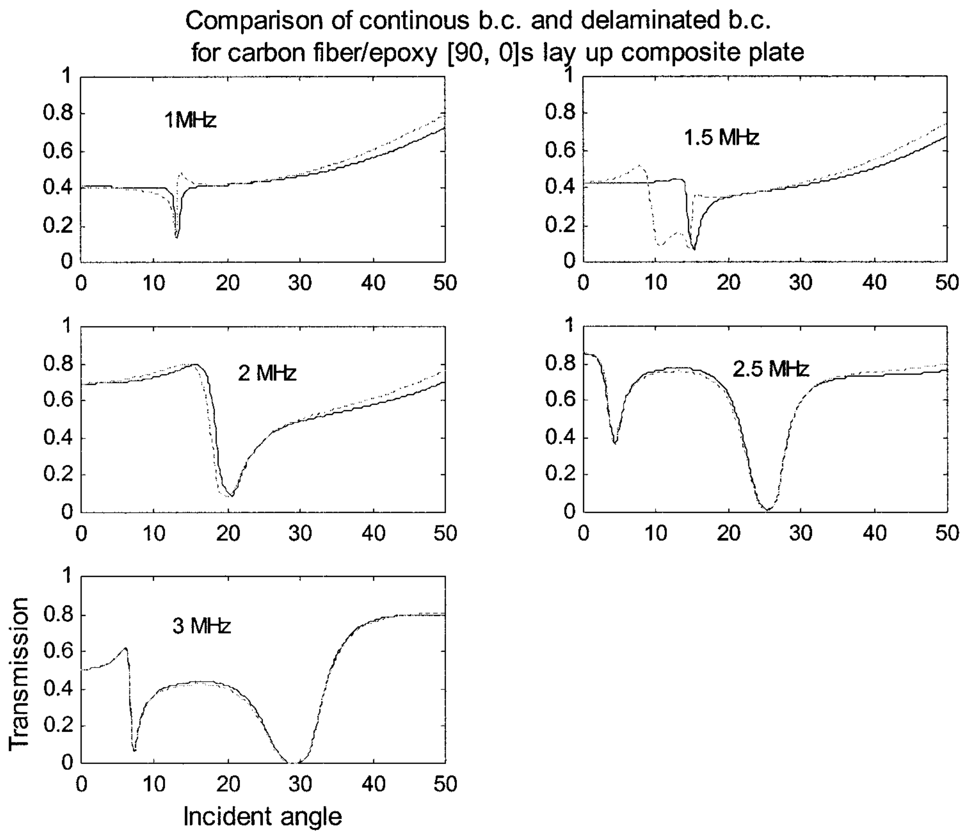

Figure J.4. Calculated curves for the comparison of continuous boundary condition and delaminated boundary condition for carbon fiber/epoxy composite plate $[90, 0]_S$ lay up

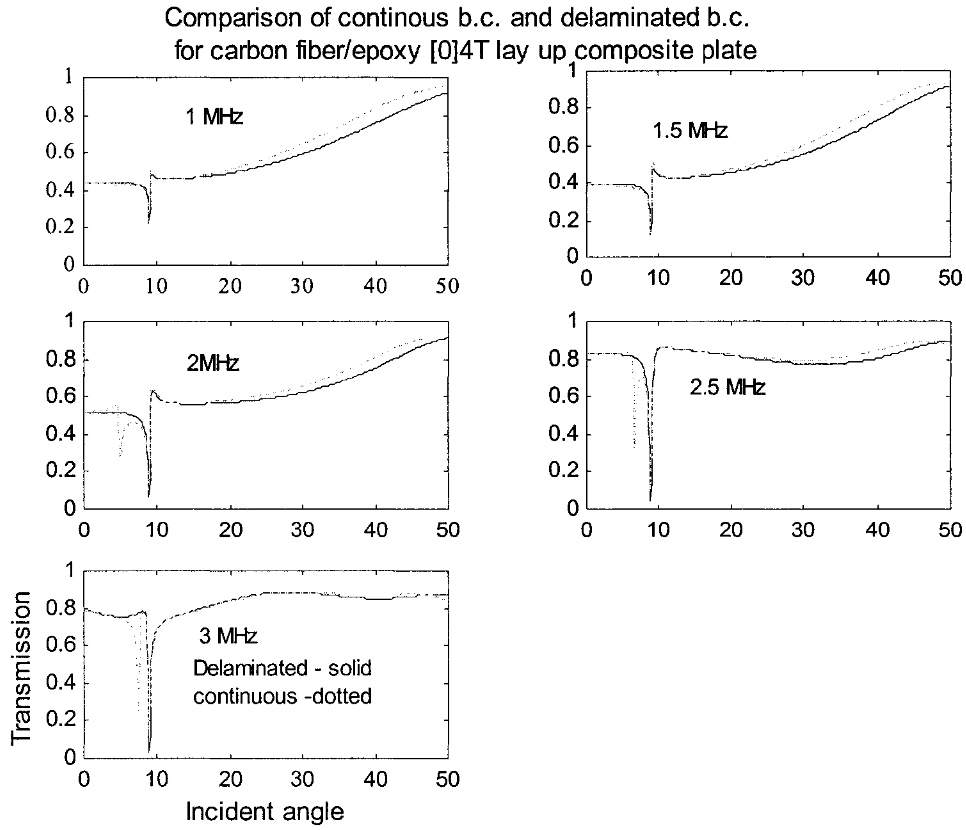

Figure J.5 Calculated curves for the comparison of continuous boundary condition and delaminated boundary condition for carbon fiber/epoxy composite plate $[0]_{4T}$ lay up

J.4 References

Brekhovskikh, L. M. and. Godin, O.A, 1990, *Acoustics of Layered Media I*, Springer-Verlag, New York.

Downs, J., Zhang, P. and Peterson, M. L., 1999, 'a High-Speed High-Resolution Ultrasonic Inspection Machine', IEEE/ASME Transactions on Mechatronics, Vol. 4, no.1, 301-311.

Nayfeh, Adnan H., 1995, *Wave Propagation in Layered Anisotropic Media*, Elsvier, New York.

Nayfeh, Adnan H. and Chimenti, D. E., 1989, 'Free Wave Propagation in Plates of General Anisotropic Media', J. Applied Mechanics, 56, 881-886.

Zhang, P. and Peterson, M. L., 1998, 'Transmission Coefficient for Multi-Layered Structures at Arbitrary Incident Angle', Review of Progress in Quantitative Evaluation, vol. 18.